# THE KUMAMOTO JAPAN EARTHQUAKES OF 14 AND 16 APRIL 2016

## A FIELD REPORT BY EEFIT

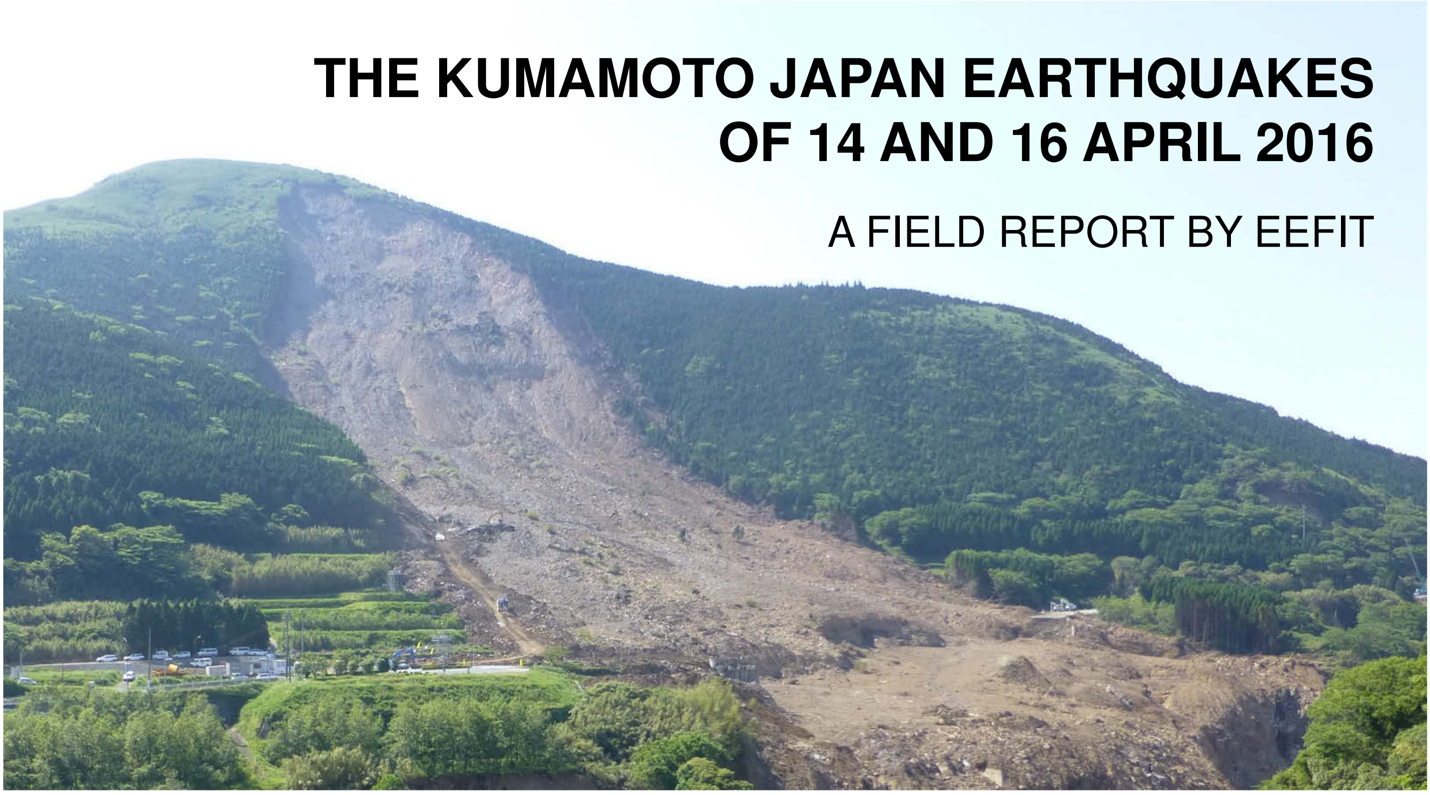


EEFIT

# THE KUMAMOTO JAPAN EARTHQUAKES OF 14 AND 16 APRIL 2016


**Dr. Katsu Goda, *University of Bristol* (Team Leader and Editor)**

**Dr. Grace Campbell, *Arup***

**Ms. Laura Hulme, *Arup***

**Mr. Bashar Ismael, *University of Manchester***

**Dr. Lin Ke, *Willis Re Japan***

**Ms. Rebekah Marsh, *Mott MacDonald***

**Prof. Peter Sammonds, *University College London***

**Dr. Emily So, *University of Cambridge***

**Report prepared in association with:**

**Dr. Yoshihiro Okumura, *Kyoto University***

**Miss Saki Yotsui, *Kyoto University***

**Dr. Maki Koyama, *Gifu University***

**Dr. Nozar Kishi, *Karen Clark & Company***

**Report reviewed by:**

**Mr. Antonios Pomonis, *World Bank*, Consultant; Social, Urban, Rural & Resilience (GSURR)**

## Acknowledgements

The EEFIT Kumamoto team would like to express our sincere gratitude to the following individuals and organisations for their support prior to, during and following this mission, without whom we would not have been able to carry out the field trip and research effectively.

- Ms. Berenice Chan, *Institution of Structural Engineers*
- Dr. Tristan Lloyd, *AIR Worldwide*
- Dr. Sean Wilkinson, *Newcastle University*
- Prof. Junji Kiyono, *Kyoto University*
- Dr. Takashi Kiyota, *University of Tokyo*
- Prof. Shinji Toda, *Tohoku University*
- Miss Zoe Mildon, *University College London*

Thanks are also due to the following organisations for funding the participation of team members:

- EPSRC (EP/I01778X/1) for funding Dr. Katsu Goda, Prof. Peter Sammonds, Dr. Emily So, and Mr. Bashar Ismael
- Arup for funding Dr. Grace Campbell and Ms. Laura Hulme
- Mott MacDonald for funding Ms. Rebekah Marsh
- Willis Towers Watson for funding Dr. Lin Ke

EEFIT would like to acknowledge the on-going support of corporate sponsors: AECOM, AIR Worldwide, Arup, British Geological Survey, ch2m, GUY CARPENTER, RMS, Mott MacDonald, Sellafield Ltd, and Willis Towers Watson.

EEFIT

# Contents

## List of Figures

EEFIT

## List of Tables

# 1 Introduction

## 1.1 Preamble

A moderate-size earthquake struck the Kumamoto Prefecture of Kyushu Island, Japan on 14 April 2016 (21:26 PM local time). The Japan Meteorological Agency (JMA) magnitude $M_J$ of 6.5 was registered (moment magnitude $M_w$6.1). The fault rupture was originated from the northern segment of the Hinagu Fault. Intense shaking was recorded in the eastern part of Kumamoto Prefecture, and major earthquake damage was caused in Mashiki Town near the epicentre. Subsequently, on 16 April 2016 (1:25 AM local time), a larger $M_J$7.3 earthquake ($M_w$7.1) occurred along the Futagawa Fault (NE of the Hinagu Fault). This earthquake caused significantly greater damage in wider areas near the fault (e.g. Mashiki Town, Nishihara Village, and Minami Aso Village). The crustal deformation due to the mainshock was observed as ground surface ruptures at many locations along the Futagawa Fault. At several places, ground deformation up to 2 m was reported (Shirahama et al., 2016). Retrospectively, the 14 April 2016 and 16 April 2016 events are considered as foreshock and mainshock, respectively, and both are of right-lateral strike-slip type occurring at shallow depths. It is important to note that the foreshock and mainshock were originated from close but different active faults (Kato et al., 2016). The JMA intensity of 7 (highest intensity in the JMA intensity scale) was recorded in Mashiki Town during both foreshock and mainshock (i.e. double shock impact). Numerous buildings had collapsed due to the double shock in Mashiki Town. The earthquake sequence also triggered several moderate earthquakes (and some damage) at remote locations, such as Yufu City and Kokonoe Town in Oita Prefecture (both about 60 km N-NE of Mashiki Town). Moreover, an active aftershock sequence was observed in Kumamoto City.

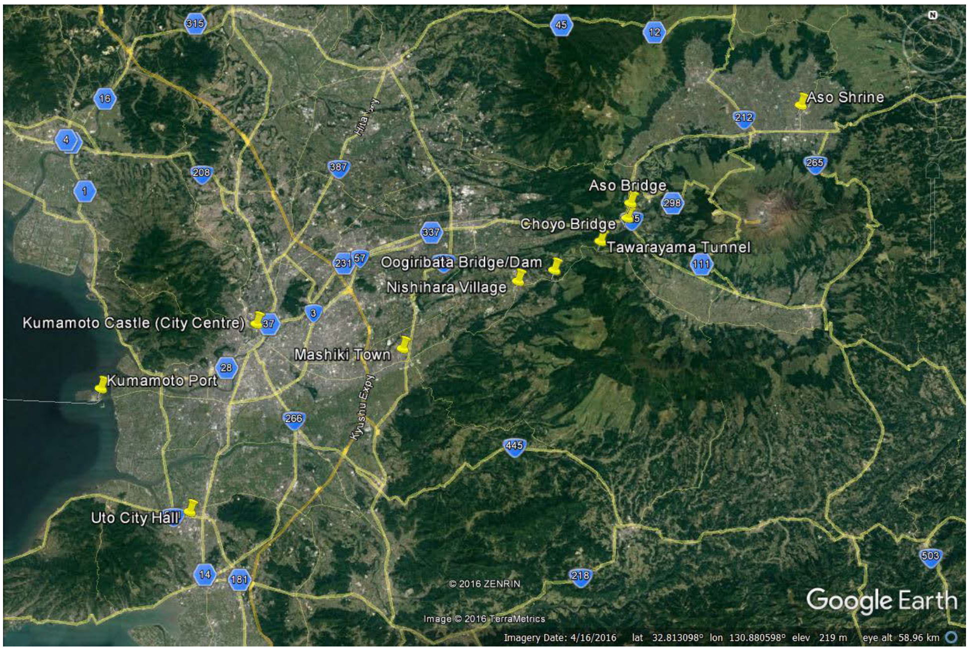


**Figure 1.1** Main locations in Kumamoto Prefecture (image source: Google Earth).

The earthquakes caused significant tangible and intangible loss. As of July 2016, the number of fatalities stood at 69 of which 9 were due to the foreshock (49 caused by direct causes, such as building collapse and landslides and 20 due to indirect causes) increasing to 115 in October 2016 and eventually reaching 225 due to many earthquake-related deaths among the displaced (see Section 6), while the total number of injured persons was 1,747 (Fire and Disaster Management Agency, 2016; **Table 1.1**). More than 180,000 people were evacuated immediately after the mainshock. The total economic loss was estimated to be 2.4 to 4.6 trillion Japanese Yen (Cabinet Office of Government of Japan, 2016), while insurance pay-out exceeded 3 billion US Dollar (General Insurance Association of Japan, 2016). Due to the Kumamoto earthquake sequence, 8,050 houses were destroyed, whereas 24,147 buildings suffered major damage (Fire and Disaster Management Agency, 2016; **Table 1.1**).

The majority of the collapsed buildings were timber houses with heavy roof, which were constructed according to the pre-1981 seismic design provisions (Nakashima and Chusilp, 2003). Several cultural heritage sites (e.g. Kumamoto Castle and Aso Shrine) were also damaged severely. The earthquakes triggered numerous landslides in the mountainous areas of the Kumamoto region, and destroyed major infrastructure and facilities. In the plain areas of Kumamoto, several sections of Kyushu Expressway (bridges and road surface cracks) were damaged due to the earthquakes, resulting in major disruption of the regional traffic network. The operation of Kyushu Shinkansen was also interrupted due to the earthquakes after the mainshock because one Shinkansen train derailed in the south of Kumamoto railway station that was travelling at 80 km/h when the mainshock struck. The railway tracks of the Aso line were destroyed by landslides, and the repairs will take a long time.

**Table 1.1** Summary of earthquake damage due to the 2016 Kumamoto sequences (as of 1 July 2016; Fire and Disaster Management Agency, 2016). The numbers include the loss and damage caused by the 14 April 2016 foreshock.

| Prefecture | Deaths | Major injury | Minor injury | Collapsed houses | Severely damaged houses | Partially damaged houses | Non-residential structural damage |
|---|---|---|---|---|---|---|---|
| Kumamoto | 69[(1)] | 364 | 1,316 | 8,044 | 24,274 | 115,702 | 1,799 |
| Oita | 0 | 4 | 24 | 6 | 140 | 4,336 | 27 |
| Others | 0 | 8 | 31 | 0 | 3 | 255 | 3 |
| Total | 69 | 376 | 1,371 | 8,050 | 24,417 | 120,293 | 1,829 |

[(1)] *This number includes the fatalities due to indirect causes.*

The 2016 Kumamoto disaster was caused by multiple cascading geological hazards. The primary damage was due to the intense shaking and ground deformation of the foreshock-mainshock sequence (which occurred only 28 hours apart). In the near-fault region, the effects of the ground deformation were remarkable; buildings and infrastructure that were right above the fault rupture were severely damaged (Goda et al., 2016). The secondary damage was induced by landslides and other ground failures, including liquefaction and lateral spreading along rivers and in coastal areas. The earthquake damage was widespread spatially over the rural areas of Kumamoto Prefecture. In particular, simultaneous damage/destruction to multiple key infrastructures, such as Aso Bridge, Oogiribata Bridge, Choyo Bridge, and Tawarayama Tunnel, disconnected main access routes (e.g. Road 57 and Road 28) between areas inside and outside Aso Caldera. As of June 2016, major detours were required to visit places inside Aso Caldera from Kumamoto City. In particular, this has caused significant difficulty and stress to evacuees and recovery activities in Minami Aso Village.

## 1.2 EEFIT Kumamoto team and collaboration

To learn key lessons from the observed damage and impact due to the Kumamoto earthquakes, an Earthquake Engineering Field Investigation Team (EEFIT) mission was organised and deployed by the Institution of Structural Engineers. The EEFIT-Kumamoto members include: Dr. Katsu Goda (team leader), Dr. Grace Campbell, Ms. Laura Hulme, Mr. Bashar Ismael, Ms. Rebekah Marsh, Dr. Lin Ke, Prof. Peter Sammonds, and Dr. Emily So. The affiliation and technical expertise of the members are summarised in **Table 1.2**.

**Table 1.2** EEFIT-Kumamoto members.

| Name | Affiliations | Expertise |
|---|---|---|
| Dr. Katsu Goda (KG) *(Team Leader)* | Senior Lecturer in Civil Engineering, University of Bristol | Engineering seismology & ground motion |
| Dr. Grace Campbell (GC) | Geologist, Arup | Earthquake geology & geophysics |
| Ms. Laura Hulme (LH) | Structural engineer, Arup | Structural engineering |
| Mr. Bashar Ismael (BI) | PhD student, University of Manchester | Geotechnical engineering |
| Dr. Lin Ke (LK) | Geotechnical Engineer, Willis Towers Watson | Geotechnical engineering |
| Ms. Rebekah Marsh (RM) | Geologist, Mott MacDonald | Engineering geology |
| Prof. Peter Sammonds (PS) | Professor of Geophysics, University College London | Geophysics & earthquake mechanism |
| Dr. Emily So (ES) | Senior Lecturer, University of Cambridge | Earthquake impact & recovery |

The mission was generously supported by many colleagues from Japan and the US (see the full list of the contributors on the Acknowledgements page). In particular, Dr. Yoshihiro Okumura and Miss Saki Yotsui from Kyoto University, Dr. Maki Koyama from Gifu University, and Dr. Nozar Kishi from Karen Clark & Company participated in the field work (**Figure 1.2**). The main earthquake reconnaissance survey was conducted between 22 May and 26 May 2016. Dr. So extended her stay to continue the interviews and hearing from the evacuees as well as disaster management officials from various organisations. The itinerary of the EEFIT-Kumamoto mission is summarised in **Table 1.3**, and the main locations visited are marked in **Figure 1.1**.

**Figure 1.2** EEFIT Kumamoto team in Minami Aso with Dr. Yoshihiro Okumura (1st from left, front), Miss Saki Yotsui (3rd from left, front), and Dr. Nozar Kishi (2nd from left, back).

**Table 1.3** Visited locations by the EEFIT-Kumamoto members.

| Date | Locations visited | EEFIT member | Accompanied by |
|---|---|---|---|
| Day 1 (22 May) | Kumamoto City (downtown) and Mashiki Town | All | - |
| Day 2 (23 May) | Aso City and Minami Aso Village | All | Dr. Okumura, Miss Yotsui, Dr. Kishi |
| Day 3 (24 May) team 1 | Mashiki Town and Nishihara Village (fault rupture and geotechnical damage) | KG, GC, PS, RM | - |
| Day 3 (24 May) team 2 | Kumamoto Port, Uto City, and Mashiki Town (geotechnical damage and building damage) | BI, LK, LH, ES | Dr. Koyama, Miss Yotsui, Dr. Kishi |
| Day 4 (25 May) team 1 | Mashiki Town and Nishihara Village (faulting and infrastructure/geotechnical damage) | GC, BI, RM, PS | Dr. Koyama, Miss Yotsui, Dr. Kishi |
| Day 4 (25 May) team 2 | Kumamoto City and Mashiki Town (faulting and building damage) | KG, LH, LK | Dr. Kishi |
| Day 4 (25 May) team 3 | Mifune Town social welfare council, Mifune Junior High School, Kumamoto City Sun Life and Gender Equality Centre, Kumamoto Prefecture Office (interviews, evacuation centre visits, and meetings with NGOs) | ES | Dr. Koyama, Miss Yotsui |
| Day 5 (26 May) team 1 | Mashiki Town (damage survey) | KG, LH, GC | Dr. Kishi |
| Day 5 (26 May) team 2 | Nishihara Village (geotechnical and infrastructure damage along Road 28) | BI, LK, RM, PS | - |
| Day 5 (26 May) team 3 | Sojo University (meeting with AIJ), Minateras (Mashiki Town interaction information centre), Mashiki Town gym (evacuation centre visits and interviews) | ES | Dr. Koyama, Miss Yotsui |
| Day 6 (27 May) | Uki City welfare centre, library, hall and community centre (evacuation centre visits and interviews) | ES | Dr. Koyama, Miss Yotsui |
| Day 7 (28 May) | Kumamoto City international centre and university (meetings with academics and city officials) | ES | Dr. Koyama, Miss Yotsui |
| Day 8 (29 May) | Nishihara Village school (meeting with village officers) | ES | Dr. Koyama, Miss Yotsui |

The field investigations were focused upon: (i) building damage, (ii) infrastructure and geotechnical damage, (iii) fault rupture, and (iv) disaster response and recovery. The main objectives of the mission were to make observations regarding:

1. Earthquake damage to buildings and infrastructure in the near-fault region (Mashiki Town, Nishihara Village, and Minami Aso Village). The particular focus was to relate observed damage and experienced ground shaking. For this purpose, building damage surveys were conducted in Mashiki Town (note: seismograms at the Mashiki Town Office recorded ground motions due to the foreshock and mainshock, and the JMA intensity of 7 was registered for both foreshock and mainshock).
2. Infrastructure damage in the near-fault region, caused by large-scale landslides and slope failures (e.g. Road 57 blockage and Aso Bridge collapse).
3. Damage caused by liquefaction and lateral spreading along rivers and near port areas.
4. Fault rupture due to the earthquake, which appeared on ground surface.
5. Earthquake response and recovery activities by emergency response teams, evacuees, volunteers, and non-governmental organisations.
6. Establish contacts and exchange information with the Japanese academic community involved in the post-event activities.

Our observations and investigations highlight considerable earthquake shaking and deformation demand in the near-fault region, and provide insights that are useful for enhancing community resilience against major earthquake disasters.

In this report, the following topics are discussed:

- Section 2: Geological and tectonic observations (main contributors – GC and PS)
- Section 3: Ground motion observations (main contributor – KG)
- Section 4: Building damage observations (main contributor – LH)
- Section 5: Infrastructure and geotechnical observations (main contributors – BI, LK, and RM)
- Section 6: Response and recovery observations (main contributors – ES and Miss Yotsui)

### 1.3 References

Cabinet Office of Government of Japan (2016). Estimated economic impact due to the 2016 Kumamoto earthquakes. Accessed on 9 June 2016 at http://www5.cao.go.jp/keizai3/kumamotoshisan/kumamotoshisan20160523.pdf.

Fire and Disaster Management Agency (2016). Accessed on 5 July 2016 at http://www.fdma.go.jp/bn/2016/.

General Insurance Association of Japan (2016). Key figures related to insurance claims due to the 2016 Kumamoto Earthquake as of June 13, 2016. Accessed on 18 June 2016 at http://www.sonpo.or.jp/en/news/2016/1606_03.html.

Goda, K., Campbell, G., Hulme, L., Ismael, B., Ke, L., Marsh, R., Sammonds, P., So, E., Okumura, Y, Kishi, N., Koyama, M., Yotsui, S., Kiyono, J., Wu, S., and Wilkinson, S. (2016). The 2016 Kumamoto earthquakes: cascading geological hazards and compounding risks. *Frontiers in Built Environment*, **2**, 19, doi: 10.3389/fbuil.2016.00019.

Kato, A., Fukuda, J., Nakagawa, S., and Obara, K. (2016). Foreshock migration preceding the 2016 $M_w$7.0 Kumamoto earthquake, Japan. *Geophysical Research Letters*, **43**, 8945–8953.

Nakashima, M., and Chusilp, P. (2003). A partial view of Japanese post-Kobe seismic design and construction practices. *Earthquake Engineering and Engineering Seismology*, **4**, 3–13.

Shirahama, Y., Yoshimi, M., Awata, Y., Maruyama, T., Azuma, T., Miyashita, Y., Mori, H., Imanishi, K., Takeda, N., Ochi, T., Otsubo, M., Asahina, D., and Miyakawa, A. (2016). Characteristics of the surface ruptures associated with the 2016 Kumamoto earthquake sequence, central Kyushu, Japan. *Earth Planets and Space*, **68**, 191, doi: 10.1186/s40623-016-0559-1.

# 2 Geology and Tectonics

This section presents the geological and tectonic setting of the 2016 Kumamoto earthquakes. The seismological aspects of the earthquake sequence are discussed in Section 3.

## 2.1 Japan tectonic setting

Japan is one of the most seismically and volcanically active regions in the world. It owes this intense activity to its location, at the intersection of three tectonic plates: the Eurasia Plate in the west, the Pacific Plate in the east, and the Philippine Sea Plate in the southeast (**Figure 2.1**). Along Japan's northern Pacific coast, the boundary of the Pacific and Eurasia Plates forms the Japan Trench (**Figure 2.1**). In the south, the boundary between the Philippines Sea Plate and the Eurasia Plate forms the Nankai Trough. These two boundaries are subduction zones along which the dense ocean crust of the Pacific and Philippines Sea Plates sinks beneath the less dense continental crust of the Eurasia Plate. Global Positioning System (GPS) velocity measurements relative to stable Eurasia indicate that the Philippines Sea and Pacific Plates move W to NW at rates of ~55 mm/year and 90 mm/year, respectively (**Figure 2.1**).

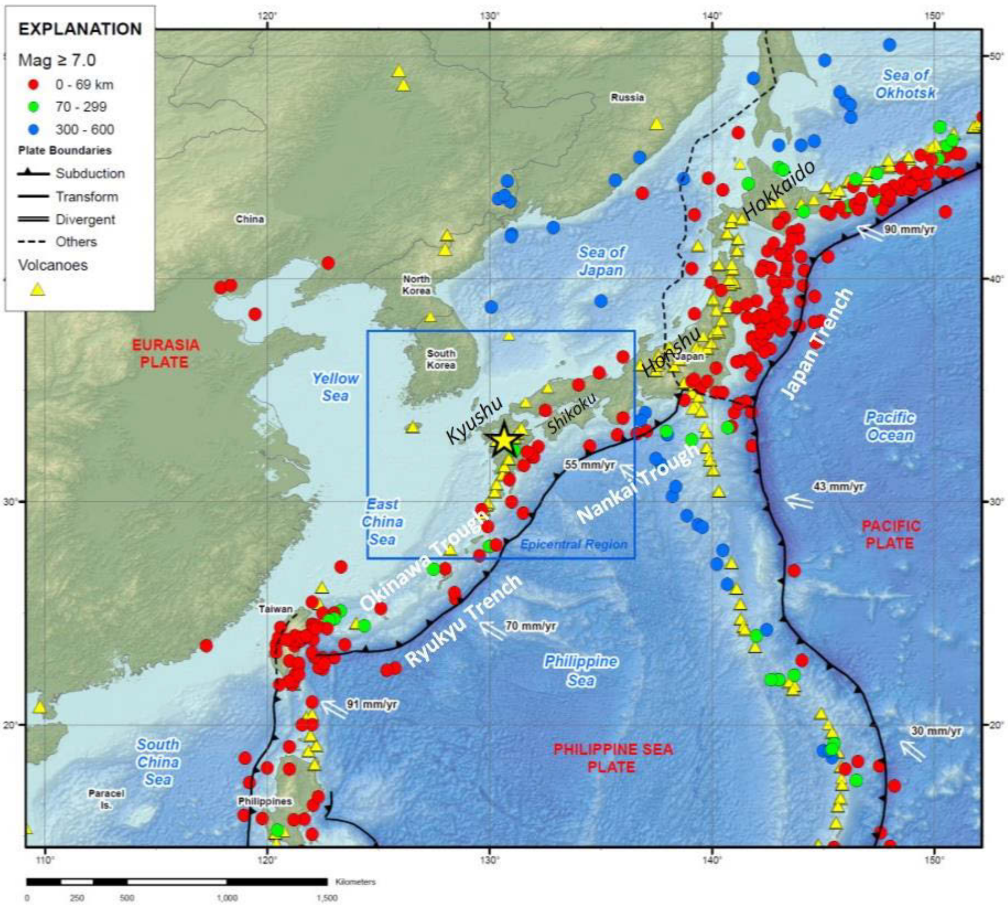


**Figure 2.1** Tectonic setting and seismicity of Japan. The yellow star indicates the epicentre of the $M_w$7.1 16 April 2016 Kumamoto mainshock (United States Geological Survey, 2016).

**Figure 2.1** shows the distribution of earthquakes with moment magnitude ($M_w$) equal to and greater than 7.0 in Japan since 1900. Convergence along the subduction boundaries is accommodated by shortening of the main subduction interface zones and also by active shallow crustal faults (less than 20 km depth) that occur up to hundreds of kilometres from the main subduction interface within the Eurasia Plate. The Kumamoto earthquakes are an example of the latter plate-interior type of faulting. Though both types of faulting (subduction and plate-interior) have generated large-magnitude, destructive earthquakes in Japan, the plate-interior crustal events are less well documented and less well known (see Section 2.3). The best-documented, instrumentally-recorded earthquake, which was similar to the Kumamoto mainshock in terms of magnitude, depth, and faulting mechanism, was the 1995 $M_w$6.9 Kobe earthquake (Kanamori, 1995), which killed over 5,500 people. In addition to the 1995 Kobe earthquake, therefore, the Kumamoto earthquakes provide a relatively unique example of plate-interior crustal faulting in Japan.

## 2.2 Active faults in Kyushu Island

Kyushu Island, which is the epicentral location of the April 2016 Kumamoto earthquakes, is the southernmost main island of Japan. This region experiences two dominant tectonic movements: 1) N-S extension, associated with active volcanism and crustal thinning and 2) E-W compression and right-lateral shear, related to the oblique motion of the Philippines Sea Plate relative to the stable Eurasia Plate. **Figure 2.2** shows the active faults in the northern and central parts of Kyushu Island (in red) as well as the epicentres of the 2016 Kumamoto foreshock and mainshock (yellow circles). In general, there are two dominant orientations of faulting: E-W and NE-SW (**Figure 2.2**). The N-S extension is largely accommodated by the E-W trending Central Kyushu rift zone, which is bounded by and contains sub-parallel faults. Major volcanic centres, such as Aso Volcano/Caldera and Unzen Volcano, align approximately E-W along the rift zone (**Figure 2.2**). In the southwest, the central rift is thought to continue down to the Okinawa Trough (**Figure 2.1**), the active back-arc spreading centre behind the Ryukyu Island arc (**Figure 2.1**), whereas at its eastern extent it continues to Beppu Bay (**Figure 2.2**). Further east of Beppu Bay, the tectonic style changes from multiple distributed ~5-10 km long sub-parallel E-W oriented faults, to the major NE-SW oriented Median Tectonic Line (MTL), an active transform (strike-slip) fault (**Figure 2.2**). In Shikoku Island (**Figure 2.1**), the MTL is very active (Okumura, 2016), however, the activity is replaced with normal faulting onshore in Kyushu (**Figure 2.2**). According to Okumura (2016), the majority of the southern margin of the Central Kyushu rift has not been active in the Quaternary (since around ≤12,000 years before present), with the exception of the Futagawa and Hinagu Faults (denoted by **F** and **H**, respectively, in **Figure 2.2**). These faults were known to be active as determined from paleo-seismological studies (Chida, 1979; Shimokawa et al., 1999), and were the causative faults of the Kumamoto foreshock and mainshock.

## 2.3 Historical crustal earthquakes

The long-documented historical and pre-historical (paleo-seismological) records of Japanese earthquakes, which span many hundreds to several thousands of years, indicate that major events occur approximately every ~180 years on average along the Nankai Trough subduction interface (e.g. Moreno et al., 2016). In contrast, the records for large-magnitude, plate-interior crustal earthquakes are relatively less well known and less complete (Moreno et al., 2016). **Figure 2.2** shows some of the known historical events with $M_w$7.0 or greater, though as expected considering the dates of these events, little is known about the fault sources or seismological aspects of these earthquakes and the impacts they had. One of the most recent historical damaging earthquakes in Kumamoto was the *M*6.3 1889 Kumamoto earthquake. Additionally, the 1792 *M*6.4 Shimabara-Shigatusaku (Unzen) earthquake (**Figure 2.2**) triggered a lava-dome flank collapse in the Unzen volcanic area, which in turn generated a big tsunami. The tsunami, which hit both sides of Ariake Bay (**Figure 2.2**), and caused over 15,000 deaths. This sequence of disasters is known as the Shimabara Catastrophe and is considered the worst disaster in the history of volcanic hazards in Japan (Inoue, 2000). The Aso volcanic region shares many similarities in terms of seismicity, faulting, and volcanism to the Unzen volcanic region, therefore, the Shimabara Catastrophe is an important analogy to consider when assessing earthquake-, volcano-, landslide-, and tsunami-hazard potential in the Aso volcanic region.

In more recent decades, the Research Group for Active Faults in Japan (1980, 1991) have comprehensively mapped and characterised many of the active faults in Japan, including Kyushu Island, however, there remains few clear examples of historical or pre-historical earthquake surface ruptures preserved in the landscape in Kyushu. The Kumamoto mainshock, which generated very clear, well-preserved surface ruptures, therefore, provides a unique opportunity to gain insight into the relationship between slip on plate-interior crustal faults in a single earthquake, and the long-term trend of the topography on Kyushu Island, which has developed over many thousands of years.

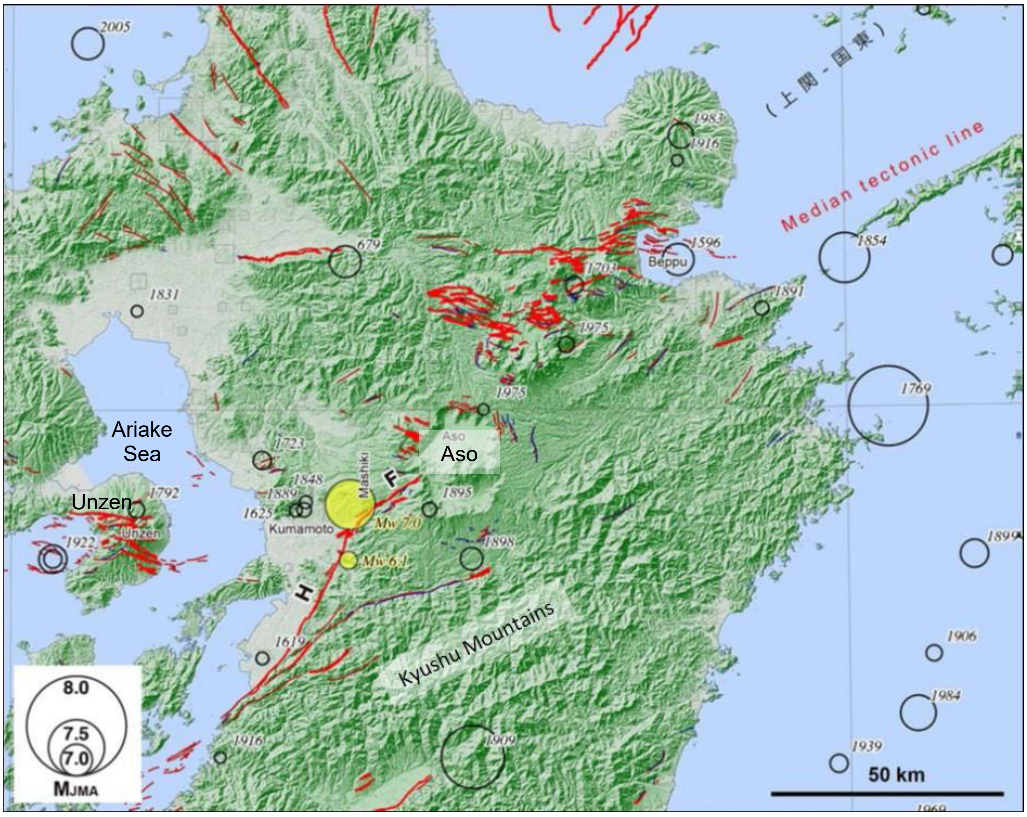


**Figure 2.2** Quaternary faults and earthquakes in Central Kyushu Island (Okumura, 2016).

## 2.4 Hinagu and Futagawa Faults

Sudden slip on the Hinagu and Futagawa Faults caused the Kumamoto foreshock and mainshock, respectively. Both faults had been previously mapped by the Research Group for Active Faults of Japan (1980, 1991) and are included in seismic hazard assessments by the Headquarters for Earthquake Research Promotion (2016). The Futagawa Fault had been mapped extending approximately 70 km WSW-ENE from Uto Peninsula in the southwest to the crater rim of Aso Caldera in the east (**Figure 2.2**). The Hinagu Fault had been mapped to extend approximately 80 km NNE-SSW and at its northern extent it merges with the western extent of the Futagawa Fault (**Figure 2.2**). The two faults accommodate both the E-W compression driven by the Philippine Sea Plate subduction and the N-S extension of the Central Kyushu rift. Based on the observed geological offsets along the faults, the dominant sense of slip is known to be right-lateral strike-slip with a lesser component south-side-up vertical displacement, associated with the N-S extension of the Kyushu rift. The uplift of the Kyushu Mountains in the south is due to the normal (south-side-up) component of the fault movement (**Figure 2.2**). Both faults dip steeply (~60-80°) with the WSW-ENE striking Futagawa Fault dipping NNW, and the NNE-SSW striking Hinagu Fault dipping WNW.

## 2.5 Mainshock surface ruptures

Two types of surface rupturing were observed after the Kumamoto mainshock: 1) right-lateral strike-slip displacements and 2) vertical offsets with a normal/extensional sense of motion. Seismological observations indicate that the mainshock was a predominantly strike-slip faulting event, with a lesser extensional component (e.g. Asano and Iwata, 2016; Kubo et al., 2016; Yagi et al., 2016) and, as expected, the dominant types of surface ruptures observed in the field (e.g. Kumahara et al., 2016; Shirahama et al., 2016; Toda et al., 2016) have been horizontal right-lateral displacements with lesser vertical offsets (e.g. **Figure 2.3**). The field rupture offset measurements and offset distributions are consistent with what has been observed from the available seismological, e.g. strong motion and broadband teleseismic waveforms, and geodetic data, e.g. high-resolution satellite imagery and Interferometric Synthetic Aperture Radar (InSAR).

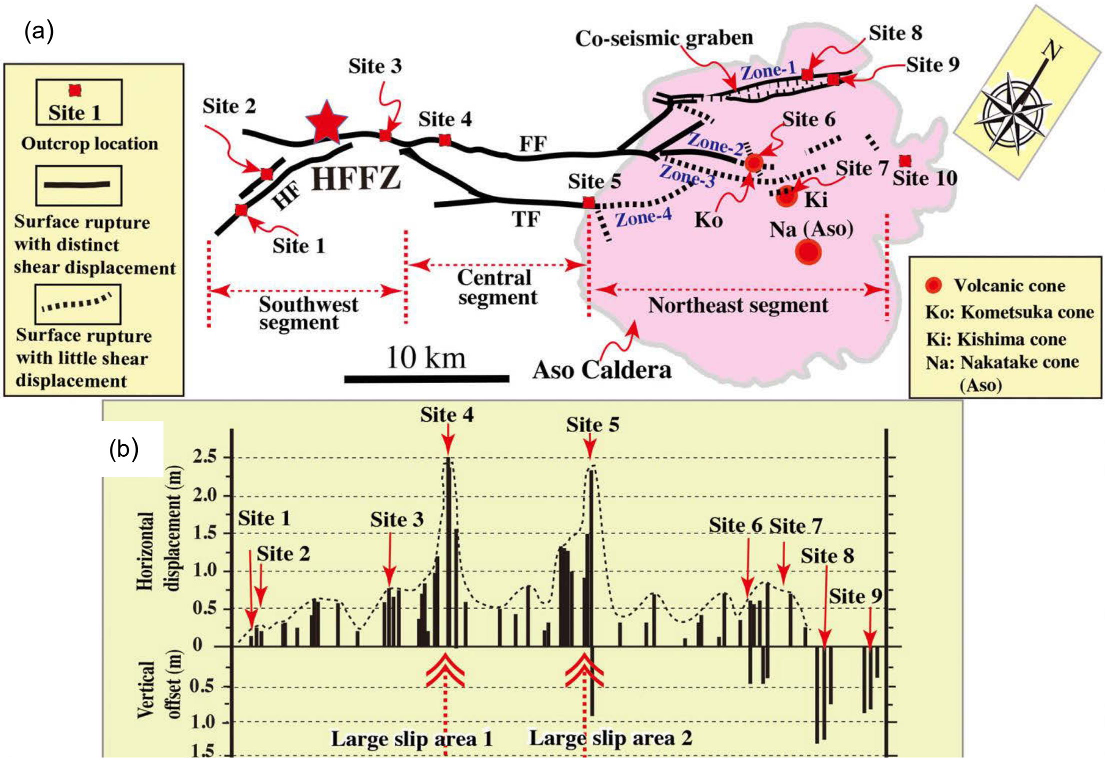


**Figure 2.3** (a) Surface rupture mapping and (b) offset measurements (Lin et al., 2016).

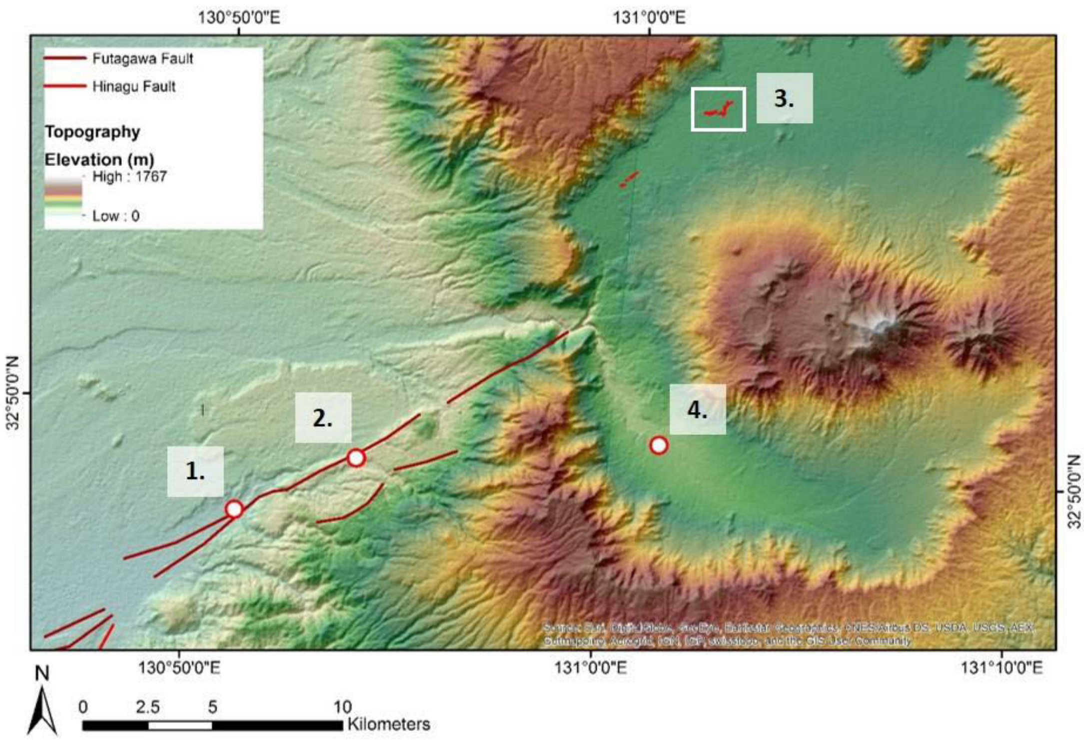


**Figure 2.4** Location map of the surface rupture sites visited by the EEFIT in the field. The number headings on the map correspond to four sites mentioned in the main text (base map: Shuttle Radar Topography Mission SRTM-1).

The EEFIT members made field observations and measurements of both types of mainshock surface ruptures along the Futagawa Fault. These observations are presented in the subsections below, starting in the southwest of the Futagawa Fault (~3.3 km east of Mashiki Town) and ending in the east within the NW and SW regions of Aso Caldera. **Figure 2.4** shows the surface-rupture locations visited by the team in the field.

### 2.5.1 *Right-lateral strike-slip surface ruptures*

At site 1 (32.7945ºN, 130.8306ºE; see **Figure 2.4**), a right-lateral strike-slip surface rupture was preserved along a ~400 m long segment of the main fault ~3.3 km east of Mashiki Town. The rupture tracked ENE-WSW across dry rice paddy fields, displacing a series of NE-SW oriented crop rows and field borders (**Figure 2.5**). In combination, these features form a perfect grid in order to quantitatively measure the sense and amount of earthquake surface deformation at this site.

Along this section of the rupture, the team carried out an aerial photography survey, using a DJI Phantom 2 unmanned aerial vehicle (UAV). The digital photos collected from the survey were used to generate an orthorectified photomosaic of this section of the rupture, in addition to a high-density point cloud of elevation data and digital elevation model (DEM). These data were derived from post-processing of the digital photos using the technique *structure from motion* (SfM) implemented in computer software. For further details of the SfM technique and data processing in relation to fault-rupture mapping, see Johnson et al. (2014).

**Figure 2.6** and **Figure 2.7** present the shaded relief DEM of the rupture section. The high-resolution DEM reveals the complexity of the surface rupture and enables quantitative measurements of the offsets to be made. Some preliminary measurements using this dataset are shown in **Figure 2.7**. Each consecutive rice paddy border X to Z has been right-laterally offset by an average of ~1 m where they cross the fault (**Figure 2.7**). The measurements of slip along this section of the surface rupture (in the field and from the DEM) are consistent with those estimated by Lin et al. (2016) at approximately the same location (site 3 in **Figure 2.3**).

**Figure 2.8a** shows a field view of one of the right-laterally offset rice paddy fields. The earthquake surface slip in this field, at the time of the mission, had been exceptionally recorded and preserved. Examples of this type of exposure and preservation are limited, yet they are crucial in order to enable comparisons between the amount of slip measured from geodetic methods, such as InSAR and GPS. **Figure 2.8b**, which shows a farmer ploughing the far northwest fields where the surface rupture is preserved, however, illustrates the transient nature of these exceptional features and highlights the importance of near-immediate post-earthquake field missions in order to make these types of measurements.


**Figure 2.5** (a) Google Earth imagery showing rice paddy fields before the mainshock and (b) aerial photo orthomosaic from the UAV survey after the earthquake showing the strike-slip surface rupture.

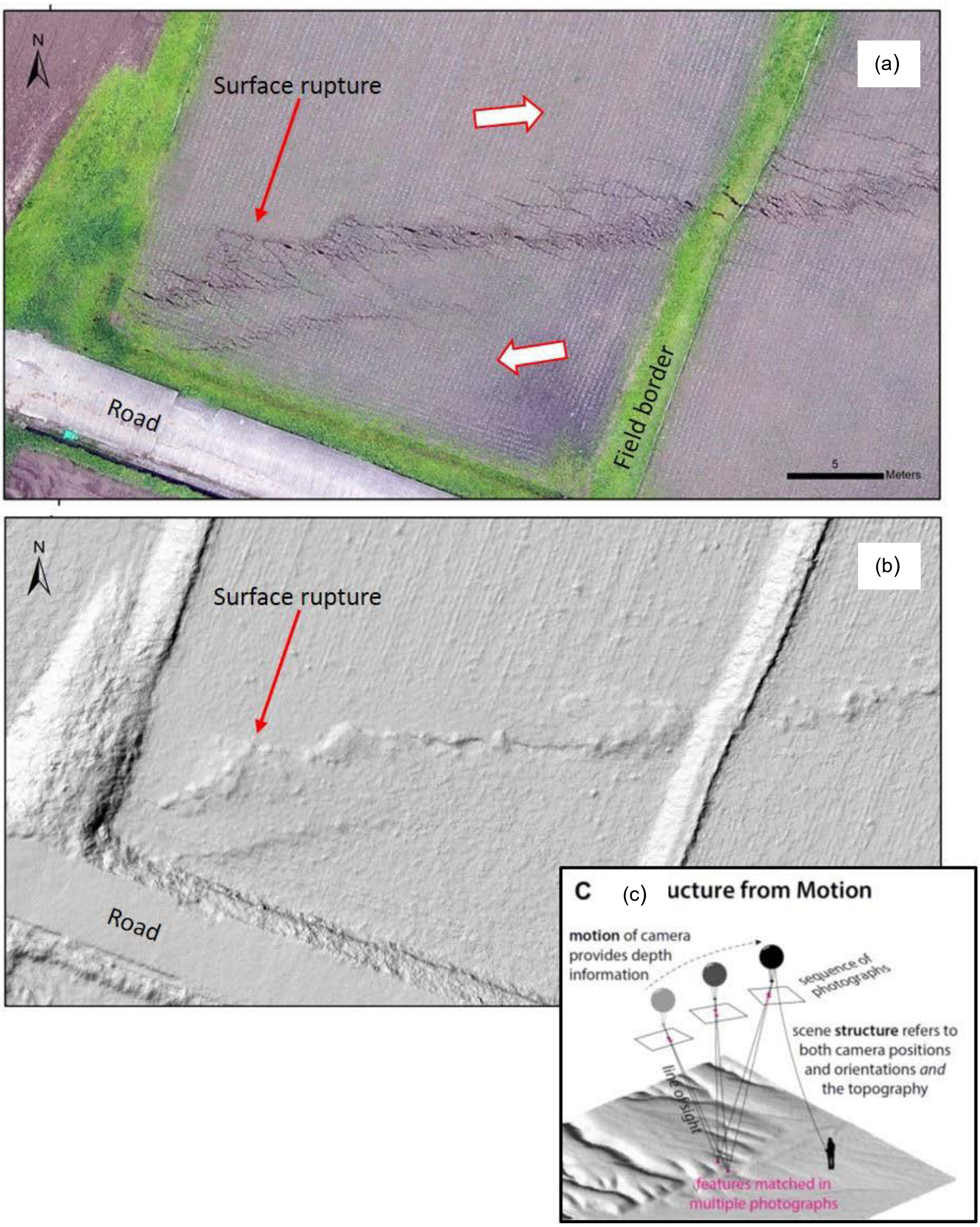


**Figure 2.6** (a) Aerial survey image of a section of the strike-slip rupture in rice paddy fields and (b) corresponding shaded relief map (3 cm grid spacing) of the DEM derived from SfM for the same area. The insert (c) shows the concept and method of SfM (Johnson et al., 2014). The approximate areas of (a) and (b) are outlined in **Figure 2.5**.

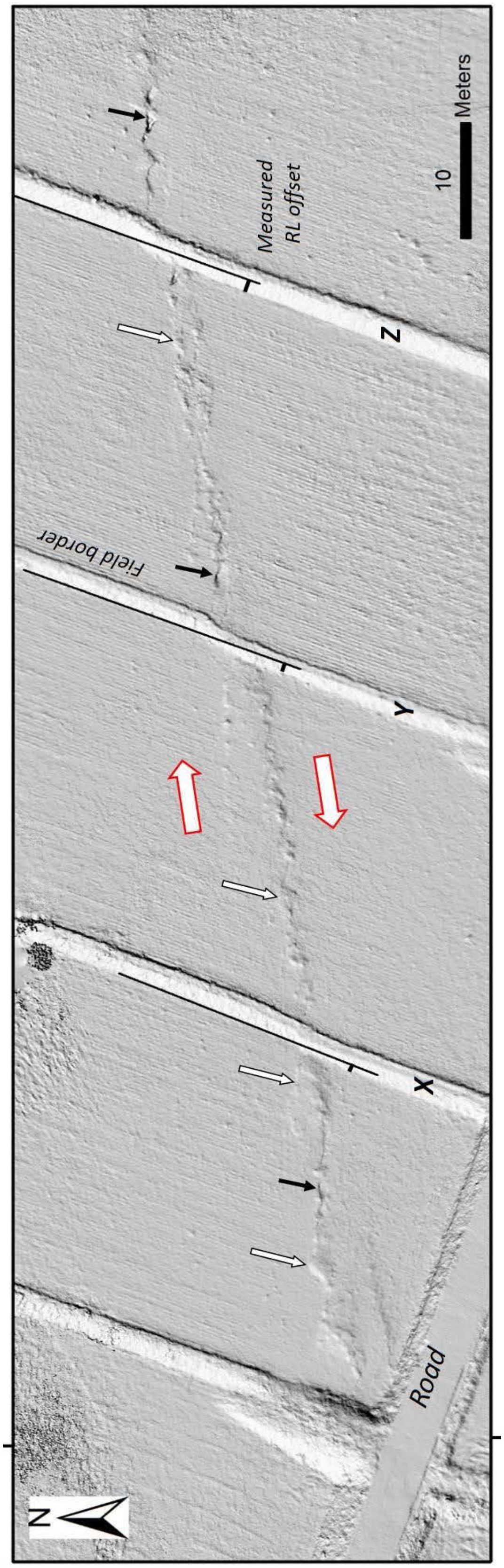


**Figure 2.7** Shaded relief DEM of the area shown in **Figure 2.5**. White and black arrows point to generally 'pushed-up' and 'dropped-down' sections, respectively.

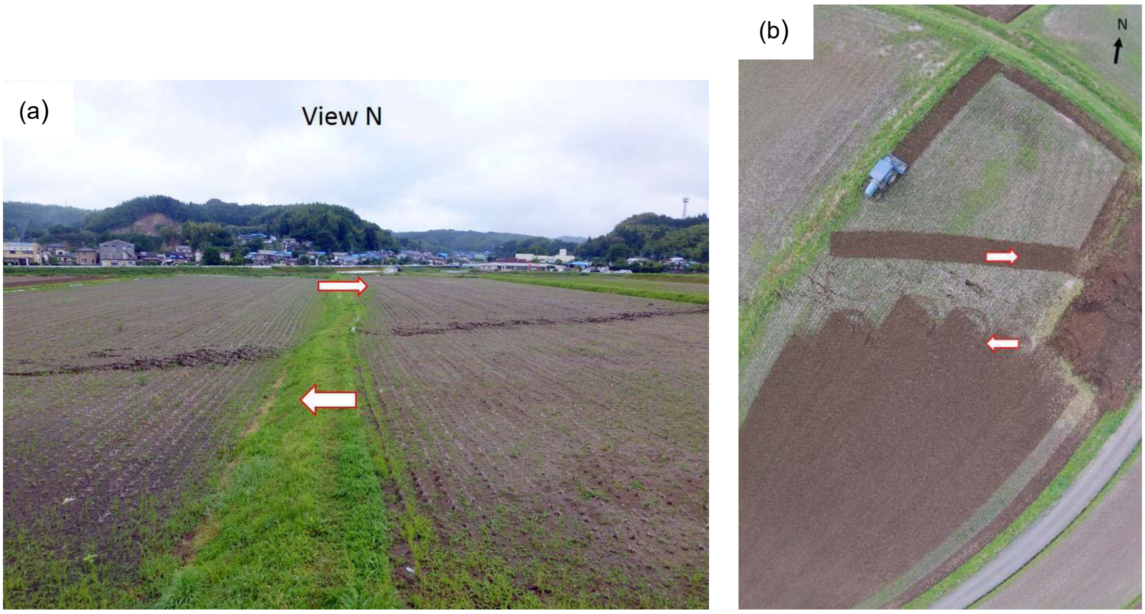


**Figure 2.8** (a) Right-lateral offset in rice paddy field and (b) rupture and fresh ploughing (see **Figure 2.5** for the photo locations).

### 2.5.2 *Normal surface ruptures*

At site 2 (32.8219ºN, 130.8847ºE; see **Figure 2.4**) surface ruptures extended through the south side of a farmer's property (**Figure 2.9**). The ruptures were oriented ENE-WSW and recorded a normal sense of motion. The team measured an average of ~1 m and ~0.5 m (north-side-down) vertical offset, in the garden south of the farm house, and in the field west of the farm house, respectively. These measurements of slip are consistent with those made by other field teams along the main fault trace.

At sites 3 and 4 (32.9563ºN, 131.0364ºE and 32.8362ºN, 131.0202ºE, respectively; see **Figure 2.4**) in the north and southwest of Aso Caldera, respectively, left-stepping en-echelon surface ruptures that are essentially parallel to the strike of the main fault strike were observed (**Figure 2.10** and **Figure 2.11**). This rupture geometry and sense of offset are consistent with predominant right-lateral strike-slip and N-S extension (as indicated from the post-earthquake surface deformation maps derived from InSAR data). The vertical slip measured at this location ranged from around 0.3 m to 2 m, depending on the local topography and near-surface site conditions.

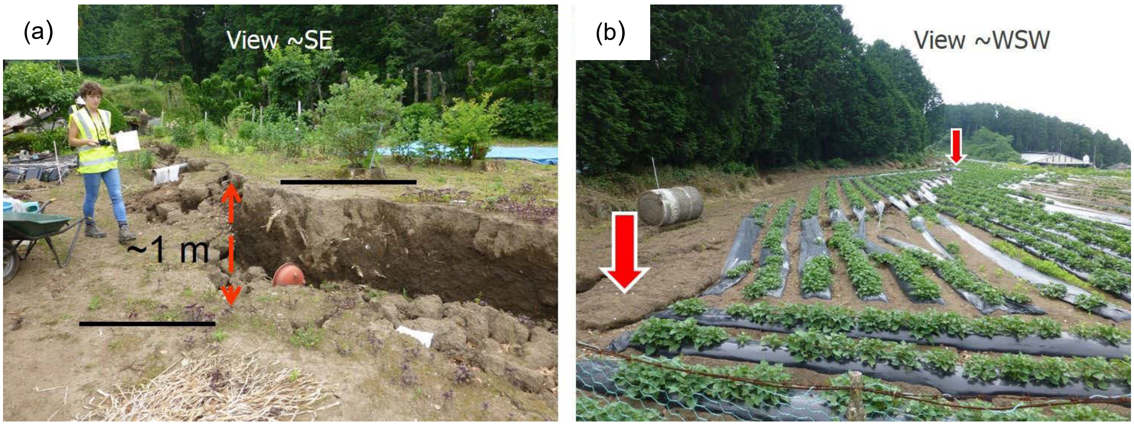


**Figure 2.9** (a) Around 1 m north-side-down vertical offset west of the farm house and (b) normal faulting rupture continuing through the farmer's field, with 0.5 m to 1 m vertical offsets measured.

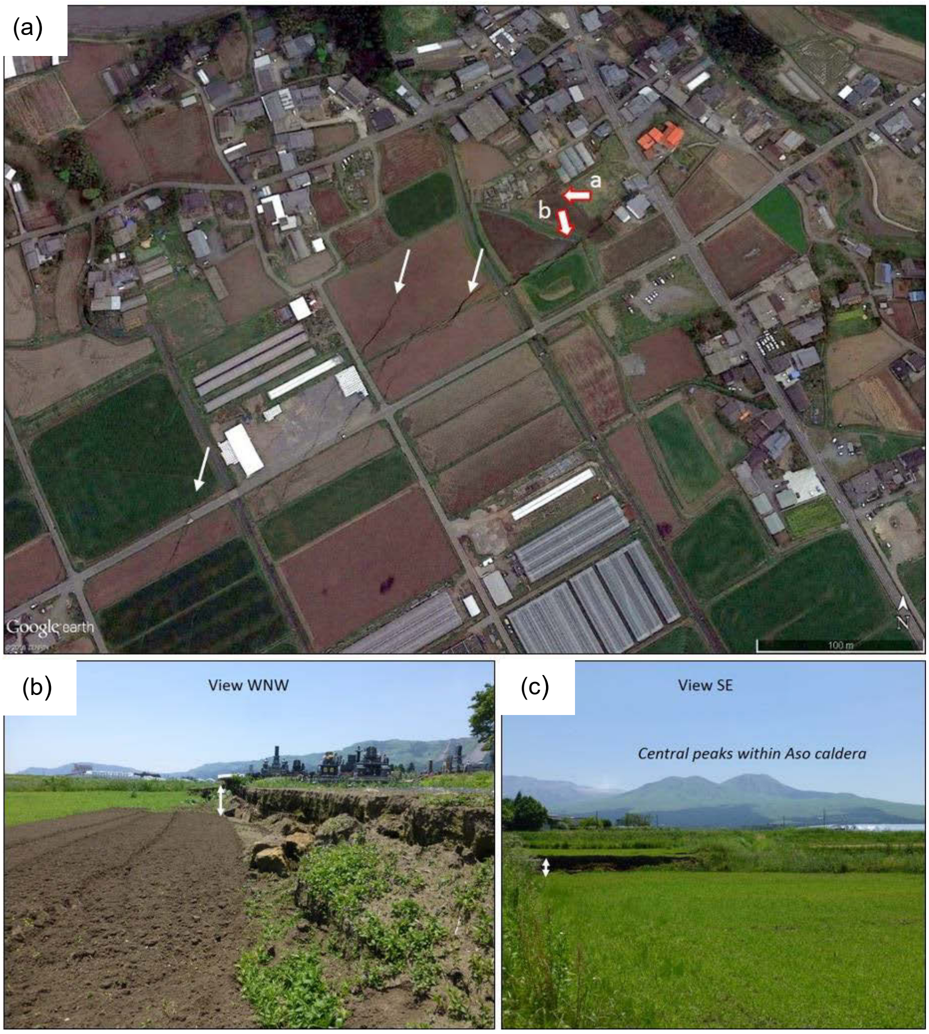


**Figure 2.10** (a) Google Earth imagery showing en-echelon extensional surface ruptures in the north of Aso Caldera (site 3 in **Figure 2.4**). (b) and (c) field photos of the vertical offsets (~1-2 m) at the locations shown in (a).

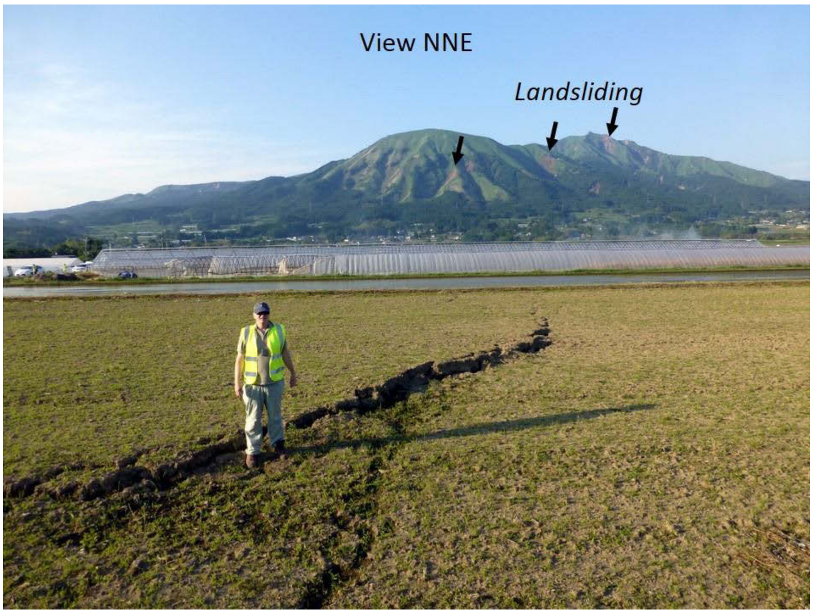


**Figure 2.11** Extensional normal surface ruptures in the southwest of Aso Caldera (site 4 in **Figure 2.4**).

### 2.5.3 *Other activated faults*

In addition to the surface ruptures observed along the main Futagawa Fault, several hundred other previously unmapped secondary faults (not directly connected with the main fault) were activated in association with either the mainshock or strong aftershocks (Fujiwara et al., 2016; **Figure 2.12**). This widespread minor faulting has been mapped using satellite InSAR data. In particular, many linear surface ruptures have been mapped in the northwest of the outer rim of Aso Caldera indicating that the caldera structure was strongly influenced by minor surface rupturing, with a normal component. These new features have been identified in the Central Kyushu region from line of sight surface deformation maps derived using methods in InSAR as shown in **Figure 2.12**. According to Fujiwara et al. (2016), many of these features are consistent with the field mapping (Shimahara et al., 2016).

### 2.5.4 *Fault rupture-caldera interaction*

As noted in the previous sections, the mainshock rupture continued ~10 km northeast into and terminated within Aso Caldera. This new section of the fault trace had not been mapped previously. Since fault length (and depth) and earthquake-magnitude potential typically scale with one another (the longer and deeper the fault, the greater the earthquake magnitude; Wells and Coppersmith, 1994), this new fault section provides important information to inform future seismic hazard assessments.

There are two other significant aspects of the fault-caldera interaction worth mentioning. The first is that new volcanic and geothermal activities were documented at several sites in the Aso region immediately after the Kumamoto earthquakes, strongly suggesting that there was a direct link between faulting and volcanic activity, a phenomena that is not yet well understood. The second is that, the rupture termination within the caldera, and the lack of aftershocks observed in this region, have both been linked with the presence of a shallow (~5 km depth) magma chamber beneath Aso (e.g. Lin et al., 2016; Uchide et al., 2016; Yagi et al., 2016). Both of these observations also have important implications for future seismic and volcanic hazard assessments in Kyushu.

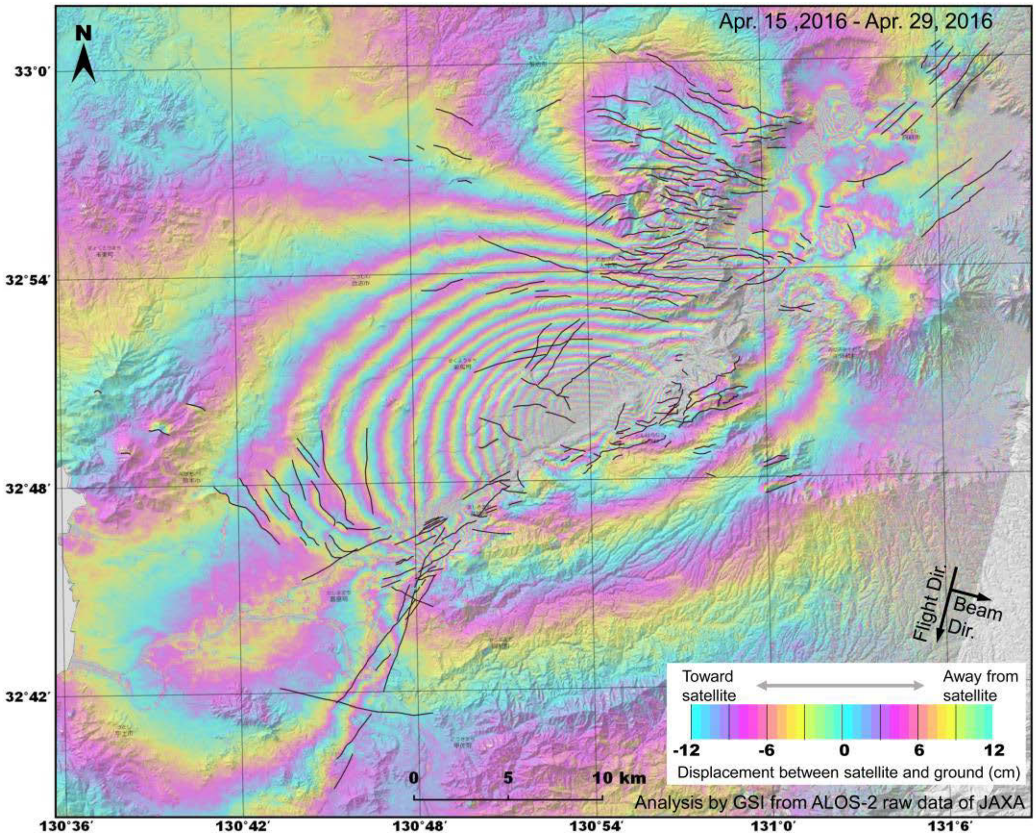


**Figure 2.12** InSAR image of the 2016 Kumamoto earthquakes with identified linear surface ruptures (Fujiwara et al., 2016).

## 2.6 Geological setting

There are two dominant types of geology in Central Kyushu Island: Neogene-Quaternary (~22 million years old to present day) volcanics and sediments in the north, and Mesozoic age (240-65 million years old) subduction-related (accretionary) sediments in the south (**Figure 2.13**). These two distinct geological regions form a boundary along the ENE-WSW Quaternary Median Tectonic Line (**Figure 2.13**).

The near-surface geology influences the strong ground motions generated in earthquakes. Kumamoto City and Mashiki Town, which both suffered structural damage, are located north of the Kumamoto alluvial plain (**Figure 2.13**). The Kumamoto plain is a Holocene (less than 12,000 years before present) alluvial plain comprised of marine and non-marine sediments. The northern half of Kumamoto City and Mashiki Town are located north of the plain on older Pleistocene (2.58 million years old to ~12,000 years before present) fluvial terraces and on a pyroclastic flow. The Futagawa Fault cuts the lava plateau and continues along the boundary between the Kumamoto plain and Cretaceous (145 to 66 million years old) rocks. The Hinagu Fault in the south juxtaposes the alluvial plain with the bedrock and continues north through bedrock to merge with the Futagawa Fault. In summary, it is estimated that 450-900 m of sediments have accumulated over a million years under the Kumamoto plain including the regions immediately north of the Hinagu and Futagawa Faults (Okumura, 2016). It is the sediment thickness in these areas that probably caused the strong ground motion amplifications of the foreshock and mainshock at Kumamoto City and, in particular, measured at the seismic recording stations in Mashiki Town (see Section 3).

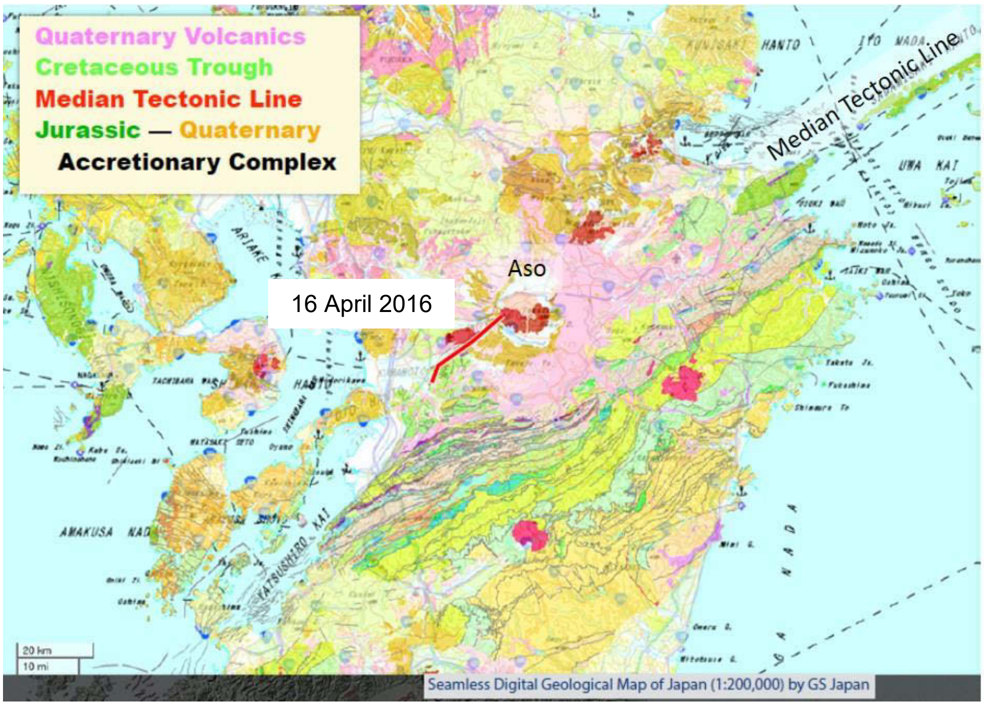


**Figure 2.13** Geological map of Central Kyushu Island. Red line indicates the approximate trace of the 16 April mainshock rupture along the Futagawa Fault (Seamless Geological Map of Japan, 2016).

## 2.7 Conclusions for the geology and tectonics

The main results from the geological and tectonic observations of the Kumamoto earthquakes are as follows:

1. The dominant tectonic forces across Central Kyushu Island are N-S extension and right-lateral shear. These forces are driven by the SE to NW subduction of the Philippines Sea Plate beneath the stable Eurasia Plate along the Nankai Trough.
2. Both the Hinagu and Futagawa Faults were known by geologists and seismologists and the faults were already (well-characterised and) included in the national seismic hazard assessments.

3. The peak ground shaking intensity and spatial distribution of shaking estimated by the national seismic hazard model, considering a large-magnitude earthquake scenario on the Futagawa Fault, has matched well the $M_w$7.1 Kumamoto mainshock event.
4. The mainshock earthquake resulted in extensive normal and right-lateral strike-slip surface ruptures along the length of the ENE-WSW Futagawa Fault. **Figure 2.14** shows a sketch of how the normal and strike-slip surface ruptures may be related to one another at depth along the main Futagawa Fault (Toda et al., 2016).
5. The previously unmapped NW section of the Futagawa Fault in Aso Caldera has implications for future seismic hazard assessments.
6. The Kumamoto mainshock is a relatively less frequent example of damaging plate-interior (non-subduction) shallow crustal earthquakes in Japan, which is useful for understanding crustal rheology and rupture dynamics in the region.
7. The mainshock has raised various questions regarding fault-caldera interaction. New volcanic activity was triggered by the earthquake. It has also been hypothesised that a shallow (5 km deep) magma chamber beneath Aso Caldera played a role in rupture termination, and resulted in the absence of aftershocks.
8. The geology of the near-fault source region is complex. The large ground accelerations recorded at Kumamoto City and Mashiki Town during the foreshock and mainshock (up to and greater than 1 *g*) are likely to have resulted from wave amplification in thick alluvial deposits that exist immediately north of the Futagawa Fault (see Section 3).

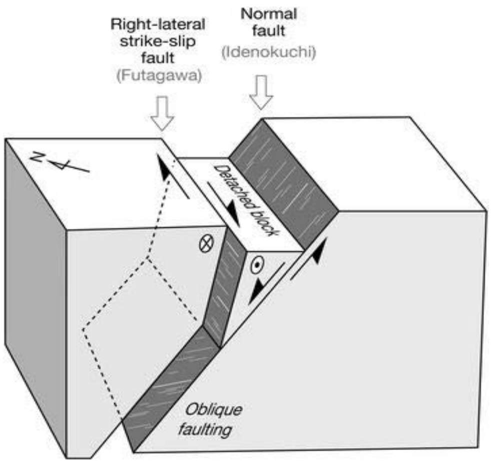


**Figure 2.14** Schematic illustration of slip partitioning from depth to the surface that occurred during the 2016 Kumamoto earthquake (Toda et al., 2016).

## 2.8 References

Asano, K., and Iwata, T. (2016). Source rupture processes of the foreshock and mainshock in the 2016 Kumamoto earthquake sequence estimated from the kinematic waveform inversion of strong motion data. *Earth Planets and Space*, **68**, 147, doi: 10.1186/s40623-016-0519-9.

Chida, N. (1979). Late Quaternary tectonic movements in central Kyushu district, southwest Japan, with special reference to the active faults distributed in the Quaternary volcanic area. *Annual Report Faculty of Education, Iwate University*, **39**, 37-75.

Fujiwara, S., Yarai, H., Kobayashi, T., Morishita, Y., Nakano, T., Miyahara, B., Nakai, H., Miura, Y., Ueshiba, H., Kakiage, Y., and Une, H. (2016). Small-displacement linear surface ruptures of the 2016 Kumamoto earthquake sequence detected by ALOS-2 SAR interferometry. *Earth Planets and Space*, **68**, 160, doi: 10.1186/s40623-016-0534-x.

Headquarters for Earthquake Research Promotion (2016). Evaluation of the Futagawa and Hinagu fault zones. Accessed on 15 May 2016 at http://www.jishin.go.jp/main/chousa/13feb_chi_kyushu/k_11.pdf.

Inoue, K. (2000). Shimabara-Shigatusaku earthquake and topographic changes by Shimabara Catastrophe in 1792. *Journal of the Japan Society of Erosion Control Engineering*, **52**, 45–54.

Johnson, K., Nissen, E., Saripalli, S., Arrowsmith, J.R., McGarey, P., Scharer, K., Williams, P., and Blisniuk, K. (2014). Rapid mapping of ultrafine fault zone topography with structure from motion. *Geosphere*, **10**, 969–986.

Kanamori, H. (1995). The Kobe (Hyogo-ken Nanbu), Japan, earthquake of January 16, 1995. *Seismological Research Letters*, **66**, 6–10.

Kubo, H., Suzuki, W., Aoi, S., and Sekiguchi, H. (2016). Source rupture processes of the 2016 Kumamoto, Japan, earthquakes estimated from strong-motion waveforms. *Earth Planets and Space*, **68**, 161, doi: 10.1186/s40623-016-0536-8.

Kumahara, Y., Goto, H., Nakata, T., Ishiguro, S., Ishimura, D., Ishiyama, T., Okada, S., Kagohara, K., Kashihara, S., Kaneda, H., Sugito, N., Suzuki, Y., Takenami, D., Tanaka, K., Tanaka, T., Tsutsumi, H., Toda, S., Hirouchi, D., Matsuta, N., Mita, T., Moriki, H., Yoshida, H., Watanabe, M. (2016). Distribution of surface rupture associated the 2016 Kumamoto earthquake and its significance. *Japan Geoscience Union Meeting*, Makuhari, Chiba, MIS34-05.

Lin, A., Satsukawa, T., Wang, M., Asl, Z.M., Fueta, R., and Nakajima, F. (2016). Coseismic rupturing stopped by Aso volcano during the 2016 $M_w$7.1 Kumamoto earthquake, Japan. *Science*, **354**, 6314, 869–874.

Moreno, T., Wallis, S.R., Kojima, T., Gibbons W. (2016). The Geology of Japan. *Geological Society of London*, London, United Kingdom, 536 p.

Okumura, K. (2016). Accessed on 1 December 2016 at http://home.hiroshima-u.ac.jp/kojiok/kumamoto2016KOreport2.pdf.

Research Group for Active Faults in Japan (1980). Active faults in Japan, sheet maps and inventories. *University of Tokyo Press*, Tokyo, Japan, 363 p. (in Japanese with English Abstract).

Research Group for Active Faults in Japan (1991). Active faults in Japan, sheet maps and inventories, revised edition. *University of Tokyo Press*, Tokyo, Japan, 437 p. (in Japanese with English Abstract).

Seamless Geological Map of Japan (2016). Accessed on 1 December 2016 at https://gbank.gsj.jp/seamless/seamless2015/2d/index.html?lang=en.

Shimokawa, K., Kinugasa, Y., and Tanaka, T. (1999). Paleoseismology and activity study of the Hinagu Fault system, southwest Japan. In *Program of Workshop on Paleoseismology,* Tsukuba, Japan, 59 p.

Shirahama, Y., Yoshimi, M., Awata, Y., Maruyama, T., Azuma, T., Miyashita, Y., Mori, H., Imanishi, K., Takeda, N., Ochi, T., Otsubo, M., Asahina, D., and Miyakawa, A. (2016). Characteristics of the surface ruptures associated with the 2016 Kumamoto earthquake sequence, central Kyushu, Japan. *Earth Planets and Space*, **68**, 191, doi: 10.1186/s40623-016-0559-1.

Toda, S., Kaneda, H., Okada, S., Ishimura, D., and Mildon, Z.K. (2016). Slip-partitioned surface ruptures for the $M_w$7.0 16 April 2016 Kumamoto, Japan, earthquake. *Earth Planets and Space*, **68**, 188, doi: 10.1186/s40623-016-0560-8.

Uchide, T., Horikawa, H., Nakai, M., Matsushita, R., Shigematsu, N., Ando, R., and Imanishi, K. (2016). The 2016 Kumamoto–Oita earthquake sequence: aftershock seismicity gap and dynamic triggering in volcanic areas. *Earth Planets and Space*, **68**, 180, doi: 10.1186/s40623-016-0556-4.

United States Geological Survey (2016). Accessed on 15 May 2016 at https://earthquake.usgs.gov/archive/product/poster/20160415/us/1462205824007/poster.jpg.

Yagi, Y., Okuwaki, R., Enescu, B., Kasahara, A., Miyakawa, A., and Otsubo, M. (2016). Rupture process of the 2016 Kumamoto earthquake in relation to the thermal structure around Aso volcano. *Earth Planets and Space*, **68**, 118, doi: 10.1186/s40623-016-0492-3.

# 3 Ground Motions

## 3.1 Earthquake sequence

The Futagawa Fault stretches from the outskirt of Aso Caldera to Uto Peninsula (Headquarters for Earthquake Research Promotion, 2016). Its orientation is ENE-WSW. The total length of the fault exceeds 70 km and consists of three segments: Futagawa segment (circa 29 km), Uto segment (circa 20 km), and Uto Peninsula segment (circa 27 km). On the other hand, the Hinagu Fault touches on the Futagawa Fault in the north (near Mashiki Town) and extends to Yatsushiro Sea in the south (NE-SW orientation). The total length exceeds 80 km, consisting of three segments: Takano-Shirahata segment (circa 16 km), Hinagu segment (circa 40 km), and Yatsushiro Sea segment (circa 30 km). Both Futagawa and Takano-Shirahata segments are of right-lateral strike-slip type. Historically, there were damaging earthquakes in the Kumamoto region. For instance, the *M*6.3 1889 earthquake caused notable damage in Kumamoto City (20 deaths, 54 injuries, and 239 house collapses; Headquarters for Earthquake Research Promotion, 2016). However, the damage severity and earthquake impact of the 2016 sequence are far greater. **Figure 3.1a** shows the Futagawa segment and the Hinagu (Takano-Shirahata) segment, based on the active fault database by the National Institute of Advanced Industrial Science and Technology (2015). In **Figure 3.1a**, epicentral locations of the 14 April 2016 foreshock and the 16 April 2016 mainshock (based on the unified JMA catalogue, available from Hi-net at http://www.hinet.bosai.go.jp/) as well as locations of Kumamoto City, Mashiki Town, Nishihara Village, and Minami Aso Village are shown. The thin grey lines represent political boundaries of the municipalities in the Kumamoto region. **Figure 3.1b** shows a digital elevation model of the Kumamoto region based on the GDEM database (http://www.jspacesystems.or.jp/library/archives/ersdac/GDEM/E/index.html).

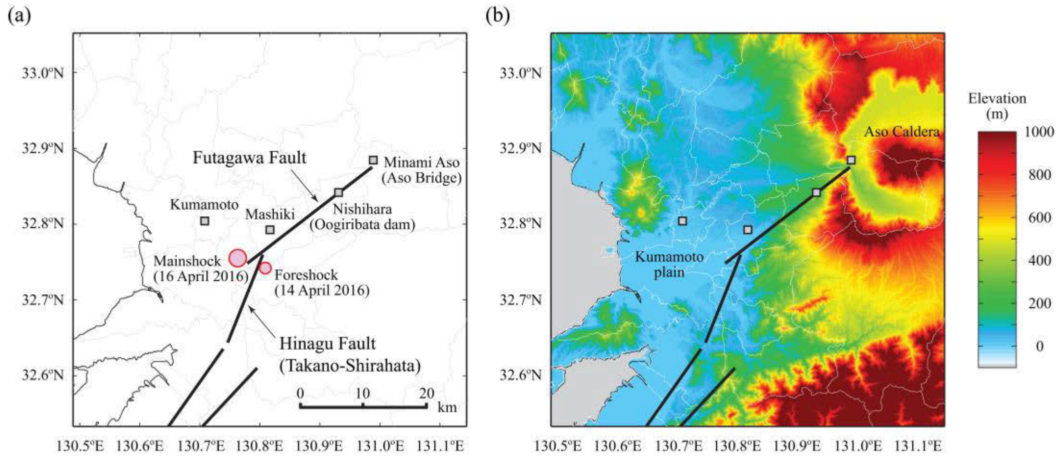


**Figure 3.1** (a) Locations of the Futagawa-Hinagu Faults and (b) digital elevation model for Kumamoto.

The most recent seismic hazard assessments by the Headquarters for Earthquake Research Promotion (2016) have taken into account rupture scenarios from the Futagawa and Hinagu Faults. In the assessments, the scenario magnitude for the Futagawa segment is set to $M_w$7.0 with occurrence probability of less than 1% in 30 years, noting that there is a possibility that all three segments of the Futagawa Fault rupture simultaneously (in this case, the magnitude is estimated to be in the range of $M_w$7.5 to $M_w$7.8). On the other hand, the scenario magnitude for the Hinagu (Takano-Shirahata) segment is considered to be $M_w$6.8 with unknown occurrence probability; similar to the Futagawa Fault, there is a possibility that all three segments of the Hinagu Fault rupture simultaneously, resulting in a $M_w$7.7 to $M_w$8.0 earthquake. Moreover, because of the adjacency of the Futagawa segment and the Takano-Shirahata segment, the earthquake might rupture both faults, potentially leading to a $M_w$7.8 to $M_w$8.2 event. Importantly, during the 2016 Kumamoto earthquake sequence, numerous events occurred initially along the Takano-Shirahata segment (e.g. 14 April foreshock), and then along the Futagawa segment (e.g. 16 April mainshock).

A prolific sequence of earthquakes was observed in the Kumamoto region, after the triggering foreshock event occurred on 14 April 2016. **Figure 3.2** shows the temporal variation of earthquakes having $M_J$ > 3 over a period between 13 April 2016 and 18 April 2016, while **Figure 3.3** shows the spatial distribution of earthquakes occurring in different time periods. The $M_J$6.5 foreshock induced an active sequence of dependent events (including a $M_J$6.4 event on 15 April 2016). From the spatial distribution of the events that occurred between the foreshock and the mainshock (**Figure 3.3d**), the triggered events are clustered along the Hinagu Fault. Subsequently, the mainshock occurred on the southern tip of the Futagawa Fault, and triggered an even more active subsequence of aftershocks (**Figure 3.2** and **Figures 3.3e** and **3.3f**). The aftershock sequence is not only concentrated along the Futagawa-Hinagu Faults but also in the Aso region. The migration of seismic activities over a relatively wide spatial scale is a notable feature of the 2016 Kumamoto earthquake sequence (Kato et al., 2016).

Using the observed earthquake data in the Kumamoto region, statistical analysis of aftershocks is carried out by applying the Gutenberg-Richter law (i.e. frequency-magnitude characteristics of an aftershock sequence) and the modified Omori law (temporal decay of an aftershock occurrence rate; Guo and Ogata, 1997; Shchervakov et al., 2005). It is considered that the JMA catalogue is complete above $M_J$3.5. In fitting these seismological models, the entire catalogue is divided into two parts: events that occurred between the foreshock and the mainshock (72 earthquakes), and events after the mainshock (248 earthquakes). The results are shown in **Figure 3.4**. Due to the longer period and the larger triggering event, the mainshock-aftershock sequence is more prolific than the foreshock-mainshock sequence. The *b*-value of the mainshock-aftershock sequence is steeper and has a value close to a typical *b*-value of 1.0 (Guo and Ogata, 1997). For the modified Omori law, the temporal decay parameter (*p*-value) for both datasets is estimated as 1.0, which is broadly consistent with the past studies of aftershock statistics (Guo and Ogata, 1997).

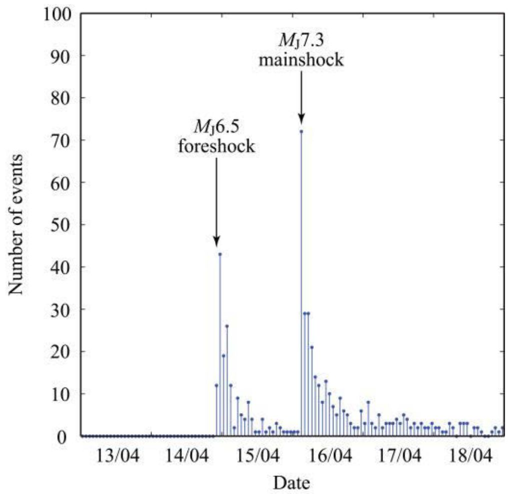


**Figure 3.2** Number of earthquakes with $M_J$ > 3 that occurred in the Kumamoto region during the foreshock-mainshock-aftershock period.

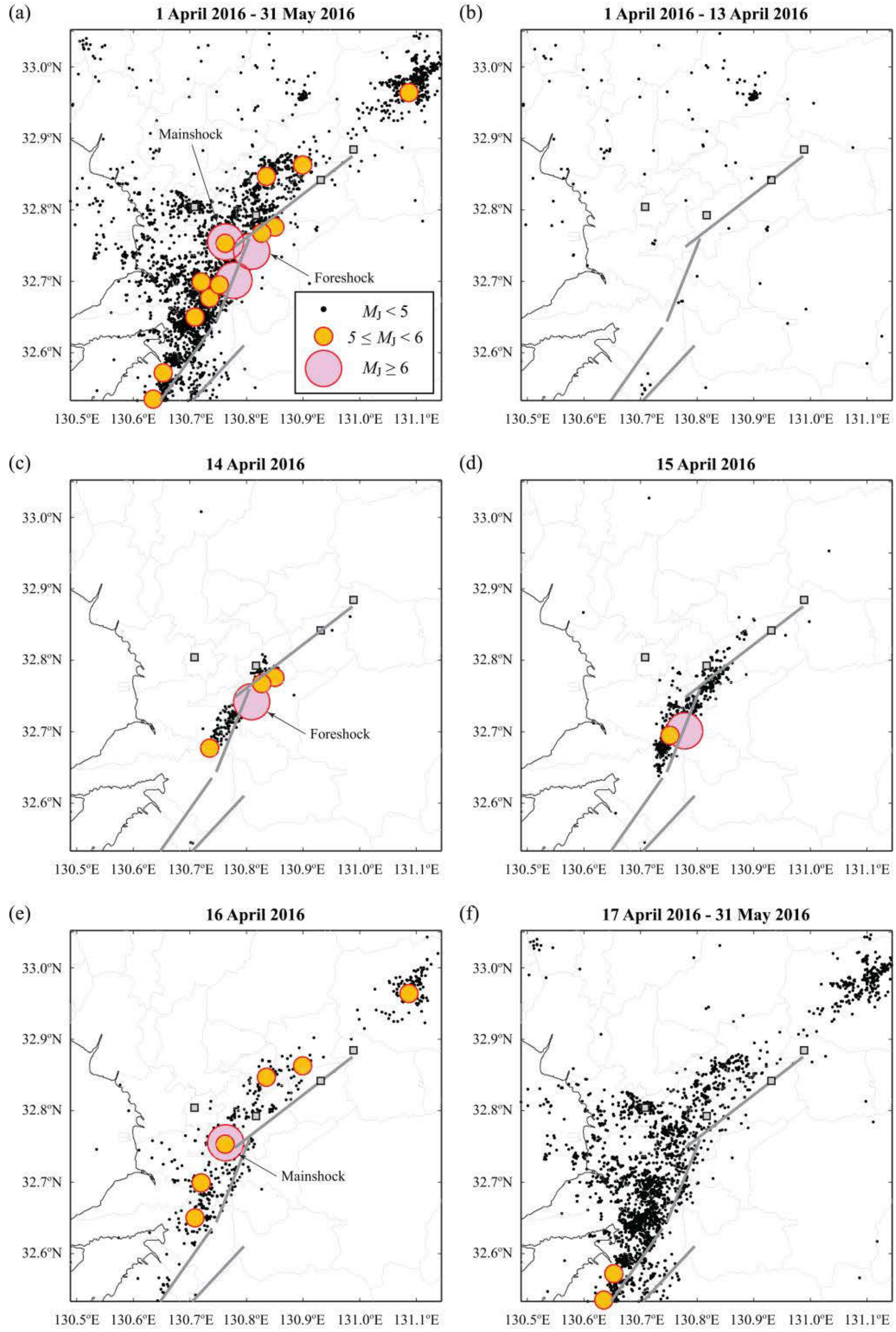


**Figure 3.3** Spatial distribution of earthquakes in the Kumamoto region: (a) 1 April 2016 to 31 May 2016, (b) 1 April 2016 to 13 April 2016, (c) 14 April 2016, (d) 15 April 2016, (e) 16 April 2016, and (f) 17 April 2016 to 31 May 2016.

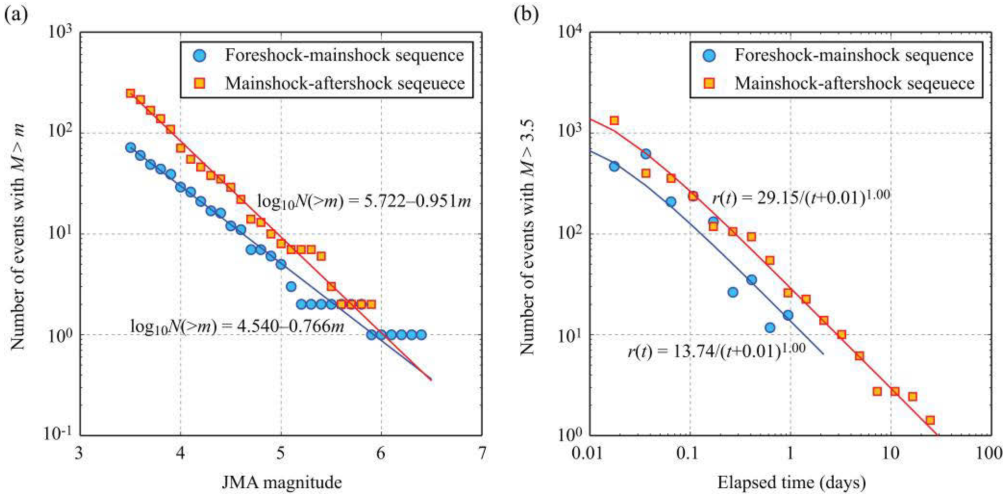


**Figure 3.4** Characteristics of foreshock-mainshock and mainshock-aftershock sequences: (a) Gutenberg-Richter models and (b) modified Omori models.

### 3.2 Finite-fault models and estimated ground deformation

Finite-fault source models, which are obtained through source inversion analysis, provide plausible images of earthquake rupture processes by achieving the consistency between observed data and geophysical model predictions (e.g. geodetic, teleseismic, strong motion, and tsunami). After the Kumamoto foreshock and mainshock, several such models have been developed and some were published in the literature (Asano and Iwata, 2016; Kubo et al., 2016; Yagi et al., 2016). For example, the Geospatial Institute of Japan (GSI) developed finite-fault models for the Kumamoto foreshock and mainshock based on GEONET GPS observations. The finite-fault parameters of the GSI models for the foreshock and mainshock are summarised in **Table 3.1**. The geometry of the finite-fault models for the foreshock and mainshock is shown in **Figure 3.5a**, and is consistent with the fault strike by the National Institute of Advanced Industrial Science and Technology (**Figure 3.1a**). The estimated slip values for the foreshock and mainshock are 0.62 m and 3.50 m, respectively (assumed to be uniform over the fault plane). For the mainshock, at the Kumamoto GEONET station (32.8421ºN, 130.7648ºE), 0.75 m horizontal deformation in the ENE direction and 0.2 m downward deformation were recorded, while at the Choyo GEONET station (32.8707ºN, 130.9962ºE), 0.97 m horizontal deformation in the SW direction and 0.23 m upward deformation were recorded. These observations serve as important constraints in developing finite-fault models for the mainshock, indicating that the fault strike (approximately SW-NE to WSW-ENE) should lie between the Kumamoto and Choyo stations.

Using the geometry and slip distribution of a finite-fault model, elastic deformation due to an earthquake can be calculated using the Okada (1985) equations. The analytical formulae allow the estimation of NS, EW, and UD components of ground surface deformation. The results of the calculated elastic deformation profiles based on the GSI finite-fault models are shown in **Figure 3.6** and **Figure 3.7** for the foreshock and mainshock, respectively. The results display the spatial deformation patterns clearly. The estimated NS, EW, and UD deformations at the Kumamoto station are 0.00 m (northward), 0.85 m (eastward), and -0.30 m (downward), while those at the Choyo station are -0.57 m (southward), -0.50 m (westward), and 0.25 m (upward); see **Table 3.2**. These estimated deformations are in agreement with the observed GPS measurements, which is expected because these data were used in calibrating the finite-fault models. The GSI models are particularly useful for estimating permanent deformation at unmonitored locations due to the earthquake.

As a part of this investigation, another set of finite-fault models for the foreshock and mainshock developed by Asano and Iwata (2016) is implemented. These are referred to as DPRI (Disaster Prevention Research Institute) models. The DPRI models were calibrated based on strong motion observations and can provide finer details of the earthquake slip along the fault plane (e.g. asperities). The models are particularly useful for predicting strong ground motions at unobserved locations. The DPRI model for the mainshock is shown in **Figure 3.5b** (note: the counterpart for the foreshock is not shown intentionally because the fault dip angle is steep (89º); i.e. it is essentially shown as a line).

The estimated elastic deformation profiles based on the DPRI models are shown in **Figure 3.8** and **Figure 3.9** for the foreshock and mainshock, respectively. In comparison with the GSI's mainshock model, the dimensions of the DPRI mainshock model are larger (and spread over both Futagawa and Hinagu Faults) and consequently, overall its mean slip (about 1.87 m) and the estimated deformations are smaller. The predicted NS, EW, and UD deformations at the Kumamoto station are 0.39 m (northward), 0.19 m (eastward), and -0.19 m (downward), while those at the Choyo station are -0.12 m (southward), -0.02 m (westward), and 0.04 m (upward); see **Table 3.2**. Therefore, the DPRI model may underestimate the deformations near the eastern end of the fault plane (nevertheless, the DPRI model is expected to predict high-frequency ground motions well).

**Table 3.1** Finite-fault parameters of the GSI (2016) models for the foreshock and mainshock.

| | Upper-left corner | | | Length (km) | Width (km) | Strike (º) | Dip (º) | Rake (º) | Slip (m) | $M_w$ |
|---|---|---|---|---|---|---|---|---|---|---|
| | Latitude (º) | Longitude (º) | Depth (km) | | | | | | | |
| Foreshock | 32.77 | 130.830 | 0.547 | 17.8 | 10.0 | 210 | 78 | 167 | 0.62 | 6.32 |
| Mainshock | 32.90 | 131.017 | 0.1 | 27.1 | 12.3 | 235 | 60 | -161 | 3.5 | 7.0 |

**Table 3.2** Comparison of the observed and estimated deformations at the Kumamoto and Choyo GPS stations for the mainshock.

| GPS station | Observation | | GSI model | | | DPRI model | | |
|---|---|---|---|---|---|---|---|---|
| | Horizontal (m) | Vertical (m) | NS (m) | EW (m) | UD (m) | NS (m) | EW (m) | UD (m) |
| Kumamoto | 0.75[(1)] | -0.20 | 0.0 | 0.85 | -0.30 | 0.39 | 0.19 | -0.19 |
| Choyo | 0.97[(2)] | 0.23 | -0.57 | -0.50 | 0.25 | -0.12 | -0.02 | 0.04 |

*[(1)] Approximately ENE direction; [(2)] Approximately SW direction.*

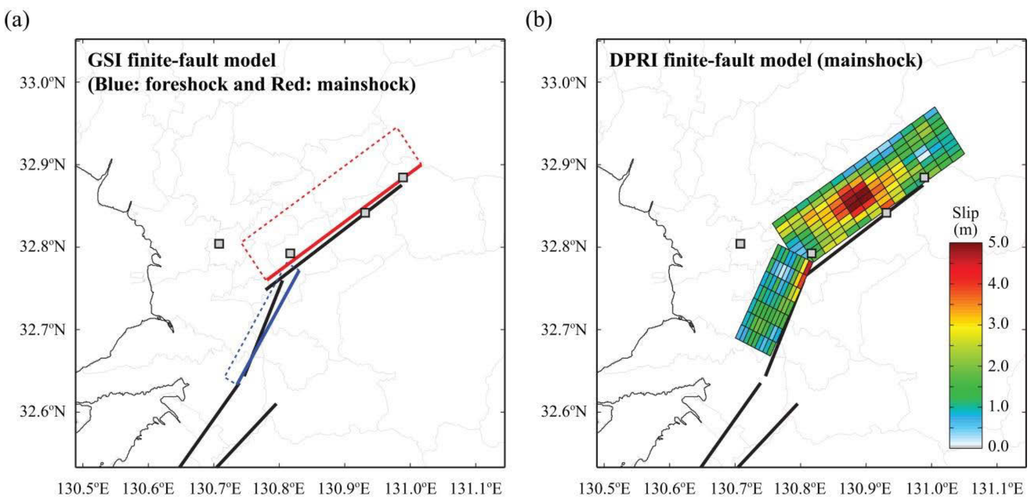


**Figure 3.5** (a) Finite-fault models by GSI (2016) for the foreshock and mainshock and (b) finite-fault model by Asano and Iwata (2016) for the mainshock.

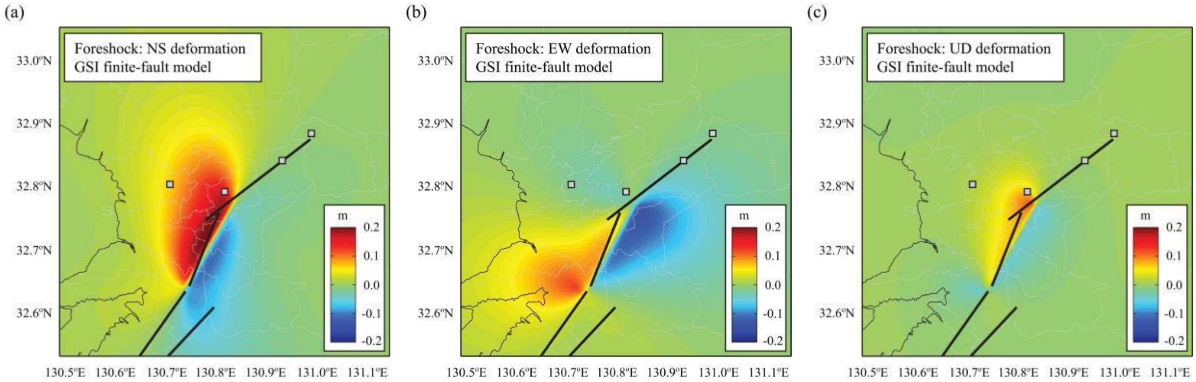


**Figure 3.6** Estimated elastic deformation profiles based on the GSI finite-fault model for the foreshock: (a) NS deformation, (b) EW deformation, and (c) UD deformation.

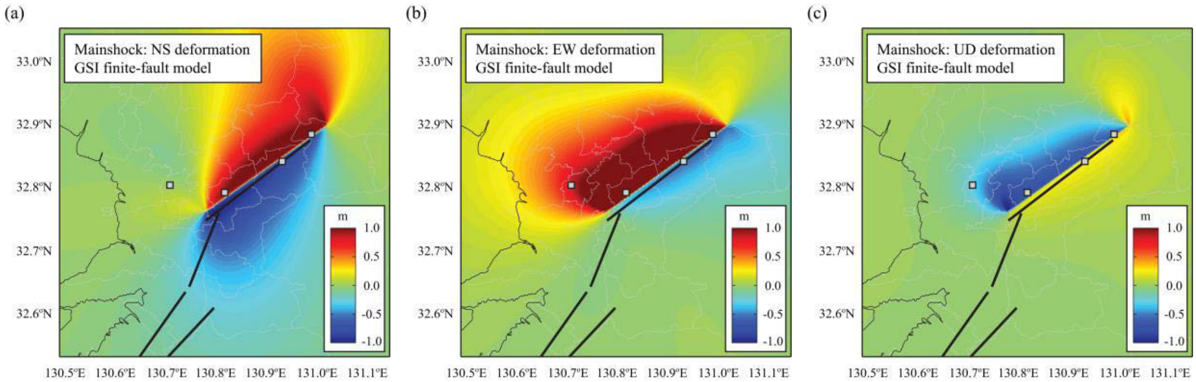


**Figure 3.7** Estimated elastic deformation profiles based on the GSI finite-fault model for the mainshock: (a) NS deformation, (b) EW deformation, and (c) UD deformation.

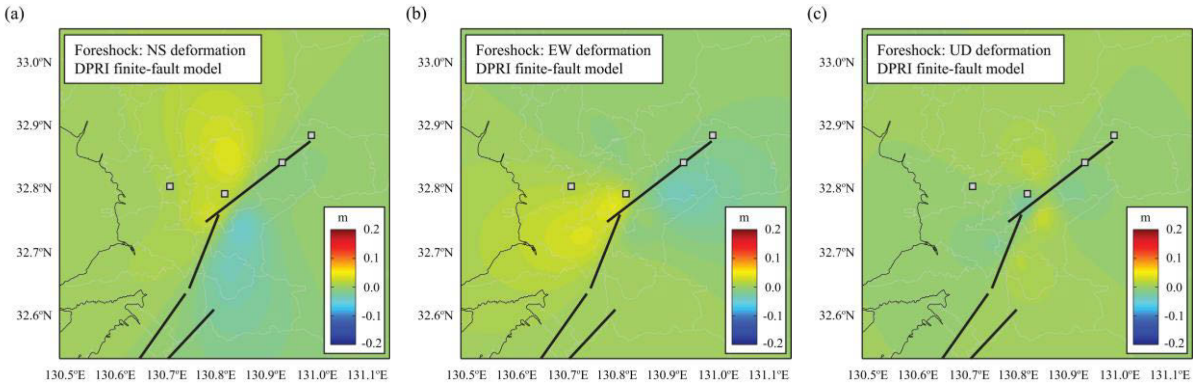


**Figure 3.8** Estimated elastic deformation profiles based on the DPRI finite-fault model for the foreshock: (a) NS deformation, (b) EW deformation, and (c) UD deformation.

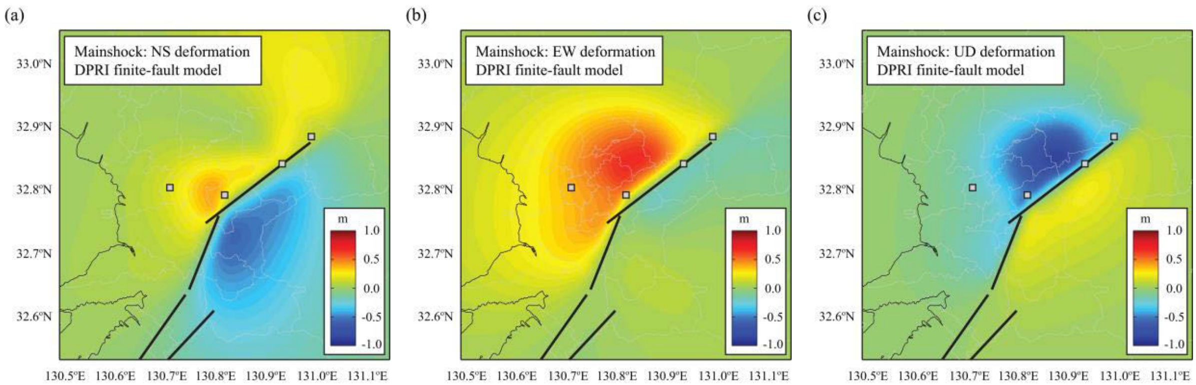


**Figure 3.9** Estimated elastic deformation profiles based on the DPRI finite-fault model for the mainshock: (a) NS deformation, (b) EW deformation, and (c) UD deformation.

### 3.3 Strong ground motion characteristics

In Japan, national strong motion networks, K-NET and KiK-net (http://www.kyoshin.bosai.go.jp/), were established in the aftermath of the 1995 Kobe earthquake, and currently more than 1700 stations are operational. For the 2016 Kumamoto earthquakes, an extensive set of ground motion data is available. In this section, characteristics of observed strong ground motions in the Kumamoto region are investigated. The following aspects are discussed in this section: (i) strong motion characteristics in the near-fault region, (ii) regional ground motion characteristics and directivity of the recorded ground motions with respect to the fault geometry/orientation, and (iii) comparison of observed ground motion recordings with an existing prediction equation.

For these purposes, all available ground motion data for 20 seismic events that occurred in April 2016 ($M_J \geq 4.3$) are downloaded from the K-NET/KiK-net (in total, 6177 records, including borehole recording data for the KiK-net; each record has 3 components), and are processed uniformly to compute acceleration/velocity waveforms as well as various ground motion parameters (peak ground acceleration, PGA, and 5%-damped spectral acceleration, SA). For the record processing, a standard procedure (e.g. tapering, zero-padding, and band-pass filtering) suggested by Boore (2005) is implemented.

#### 3.3.1 *Strong motion characteristics in the near-fault region*

In this section, recorded ground motion data at three stations, i.e. KMMH16 (Mashiki; 32.7967ºN, 130.8199ºE), KMM006 (Kumamoto; 32.7934ºN, 130.7772ºE), and KMM008 (Uto; 32.6878ºN, 130.6582ºE), are analysed in detail; the locations of these stations are shown in **Figure 3.21**. These near-fault locations are selected because the earthquake damage surveys were carried out during the EEFIT mission (Goda et al., 2016; see Section 4). The KMMH16 station is from the KiK-net and thus two sets of three component recordings at ground surface and in borehole are available. Another particularly important aspect of the selected records is that KMMH16 and KMM006 are in the hanging wall region of the mainshock (i.e. within a projected fault plane on the ground surface), and thus very intense ground shaking was observed during the mainshock. Moreover, at KMMH16, strong shaking due to the foreshock preceded the mainshock, resulting in double-shock ground motions.

**Figure 3.10** shows a borehole log and shear wave velocity profile at the KMMH16 station (in Mashiki Town). Relatively soft soil layers exist in the top 15 m (shear wave velocity less than 250 m/s), underlain by firm rock layers. The borehole recording is installed at a depth of 255 m (ground surface is at 55 m altitude). Therefore, major site amplification is anticipated between ground surface and borehole at this site because of high contrast of the shear wave velocities. The average shear wave velocity in the top 30 m of the soil is calculated as 280 m/s (i.e. NEHRP site class D).

**Figure 3.11** shows observed acceleration as well as velocity time-histories (3 components) at KMMH16 for the foreshock and mainshock. The blue curves are for the ground surface recordings, whereas the red curves are for the borehole recordings. The significant amplification of the ground motions can be visually inspected by comparing the blue and red curves. Another notable observation is that for the velocity time-histories for the mainshock (i.e. **Figure 3.11d**), relatively large long-period velocity waves are present at both ground surface and borehole (particularly for vertical motions). This indicates that site amplification for short-period components is significantly influenced by near-surface soil characteristics, while that for long-period components is more coherent at ground surface and borehole. The latter may also be attributed to the ground surface rupture near the Mashiki areas (see Section 2).

To examine the spectral content of the observed ground motions at KMMH16, 5%-damped response spectra for the foreshock and mainshock are calculated and shown in **Figure 3.12**. The results for the ground surface motions are presented with solid lines, while those for the borehole motions are shown with broken lines. The comparison of the response spectra indicates: (i) amplitudes of the response spectra are large, exceeding 1 *g* up to a period of about 1 s for the foreshock and about 2 s for the mainshock; (ii) generally site amplification is significant for all three components; (iii) horizontal motions are amplified in a period range between 0 s (i.e. PGA) and about 2 to 3 s, while vertical motions are significantly amplified at vibration periods less than 0.5 s.

To investigate the site amplification at KMMH16 in detail, the borehole-to-surface ratios of Fourier amplitude spectra are computed (Ghofrani et al., 2013), and are shown in **Figure 3.13**. The results indicate that the site amplification is period-dependent; the horizontal ground motions are amplified significantly (by a factor of 5 or more) in the period range between 0.3 s and 2 s, while the vertical ground motions are mainly amplified in the periods less than 0.5 s. To further examine the site amplification observed at KMMH16, borehole-to-surface spectral ratios are evaluated for all 20 earthquakes that are analysed as part of this investigation, and the results are shown in **Figure 3.14**. In the figure, the borehole-to-surface spectral ratio curves for NS, EW, and UD are shown in separate figures, and are categorised into four groups, i.e. foreshock, events occurred between the foreshock and the mainshock, mainshock, and events occurred after the mainshock. The division of the datasets is intended for studying the temporal changes of the site response related to soil nonlinearity during the Kumamoto foreshock-mainshock-aftershock sequence (e.g. Sawasaki et al., 2009; Wu et al., 2009). The results shown in **Figure 3.14** suggest that for the horizontal components, period shifts of the surface-to-borehole spectral ratios can be observed for the foreshock and mainshock in comparison with the majority of other smaller earthquakes (i.e. dominant peaks of the spectral ratios at 0.2 s to 0.4 s are significantly reduced). For the vertical component, very consistent site amplification is observed at periods less than 1 s, while the surface-to-borehole spectral ratios become more variable at longer periods. A more detailed investigation of the site amplification is warranted.

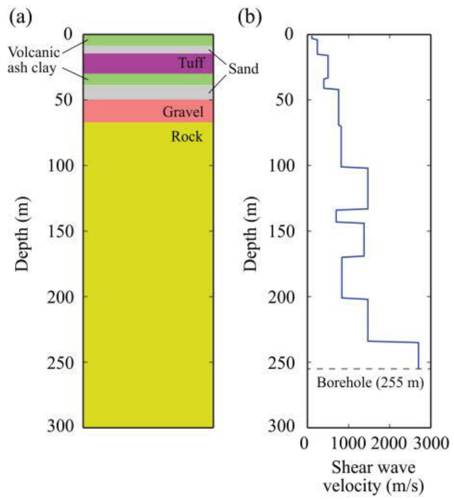


**Figure 3.10** Soil characteristics at KMMH16 (Mashiki): (a) borehole log and (b) shear wave velocity profile.

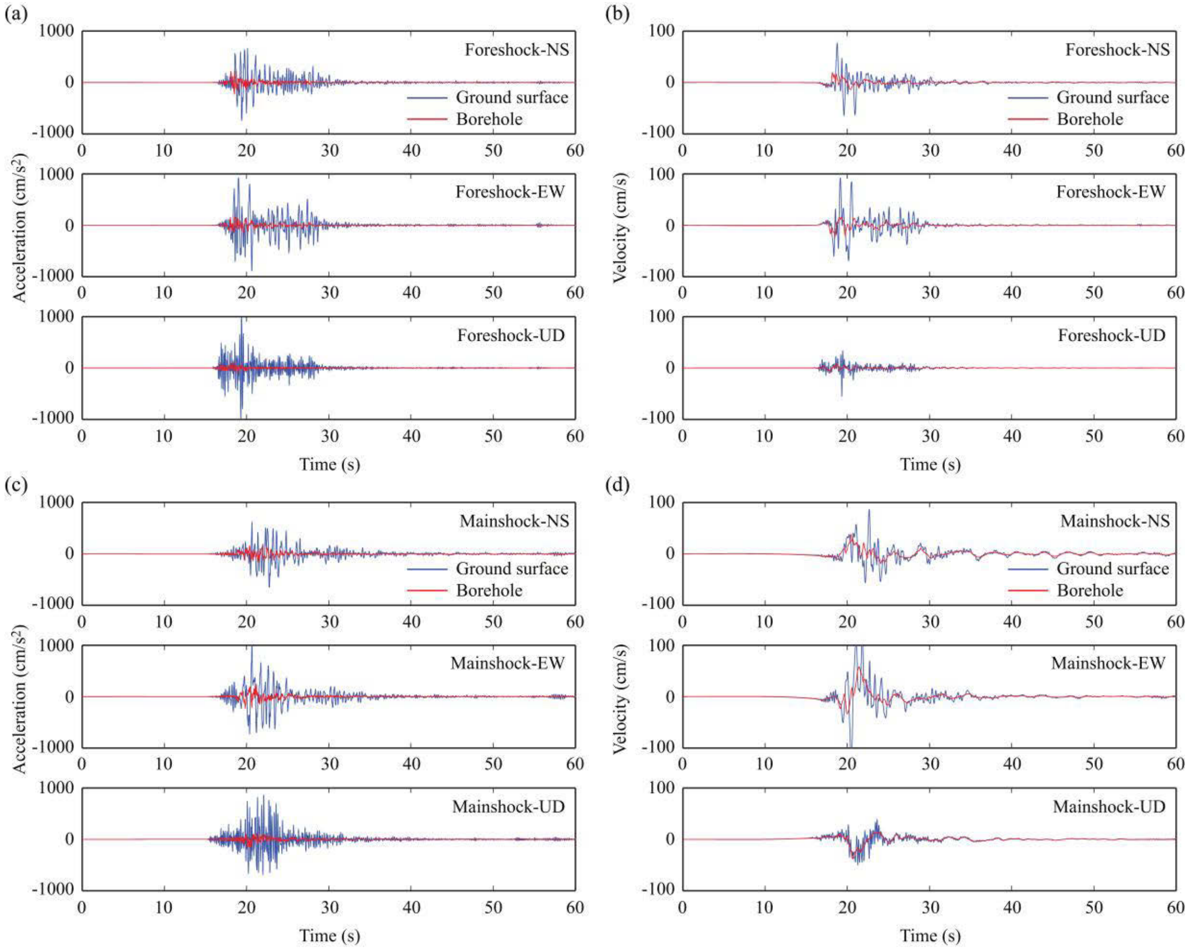


**Figure 3.11** Observed ground motion records at KMMH16 (Mashiki): (a) acceleration time-histories for the foreshock, (b) velocity time-histories for the foreshock, (c) acceleration time-histories for the mainshock, and (d) velocity time-histories for the mainshock.

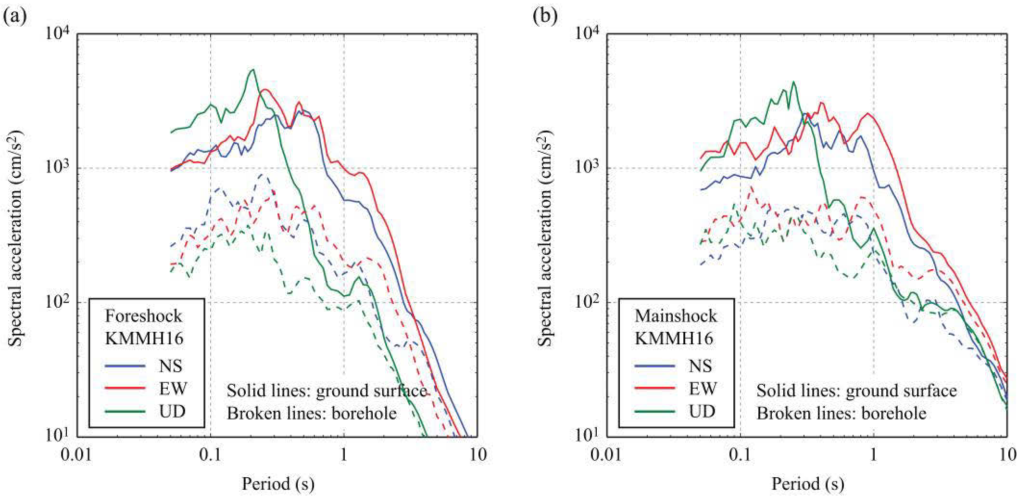


**Figure 3.12** 5%-damped response spectra at KMMH16 (Mashiki): (a) foreshock records and (b) mainshock records.

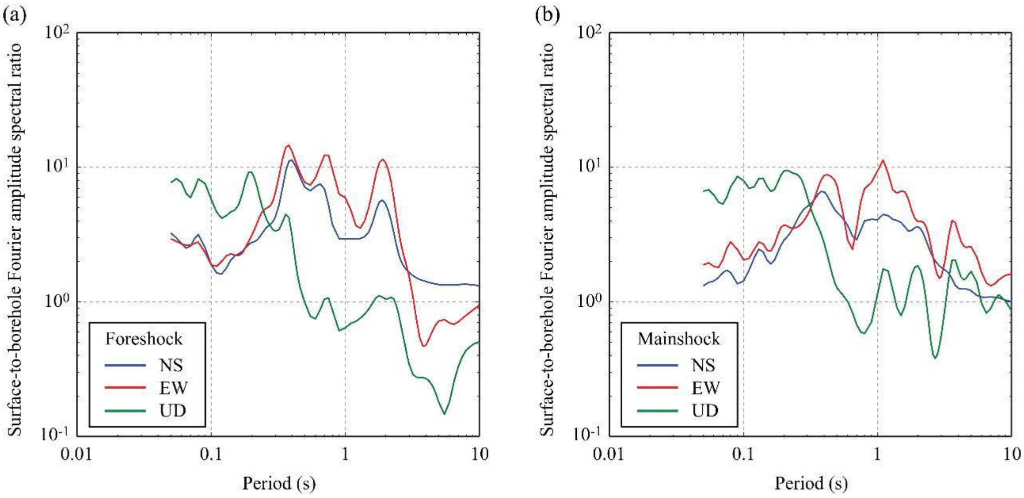


**Figure 3.13** Surface-to-borehole ratios of Fourier amplitude spectra at KMMH16 (Mashiki): (a) foreshock records and (b) mainshock records.

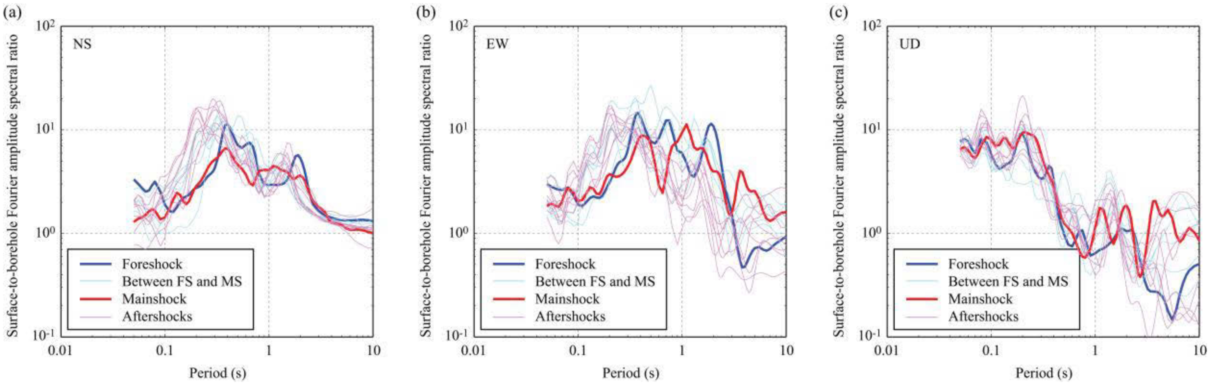


**Figure 3.14** Surface-to-borehole ratios of Fourier amplitude spectra at KMMH16 (Mashiki) for different earthquakes during the 2016 Kumamoto foreshock-mainshock-aftershock sequence: (a) NS components, (b) EW components, and (c) UD components.

**Figure 3.15** shows a borehole log, in-situ *N* blow counts (standard penetration tests), and shear wave velocity profile at the KMM006 station (in Kumamoto City). The soil data reach 20 m depth only (and no recordings are made at borehole). The top 20 m soil at KMM006 consists of relatively soft layers (all layers have shear wave velocities less than 270 m/s); in particular, up to 11 m depth, soil layers are soft (i.e. *N* values less than 5). The average shear wave velocity in the top 30 m of the soil is calculated as 246 m/s (i.e. NEHRP site class D).

**Figure 3.16** shows the ground motion records at KMM006 for the foreshock and mainshock, whereas **Figure 3.17** shows 5%-damped response spectra for the observed ground motions. The results show that intense ground motions were observed at KMM006, especially during the mainshock. At periods less than 1 s, SA values exceed 1 *g*. In comparison with KMMH16 (**Figure 3.11** and **Figure 3.12**), intensities of the ground motions at KMM006 are lower. This is consistent with the observed ground motion damage near the two stations (Goda et al., 2016). Therefore, the main slip concentration of the mainshock rupture (i.e. asperity) should be nearer to KMMH16 than KMM006 (although both stations are in the hanging wall region of the mainshock rupture; **Figure 3.5**).

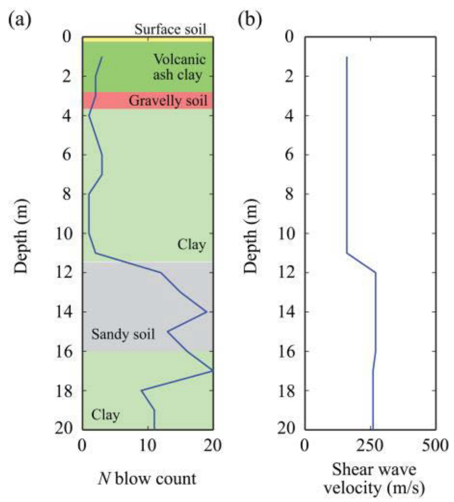


**Figure 3.15** Soil characteristics at KMM006 (Kumamoto): (a) borehole log and *N* blow count profile and (b) shear wave velocity profile.

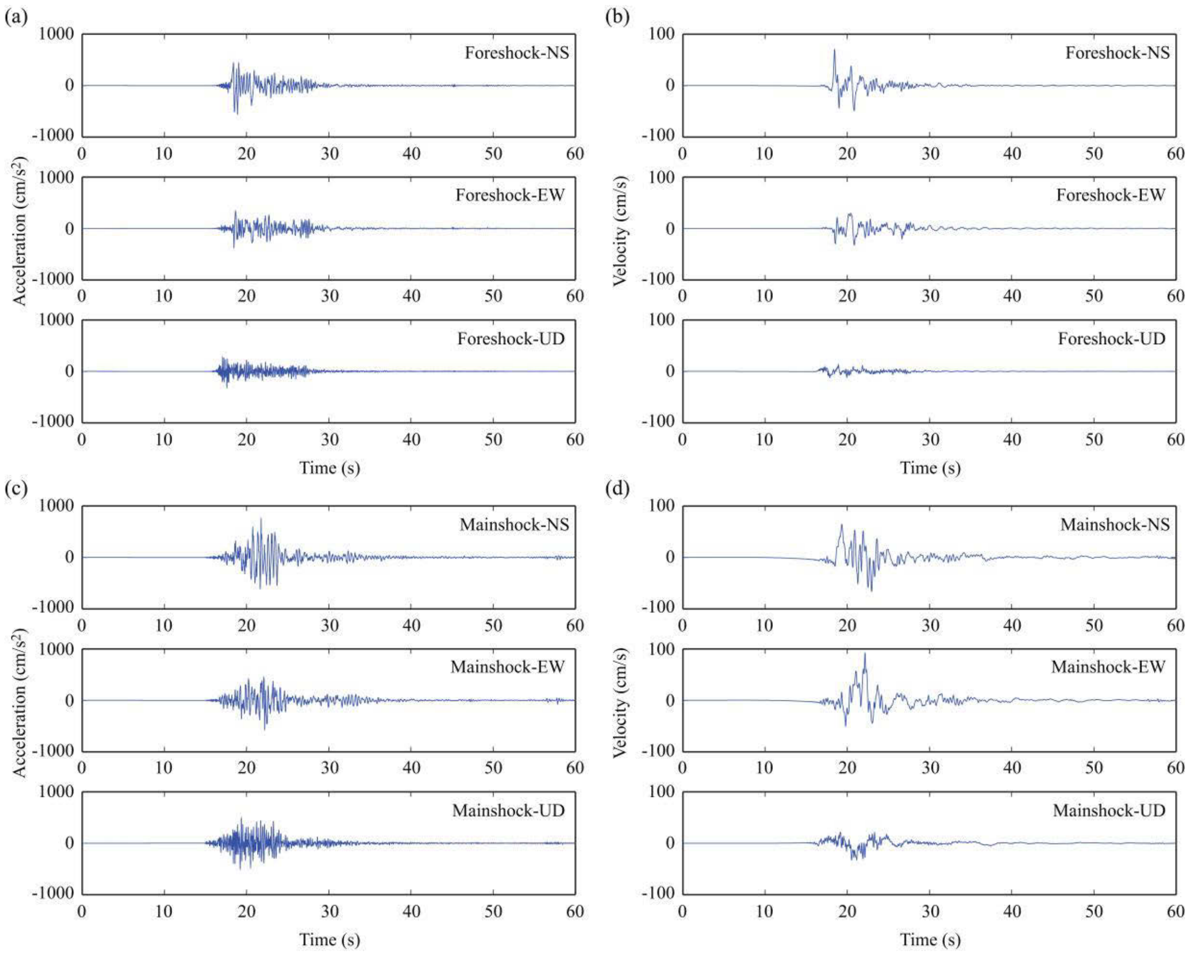


**Figure 3.16** Observed ground motion records at KMM006 (Kumamoto): (a) acceleration time-histories for the foreshock, (b) velocity time-histories for the foreshock, (c) acceleration time-histories for the mainshock, and (d) velocity time-histories for the mainshock.

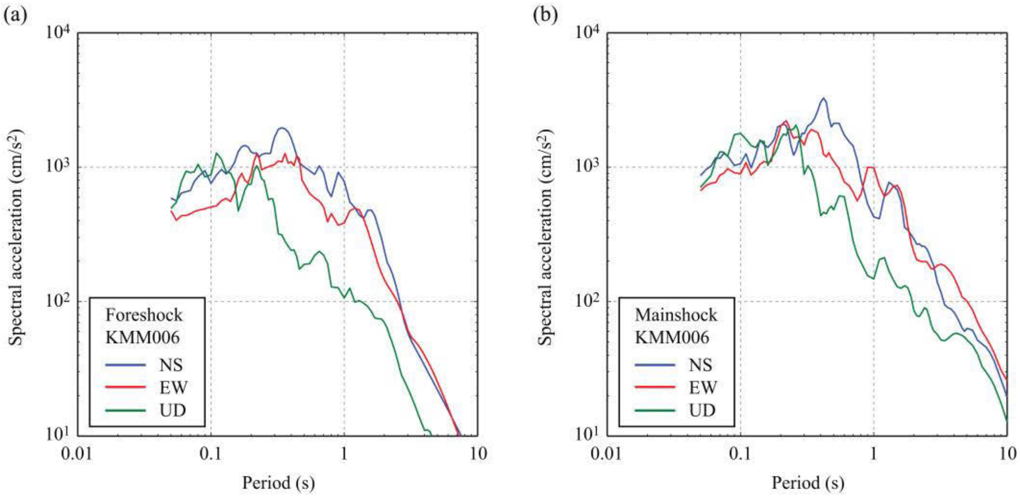


**Figure 3.17** 5%-damped response spectra at KMM006 (Kumamoto): (a) foreshock records and (b) mainshock records.

**Figure 3.18** shows a borehole log, in-situ *N* blow counts, and shear wave velocity profile at the KMM008 station (in Uto City). All soil layers at KMM008 have shear wave velocities less than 250 m/s, and there are several soft layers in the top 10 m. The average shear wave velocity in the top 30 m of the soil is calculated as 206 m/s (i.e. NEHRP site class D).

**Figure 3.19** shows the ground motion records at KMM008 for the foreshock and mainshock, whereas **Figure 3.20** shows 5%-damped response spectra for the observed ground motions. At this location, ground shaking during the foreshock was moderate, whereas ground shaking during the mainshock was intense, exceeding SA values of 1 *g* at vibration periods less than 1 s. It is noted that the location of KMM008 with respect to the Futagawa Fault and the rupture propagation during the mainshock (i.e. from WSW to ENE) corresponds to a backward directivity position.

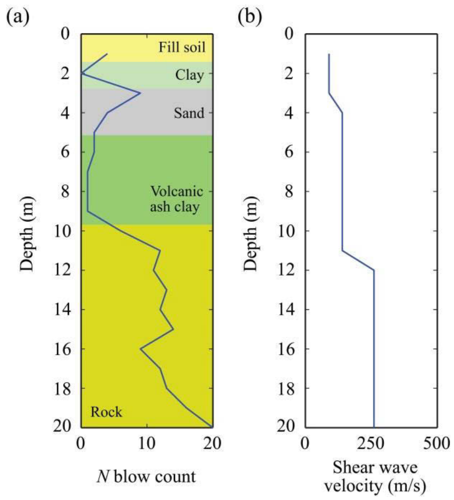


**Figure 3.18** Soil characteristics at KMM008 (Uto): (a) borehole log and *N* blow count profile and (b) shear wave velocity profile.

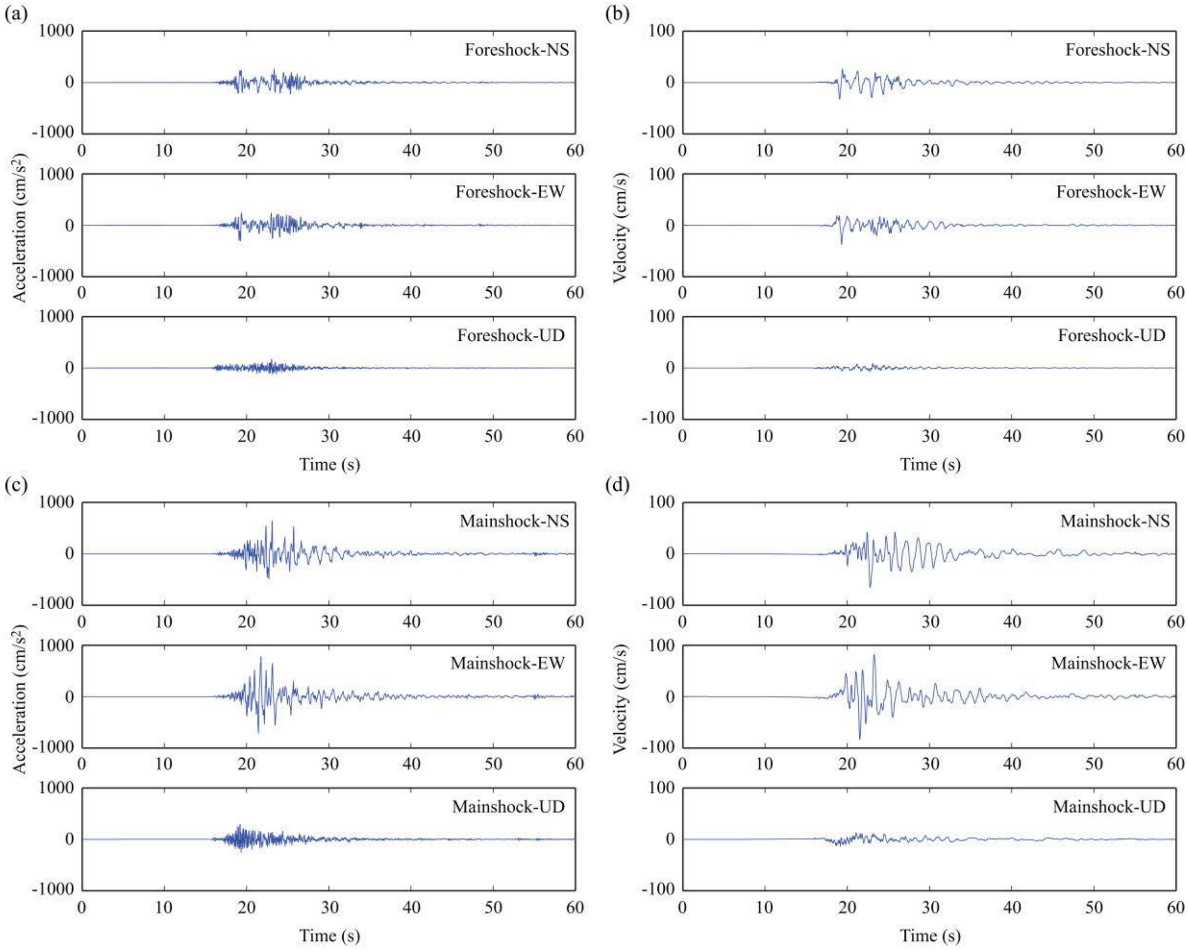


**Figure 3.19** Observed ground motion records at KMM008 (Uto): (a) acceleration time-histories for the foreshock, (b) velocity time-histories for the foreshock, (c) acceleration time-histories for the mainshock, and (d) velocity time-histories for the mainshock.

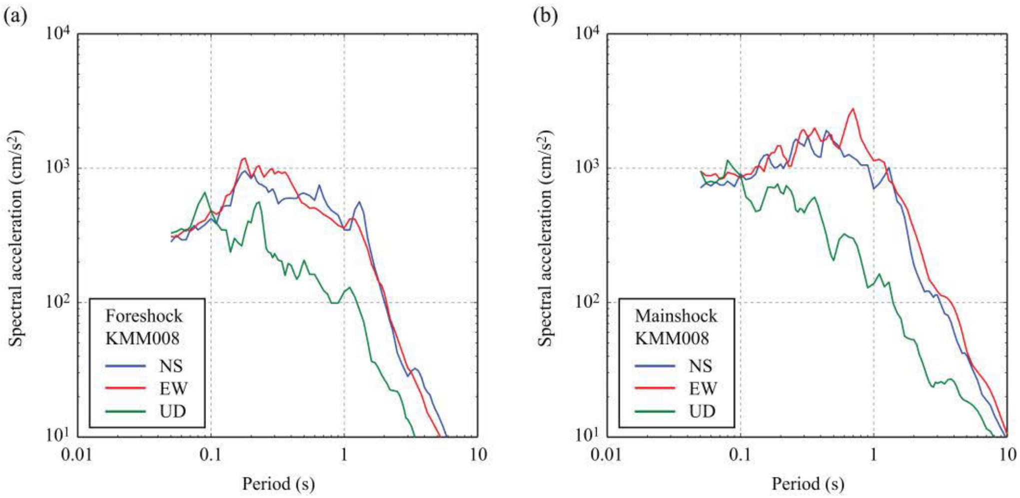


**Figure 3.20** 5%-damped response spectra at KMM008 (Uto): (a) foreshock records and (b) mainshock records.

### 3.3.2 *Regional ground motion characteristics*

The analyses of ground motion records are extended to other recording stations in the Kumamoto region. **Figure 3.21** and **Figure 3.22** show ground motion maps based on observed recordings at K-NET and KiK-net stations for the foreshock and mainshock, respectively. Four ground motion parameters, i.e. PGA and SA at 0.3 s, 1 s, and 3 s, are considered. Values of the ground motion parameters at unobserved locations are linearly interpolated and thus the ground motion maps represent crude estimates of ground motions only. **Figure 3.21** shows that during the foreshock intense ground motions were observed at KMMH16 (**Figure 3.11**) and KMM06 (**Figure 3.16**). On the other hand, **Figure 3.22** shows that intense ground motions due to the mainshock were observed at wide areas along both Futagawa and Hinagu Faults. Large values of the ground motion parameters are particularly concentrated near KMMH16. Another notable feature of the results shown in **Figure 3.22** is the observation of intense ground shaking for SA at 3 s in the north-eastern part of the map (**Figure 3.22d**).

It is interesting to investigate the orientation of ground motion parameters with respect to the fault strike (Watson-Lamprey and Boore, 2007). For this purpose, for each of the K-NET and KiK-net stations, two horizontal components are rotated to a particular azimuth and then ground motion parameters are calculated using the rotated acceleration time-history. A rotation of ground motion records is carried out over 360º with one degree increment. The results can be plotted on a polar coordinate to examine the major and minor response axes of the ground motion records (Hong and Goda, 2007), in comparison with the fault geometry. The results for the foreshock and mainshock are shown in **Figure 3.23** and **Figure 3.24**, respectively. The scale of the polar plots of the response spectra is adjusted for each ground motion parameter, noting that the same scale is adopted for the foreshock and mainshock to facilitate the visual comparison.

**Figure 3.23** shows that the recorded ground motions for the foreshock are intense at KMMH16 and KMM006, which are located in the forward directivity position (i.e. fault rupture propagates towards the location of interest). At KMMH16, rotated response spectra have circular shapes, with slightly greater responses in the fault normal direction. On the other hand, at KMM006, rotated response spectra are more polarised along the fault parallel direction.

**Figure 3.24** shows that for PGA and SAs at 0.3 s and 1 s, there is a clear dominant orientation of the ground motion parameters at KMMH16, KMM006, and KMM005 (Oozu; northeast of KMMH16), which is in parallel with the fault strike. Note that these stations are in the hanging wall region. Particularly for the short period range, the trend of the major response orientation is consistent in the near-fault region. At longer vibration periods, the orientations of the major response axes at KMMH16 and KMM005 rotate to almost fault-normal direction, while that at KMM006 remains parallel with the fault strike. It is important to note that the major response directions at short vibration periods for KMMH16 coincide with the directions of many collapsed houses in Mashiki Town (Goda et al., 2016). This indicates that in the near-fault region, effective counter-measures (e.g. bracing) can be implemented to mitigate shaking damage when the dominant direction of the ground shaking is known. Furthermore, outside the near-fault region, some consistent orientation effects can be observed. At KMMH03 (Kikuchi), the fault-normal component is dominant. On the other hand, at KMM004 (Ichinomiya), the fault-parallel component is dominant, particularly for SA at 3 s. In the EW component of the velocity time-history at KMM004, a large-amplitude velocity pulse is present.

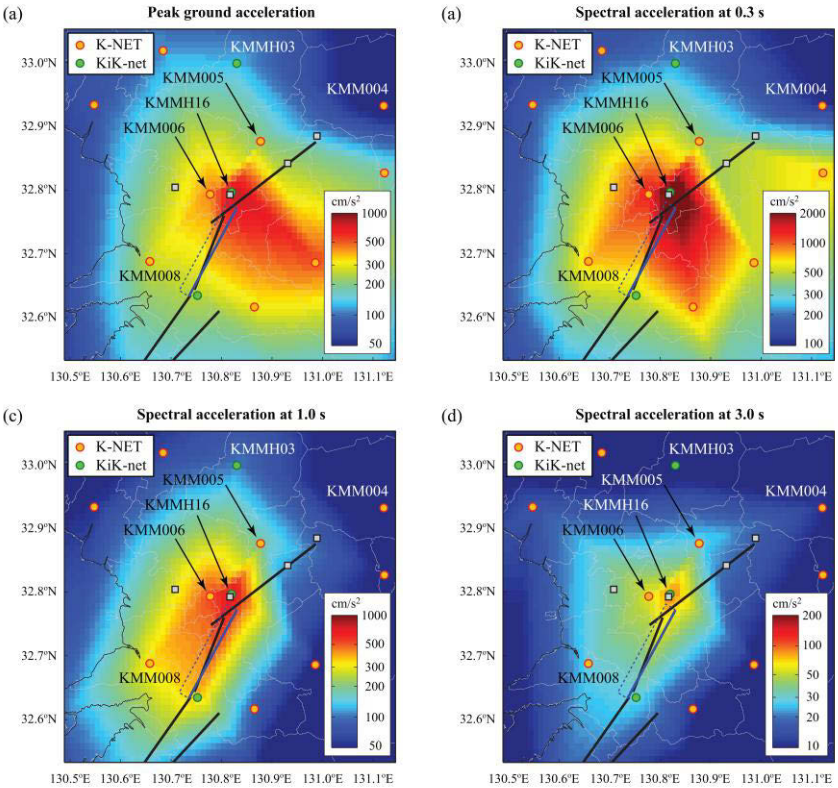


**Figure 3.21** Ground motion maps based on observed recordings for the foreshock: (a) PGA, (b) SA at 0.3 s, (c) SA at 1 s, and (d) SA at 3 s.

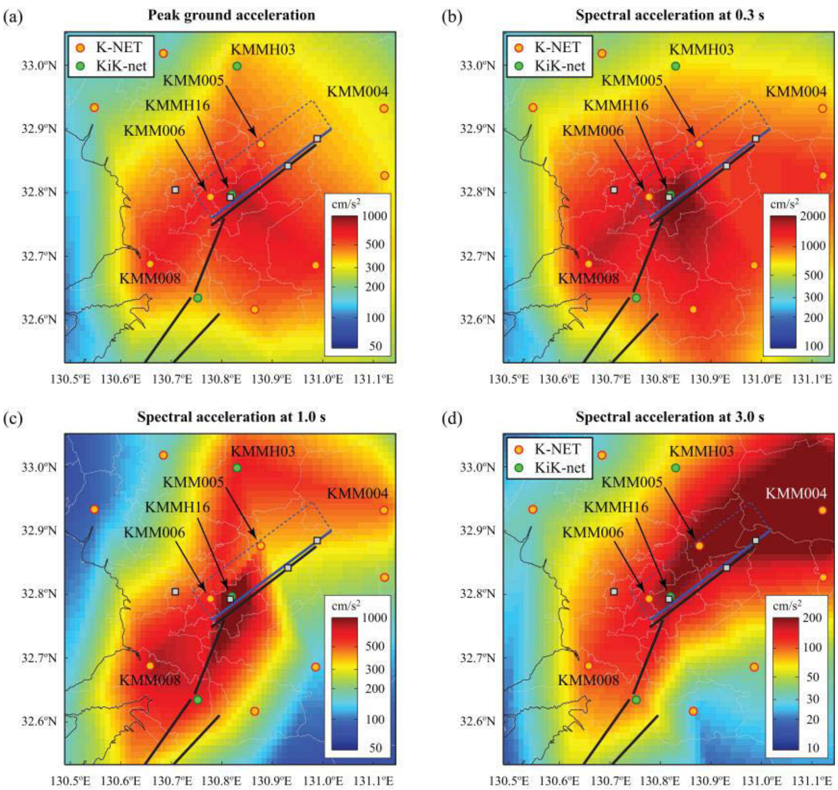


**Figure 3.22** Ground motion maps based on observed recordings for the mainshock: (a) PGA, (b) SA at 0.3 s, (c) SA at 1 s, and (d) SA at 3 s.

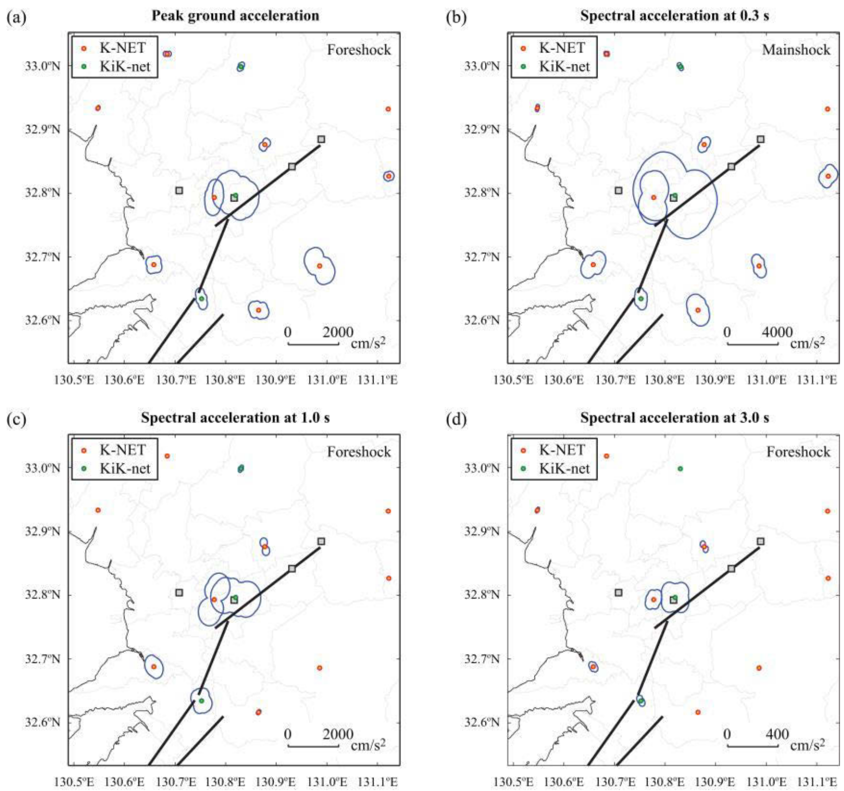


**Figure 3.23** Rotated response spectra for the foreshock: (a) PGA, (b) SA at 0.3 s, (c) SA at 1 s, and (d) SA at 3 s.

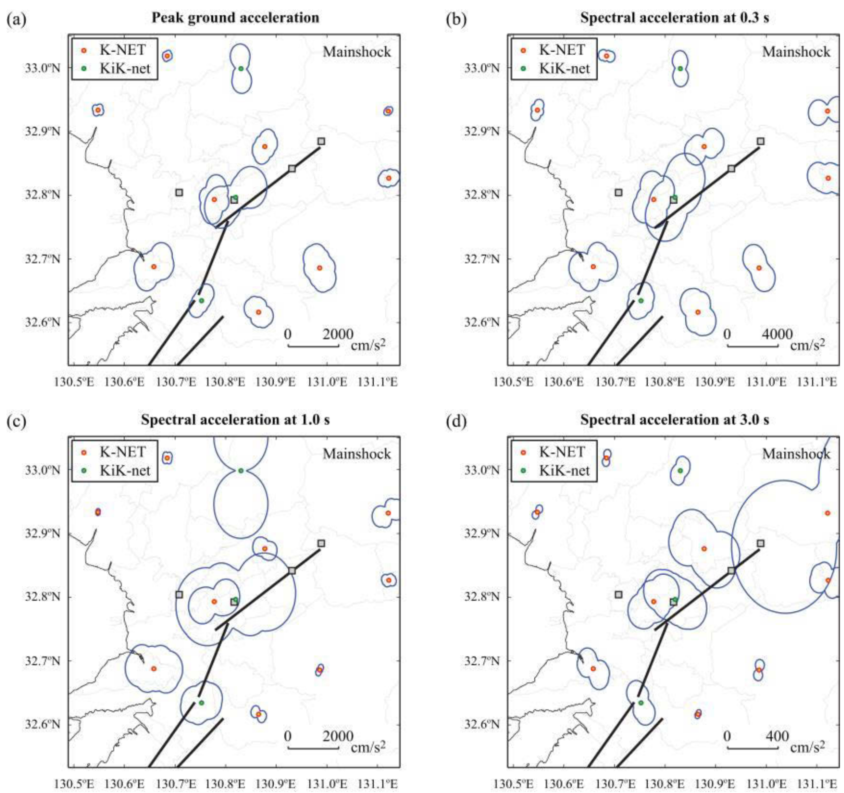


**Figure 3.24** Rotated response spectra for the mainshock: (a) PGA, (b) SA at 0.3 s, (c) SA at 1 s, and (d) SA at 3 s.

### 3.3.3 *Comparison of observed recordings and ground motion prediction equations*

It is important to compare the observed ground motions for the foreshock and mainshock with empirical prediction models in the literature. Through such a comparison, one can evaluate whether the ground motions from the Kumamoto earthquakes are unusual with respect to past events (note: such differences may arise due to various reasons, such as low/high stress drop and regional attenuation characteristics). In this study, a ground motion prediction equation (GMPE) by Boore et al. (2014) is adopted. The Boore et al. model is developed using worldwide ground motion data for shallow crustal earthquakes (including ground motion data from Japanese earthquakes) and hence is well suited for such a comparison. The moment magnitudes for the foreshock and mainshock are set to 6.1 and 7.1, respectively, according to F-net (http://www.fnet.bosai.go.jp/freesia/top.php?LANG=en). The source-to-site distance for the Boore et al. model is based on the so-called Joyner-Boore distance; for the ground motion data from K-NET and KiK-net, this distance measure is evaluated using the GSI's finite-fault plane geometry (**Figure 3.5a**). The Boore et al. model includes several adjustment parameters to refine the prediction, such as faulting mechanism and regional factor. In the comparison conducted herein, the strike-slip faulting mechanism and the regional factor for Japanese earthquakes are taken into account. For the comparison shown below, ground motion data that are recorded at sites with $V_{s30}$ between 150 m/s and 500 m/s are considered (average $V_{s30}$ is about 330 m/s). In applying the Boore et al. model, $V_{s30}$ is set to 300 m/s. For evaluating the confidence interval of the Boore et al. model, a sigma value is calculated for the intra-event case (as ground motion data from a single event are concerned).

**Figure 3.25** and **Figure 3.26** compare observed ground motions with predicted foreshock and mainshock ground motions, respectively, based on the Boore et al. model. The results for PGA and SAs at 0.3 s, 1 s, and 3 s are shown. For the foreshock, predicted values for PGA and SA at 0.3 s are consistent with the observed data, while those for SAs at 1 s and 3 s slightly overestimate the observations, especially at longer distances. For the mainshock, observed ground motions are generally consistent with the predicted values based on the Boore et al. model. In the distance range between 10 km and 100 km, there are several observation data that exceed the median plus one sigma curve; these data are mainly located in the NE of the rupture zone (i.e. Aso City and Yufu City and Kokonoe Town in Oita Prefecture). In the recorded accelerograms, the existence of a locally triggered event due to the mainshock was clearly observed; this increased the ground motion intensity at relatively remote locations. Overall, the recorded ground motion data for the foreshock and mainshock of the Kumamoto sequence are in agreement with the Boore et al. prediction models.

## 3.4 Conclusions on the ground motions

Regional earthquake catalogue data and strong motion data were analysed. In particular, the mainshock-aftershock seismic activities as well as ground deformation profiles were evaluated based on available finite-fault models for the Kumamoto earthquakes (i.e. GSI models and DPRI models), and were compared with actual GPS measurements before and after the earthquakes. Detailed analyses of recorded ground motions in the near-fault zone (e.g. KMMH16) revealed striking features of the intense ground shaking, directivity of strong motion, and site amplification. The analysed data were compared with an existing ground motion model for shallow crustal earthquakes.

The main results from the earthquake data analyses for the Kumamoto events are as follows:

1. Seismic activities of the 2016 Kumamoto sequence were distributed over a wide region, triggering numerous aftershocks. The migration of the earthquakes, originally from the Hinagu Fault zone (i.e. foreshock) to the Futagawa Fault zone (i.e. mainshock), was a notable feature of the sequence.

2. The recorded ground motions in the hanging wall region (e.g. KMMH16 in Mashiki Town) showed intense spectral acceleration amplitudes in the short-to-moderate vibration period range (exceeding 1 *g*) with significant site amplifications due to soft sediment in the Kumamoto plain. A clear directivity of ground motions in parallel with the fault strike was observed in the near-fault zone, which correlated well with the directions of collapsed buildings in Mashiki Town.

3. The observed ground motion data were in agreement with an empirical ground motion model by Boore et al. (2014).

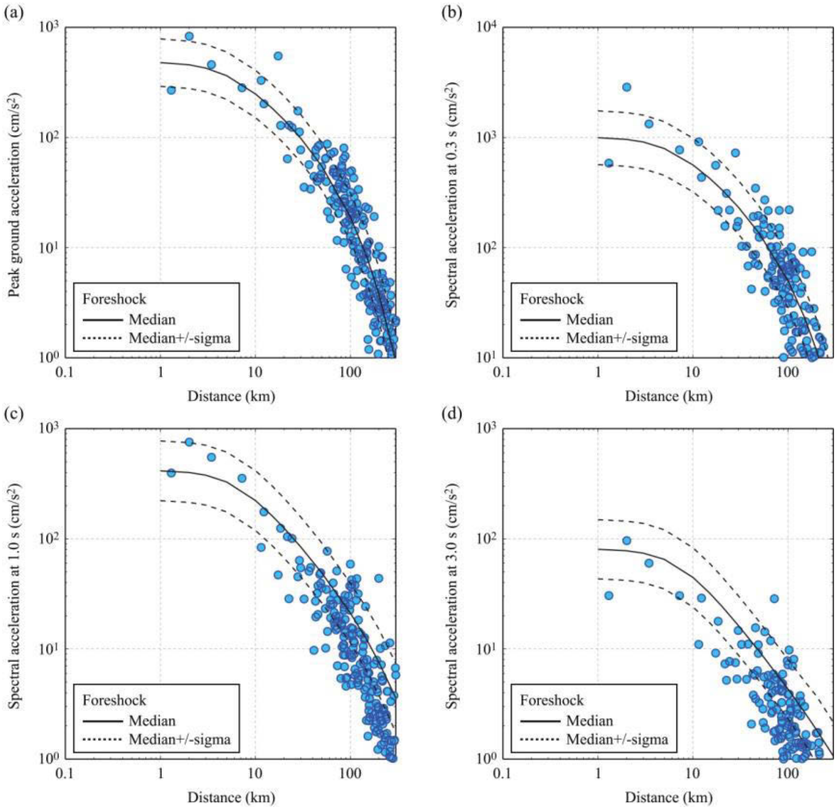


**Figure 3.25** Comparison of the observed ground motions with the prediction equations by Boore et al. (2014) for the foreshock: (a) PGA, (b) SA at 0.3 s, (c) SA at 1 s, and (d) SA at 3 s.

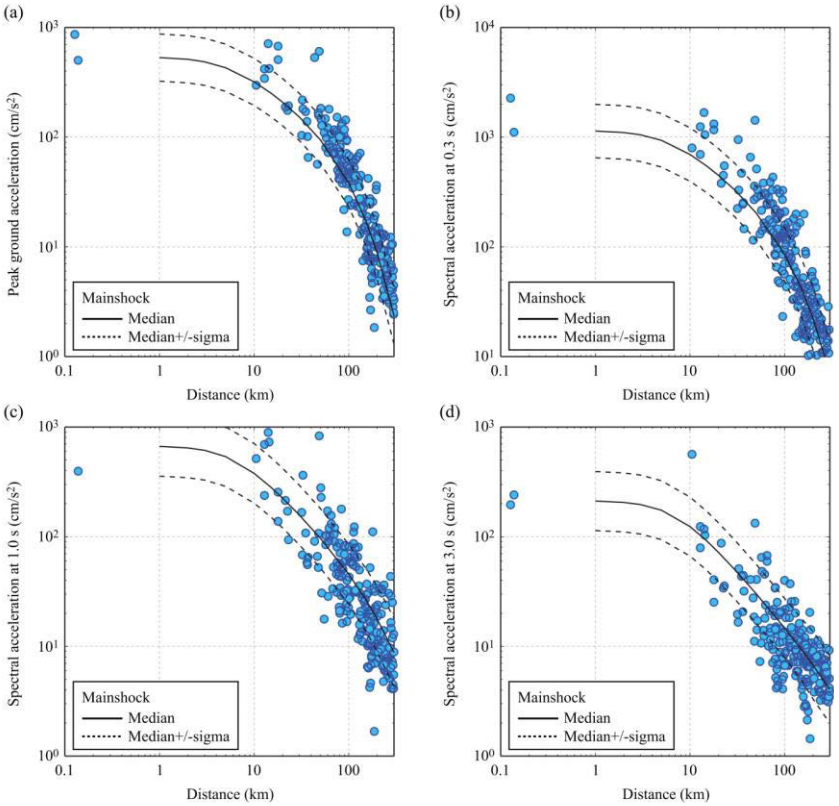


**Figure 3.26** Comparison of the observed ground motions with the prediction equations by Boore et al. (2014) for the mainshock: (a) PGA, (b) SA at 0.3 s, (c) SA at 1 s, and (d) SA at 3 s.

### 3.5 References

Asano, K., and Iwata, T. (2016). Source rupture processes of the foreshock and mainshock in the 2016 Kumamoto earthquake sequence estimated from the kinematic waveform inversion of strong motion data. *Earth Planets and Space*, **68**, 147, doi: 10.1186/s40623-016-0519-9.

Boore, D.M. (2005). On pads and filters: processing strong-motion data. *Bulletin of the Seismological Society of America*, **95**, 745−750.

Boore, D.M., Stewart, J.P., Seyhan, E., and Atkinson, G.M. (2014). NGA-West 2 equations for predicting PGA, PGV, and 5%-damped PSA for shallow crustal earthquakes. *Earthquake Spectra*, **30**, 1057–1085.

Ghofrani, H., Atkinson, G.M., and Goda, K. (2013). Implications of the 2011 M9.0 Tohoku Japan earthquake for the treatment of site effects in large earthquakes. *Bulletin of Earthquake Engineering*, **11**, 171–203.

Goda, K., Campbell, G., Hulme, L., Ismael, B., Ke, L., Marsh, R., Sammonds, P., So, E., Okumura, Y, Kishi, N., Koyama, M., Yotsui, S., Kiyono, J., Wu, S., and Wilkinson, S. (2016). The 2016 Kumamoto earthquakes: cascading geological hazards and compounding risks. *Frontiers in Built Environment*, **2**, 19, doi: 10.3389/fbuil.2016.00019.

Guo, Z., and Ogata, Y. (1997). Statistical relations between the parameters of aftershocks in time, space, and magnitude. *Journal of Geophysical Research*, **102**, B2, 2857−2873.

Headquarters for Earthquake Research Promotion (2016). Evaluation of the Futagawa and Hinagu fault zones. Accessed on 15 May 2016 at http://www.jishin.go.jp/main/chousa/13feb_chi_kyushu/k_11.pdf.

Hong H. P., and Goda, K. (2007). Orientation-dependent ground motion measure for seismic hazard assessment. *Bulletin of the Seismological Society of America*, **97**, 1525–1538.

Kato, A., Fukuda, J., Nakagawa, S., and Obara, K. (2016). Foreshock migration preceding the 2016 $M_W$7.0 Kumamoto earthquake, Japan. *Geophysical Research Letters*, **43**, 8945–8953.

Kubo, H., Suzuki, W., Aoi, S., and Sekiguchi, H. (2016). Source rupture processes of the 2016 Kumamoto, Japan, earthquakes estimated from strong-motion waveforms. *Earth Planets and Space*, **68**, 161, doi: 10.1186/s40623-016-0536-8.

National Institute of Advanced Industrial Science and Technology (2015). Active fault database of Japan. Accessed on 7 June 2016 at https://gbank.gsj.jp/activefault/index_e_gmap.html.

Okada, Y. (1985). Surface deformation due to shear and tensile faults in a half-space. *Bulletin of the Seismological Society of America*, **75**, 1135–1154.

Sawazaki, K., Sato, H., Nakahara, H., and Nishimura, T. (2009). Time-lapse changes of seismic velocity in the shallow ground caused by strong ground motion shock of the 2000 Western-Tottori earthquake, Japan, as revealed from coda deconvolution analysis. *Bulletin of the Seismological Society of America*, **99**, 352–366.

Shcherbakov, R., Turcotte, D.L., and Rundle, J.B. (2005). Aftershock statistics. *Pure and Applied Geophysics*, **162**, 1051–1076.

Watson-Lamprey, J., and Boore, D.M. (2007). Beyond $Sa_{GMRotI}$: Conversion to $Sa_{Arb}$, $Sa_{SN}$ and $Sa_{MaxRot}$. *Bulletin of the Seismological Society of America*, **97**, 1511-1524.

Wu, C., Peng, Z., and Assimaki, D. (2009). Temporal changes in site response associated with strong ground motion of 2004 M6.6 mid-Niigata earthquake sequences in Japan. *Bulletin of the Seismological Society of America*, **99**, 3487–3495.

Yagi, Y., Okuwaki, R., Enescu, B., Kasahara, A., Miyakawa, A., and Otsubo, M. (2016). Rupture process of the 2016 Kumamoto earthquake in relation to the thermal structure around Aso volcano. *Earth Planets and Space*, **68**, 118, doi: 10.1186/s40623-016-0492-3.

## 4 Building Damage

Kumamoto City is the capital city of Kumamoto Prefecture and has a population of approximately 730,000 and together with adjacent urban areas forms Japan's 11th biggest conurbation. Important industries are automotive components and electronics. The city is notable for an extensive castle complex which dates back to the 15th century and is its main tourist attraction. The surrounding Kumamoto Prefecture has a population of 1.8 million. Wide plains surrounding Kumamoto City mean that there is space for agriculture. The scenic hills and mountains to the east, including Aso Caldera, make the area popular with tourists.

The EEFIT made observations of damage to structures in a range of areas, which are indicated in **Figure 4.1**. Intense damage occurred to residential suburbs on the south-western side of Kumamoto Prefecture, such as in Mashiki Town, and to villages in close proximity to the Futagawa Fault and to the Aso Caldera wall, such as Nishihara Village and Minami Aso Village. These were the areas where the majority of human casualties occurred (Section 6). The building stock in these areas is predominantly low-rise residential timber buildings. These areas also suffered damage to bridges, including the collapse of Aso Bridge caused by a large landslide and the damage to the Tawarayama Tunnel (Section 5). Areas further from the Futagawa and Hinagu Faults, such as Uto City and Kumamoto City, suffered more localised damage to specific vulnerable buildings. As well as damage to residential dwellings, there were also a number of dramatic failures to large reinforced concrete (RC) buildings at various locations. Extensive damage also occurred at the heritage sites of Kumamoto Castle in Kumamoto city centre and Aso Shrine to the north of Mount Aso. Damage observations are described in more detail in the following sections. Japan uses a red/yellow/green tagging system for classifying buildings as unsafe (red), requiring further assessment (yellow), and cleared for re-occupancy (green). These tagging colours are referred to in the following.

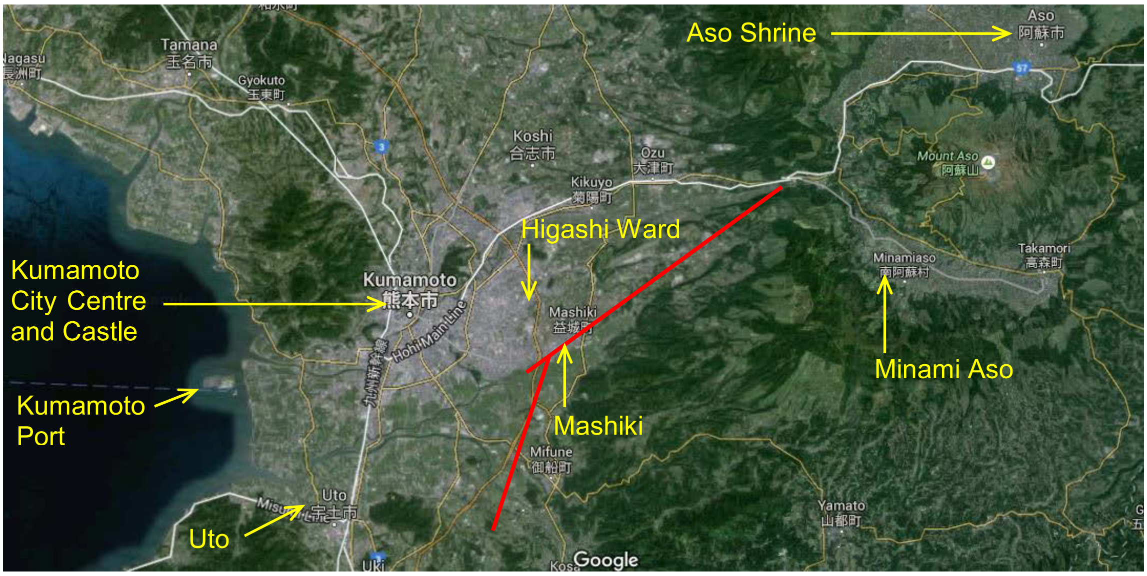


**Figure 4.1** Location map of EEFIT structural damage surveys (image source: Google Map).

### 4.1 Building regulations in Japan

Japan has a long history of earthquake engineering research and design. The 2016 Kumamoto mission is the fourth EEFIT mission to Japan. The background to Japanese building regulations has been gathered by the previous survey teams (EEFIT, 1997, 2011, 2013). This information has been repeated below (**Table 4.1**), supplemented with further information where relevant, with credit due to the previous survey teams. A more comprehensive review of the 1981 building code is provided in the EEFIT report which followed the Hyogo-Ken Nanbu (Kobe) earthquake (EEFIT, 1997). Nakashima and Chusilp (2003) provide commentary on code revisions that were carried out after the 1995 Kobe earthquake in response to lessons learned.

**Table 4.1** Summary of the Japanese building regulations for seismic design.

| Year | Summary of regulations |
|---|---|
| 1895 | The first building requirements (non-compulsory) introduced following the 1891 Nobi earthquake. |
| 1919-1920 | *City Planning Act* and *Urban Building Standards Act* introduced in response to urban expansion. Specific regulations dictating and regulating building in six major urban centres in Japan included: a height limit of 100 feet; structural design for timber, masonry, brick, RC, and steel constructions; Allowable stress design; quality of materials; dead and live loads. No seismic requirement included. |
| 1923 | Great Kanto earthquake |
| 1924 | *Urban Design Law of Japan* introduced base shear force equivalent to 0.1 *g* as a requirement for six major urban centres in Japan. |
| 1950 | Ultimate strength design introduced in the *Building Standard Law*. The design base shear was increased to 0.2 *g* and made compulsory nationwide. |
| 1968 | Tokachi-oki earthquake |
| 1971 | Amendment introduced after the 1968 Tokachi-oki earthquake to improve ductility of RC columns by reducing the required tie hoop space. |
| 1978 | Miyagi-oki earthquake |
| 1981 | Incorporating experience from the 1978 Miyagi-oki earthquake, a two-level approach (serviceability limit state and ultimate limit state) was introduced and building permission procedures were simplified for seismic isolation and active/passive vibration control (Okazaki, 2008). All buildings >31 m high must be analysed for storey drift, stiffness, lateral and torsional eccentricity, while those >60 m must be designed using dynamic analysis. Allowable storey drift was limited to 0.5% of the storey height, although this could be increased to 0.8% if guarantees of no severe damage to non-structural elements could be provided. Although seen as the most advanced code in the world at the time, criticisms included: incentive to omit shear walls/bracing to satisfy shape factor requirements; incentive to use unnecessarily large columns; structural coefficient for ultimate limit state was required for each storey rather than the whole structure; crude seismic zonation of the country; lack of provisions for sub-structure and non-structural damage; and importance factor not applied (Ishiyama, 1989). For a more detailed review of the 1981 building code, see EEFIT (1997). |
| 1995 | Kobe earthquake |
| 1995 | *Act for Promoting Seismic Retrofitting of Existing Buildings* stated that building owners of special buildings (which include most buildings except for private houses) should strive to carry out seismic assessment and strengthening. There was no mandatory requirement to strengthen, or to achieve a minimum strengthening level. |
| 2000 | Amendment of the *Building Standard Law* to include performance-based regulation. The revised code precisely defined seismic performance requirements and verification based on earthquake response spectra at engineering bedrock and additional surface-soil-layer amplification factors. This approach retained the use of life safety and damage limitation limit states introduced previously, with design ground motion damage limitation limit state reduced to 1/5 of that for life safety, which was based on an earthquake with a return period of 500 years (Kuramoto, 2006). |
| 2001 | Publishing of the advisory standards *Standard for Seismic Evaluation and Guidelines for Seismic Retrofit of Existing Reinforced Concrete Buildings* (JBDPA, 2001). These standards are not mandatory, but contain guidance about techniques for voluntary assessment and strengthening. |
| 2011 | Tohoku earthquake |
| 2013 | An amendment to the *1995 Act for Promoting Seismic Retrofitting of Existing Buildings* has placed an obligation on owners to carry out seismic assessment and report on building strength, but it is not mandatory to strengthen. |

## 4.2 Damage to timber buildings in Mashiki Town

Mashiki Town is in close proximity to the activated faults of the 2016 Kumamoto earthquakes (Section 2), and suffered severe damage and casualties. Measurements at the KMMH16 station in Mashiki Town showed response accelerations (**Figure 4.2**). Spectral accelerations were particularly high around 1 s in the EW direction. Vertical accelerations were also high. As a residential suburb, the building stock in Mashiki is dominated by single-family dwelling timber buildings of one and two storeys. There are also a number of low-to-medium-rise RC apartment buildings. Along the commercial (retail) streets (Road 28 and Road 235), buildings were generally one- to three-storey steel frames. **Figure 4.3** provides an aerial view of Mashiki Town prior to the earthquakes. It can be seen that the timber frame houses are generally detached with clearance between houses, but are often constructed tight to the narrow streets. **Figure 4.4** shows the same view after the earthquakes. An impression of the proportion of houses that have suffered roof damage can be seen from the blue weatherproofing sheeting; however, there are also many cases of severely damaged buildings that had not been sheeted, as the loss had been total.

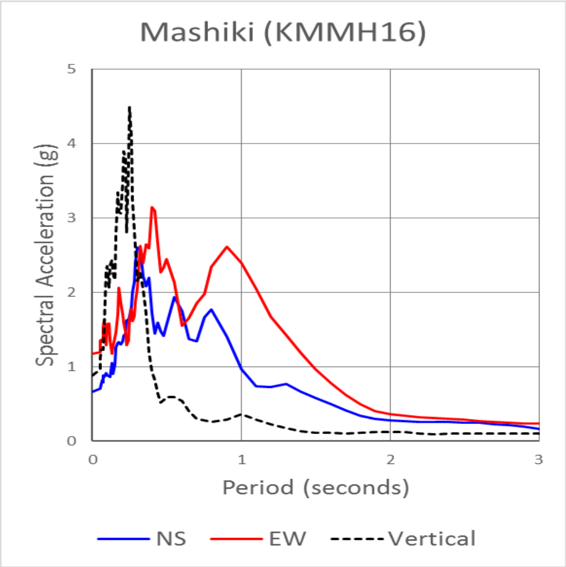


**Figure 4.2** Measured 5%-damped spectral accelerations in Mashiki Town.


**Figure 4.3** Aerial view of Mashiki Town prior to the 2016 Kumamoto earthquakes (image source: Google Earth).


**Figure 4.4** Aerial view of Mashiki Town after the 2016 Kumamoto earthquakes (image source: Google Earth).

Failures of timber buildings occurred in a number of modes. The most catastrophic failures had resulted in complete collapse, and disintegration of timber walls and roofs (**Figure 4.5a**). These types of failures were typical of older buildings constructed in traditional styles that were built before the 1981 building code. There were also many cases of failure of more modern buildings, including many cases of collapsed bottom storeys in two-storey houses (**Figure 4.5b**). In many cases buildings had suffered significant drift of bottom storeys, but had not collapsed. In these cases, often cladding had fallen and the structure of vertical timber studs and horizontal timber boarding lying behind could be seen (**Figure 4.5c**). These walls were not strengthened by sheathing boards, and it appeared that the lateral design instead used diagonal timber struts as observed in Minami Aso Village (see **Figure 4.7a**). At the levels of drifts illustrated in **Figure 4.5c**, it is likely that diagonal timber braces would be ineffective; however, many similar cases where buildings had suffered extreme loss of form without collapse were also observed. It is possible that the horizontal wooden laths were providing some resistance by offering an alternative vertical load path and restraining the buckling of vertical studs. To gain an understanding of the distribution and intensity of damage in Mashiki Town, the EEFIT carried out a systematic damage survey, which is described in Section 4.9.


**Figure 4.5** Damage to timber frame houses in Mashiki Town: (a) complete collapse of a pre-1981 structure, (b) bottom storey collapse, (c) significant drift, and (d) soft-storey collapse mechanism of a modern building.

### 4.3 Ground-induced building damage in Minami Aso Village

The EEFIT visited the student village next to Tokai University (Aso campus) in the Kawayo district of Minami Aso Village (**Figure 4.6**). Buildings in this area were a mixture of one- and two-storey timber residential buildings, and also a number of two- to five-storey RC residential buildings. The RC buildings were generally located in the lower parts of the area close to the Shirakawa River gorge. Significant damage had occurred to the majority of timber frame buildings (Goda et al., 2016). Damage to structures had occurred due to ground movement as well as shaking damage. The yellow lines in **Figure 4.6** indicate locations of significant ground ruptures.

In area A, a series of parallel ruptures suggest movement of ground towards the northwest. All timber frame houses in this area had suffered significant damage, loss of cladding and permanent drifts. An example is shown in **Figure 4.7a**.

In area B a significant single rupture had occurred, having dramatic impact on the buildings crossed by the rupture.

- Building 1 (**Figure 4.7b**) was leaning at an angle of approximately 15º. The building appeared to have suffered foundation failure to the south elevation and failure of the stud wall base connections to the north elevation, resulting in uplift of the north elevation and significant tilt. The *P*-Δ overturning moments induced by this degree of tilt put the building at high risk of collapse. The fact that it had retained its shape and not collapsed suggested that it must have robust floor and roof ties and effective cross-walls.
- Building 2 (**Figure 4.7c**) suffered complete collapse of the lower storey. Due to the extent of damage, it was not possible to determine whether this had been caused predominantly by ground deformation or by shaking forces.
- Building 3 (**Figure 4.7d**) was a two-storey timber frame student residence apartment, with steel framed walkways to the perimeter. The building had been subjected to significant shearing and extension from a ground rupture crossing the building in the transverse direction. This caused longitudinal stretching of the bottom of the building, while the upper storey remained unstretched, resulting in large tilting of columns, but no local collapse. It is likely that the presence of the steel walkways had been beneficial in providing some additional lateral resistance.

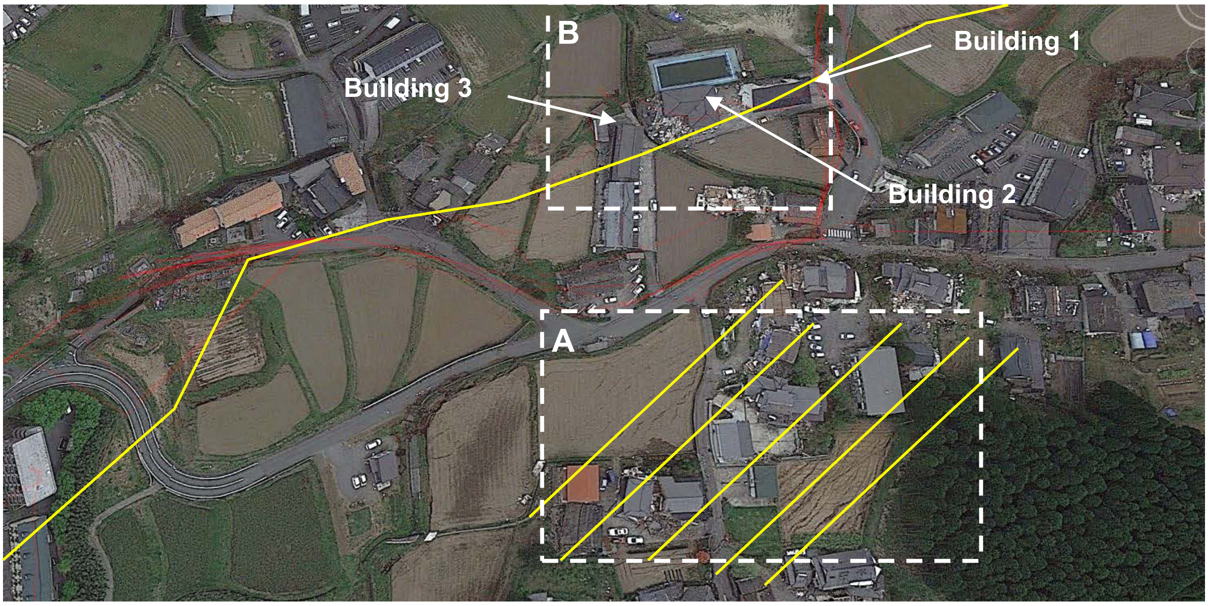


**Figure 4.6** Aerial view of a student complex in the Kawayo district of Minami Aso Village (image source: Google Map).


**Figure 4.7** Damage to timber frame buildings in the Kawayo district of Minami Aso Village: (a) heavily damaged house in Area A, (b) Building 1 in Area B, (c) Building 2 in Area B, and (d) Building 3 in Area B with visible traces of the ground rupture that crossed underneath.

### 4.4 Damage to reinforced concrete buildings

A damage survey was carried out by the University of Tokyo team a few days after the earthquakes (Tajiri et al., 2016). The survey report documented a number of examples of RC building failures, including 8 cases of collapse due to soft-storey failure (**Figure 4.8a**). RC frame failure examples were also collated by EERI desk studies by Tasdemir and Paul (2016), which included numerous images from the University of Tokyo damage survey and news media. Although the EEFIT did not observe the cases of soft-storey collapse, cases of moderate and heavy damage to RC buildings in the form of shear cracking to RC shear walls and joint damage to poorly detailed RC frames were observed (e.g. **Figures 4.9** and **4.10**).

The Uto City Office suffered from a mid-storey partial collapse mechanism (**Figure 4.8b**). The building was constructed prior to the 1981 building law. The partial collapse had occurred to the fourth storey as a result of extreme damage to a central edge column. An outer façade of more closely-spaced non-structural mullions had suffered extensive deformation. The damage to RC columns and beams could be seen clearly because the structure was exposed and the cracks to the columns and beams were wide (**Figure 4.8c**). The damage appeared to be due to poor detailing of RC elements, which may have been exacerbated by an irregular building form. Although the column grid appears regular (**Figure 4.8d**), two cores to the back of the building could possibly be causing differential stiffness of the framing lines. Only minor damage had generally occurred to other buildings nearby the Uto City Office, making this damage striking in comparison.


**Figure 4.8** Damage to RC frame buildings: (a) soft-storey collapse of an apartment building in Kumamoto City (Tajiri et al., 2016), (b) west façade of the Uto City Office, (c) column damage to the Uto City Office, and (d) structural layout of the Uto City Office – the blue lines are the front face of the building where structural damage to the RC frame is visible as shown in (b) and (c) (aerial view from Google Earth).

Mashiki Town Office is a strengthened RC building in the centre of Mashiki Town, comprising a three-storey southern block and two-storey northern block connected by a link bridge. RC frame strengthening had been applied to the southern elevation of the building (**Figure 4.9a**). This part of the building appeared undamaged, except for some hairline cracking to the concrete shear link beams connecting the retrofitted frame to the original frame. The strengthening solution uses an RC frame offset from the original façade to limit disruption to the existing building, albeit with some aesthetic and daylight disadvantages. The solution looks similar to techniques described in JBDPA (2001) and Takeda et al. (2013). The retrofit frame had a stepped shape, presumably to spread the intensity of column axial loads to the end bays and to improve efficiency of foundations. Although the retrofit appeared to be successful, localised damage had occurred to the link bridge structure joining the two blocks (**Figure 4.9b**). The link bridge had clearly been detailed with a movement joint to the northern end to permit horizontal differential movement between the two buildings. Independent vertical support was provided to the link bridge at its northern end. Damage appeared to have occurred due to the hard vertical support, which had transferred high shears into the link bridge as the southern block swayed.

**Figure 4.10** shows an example of a typical RC frame apartment building in Mashiki Town. These buildings were RC moment-resisting frames with large columns and regular column grids. All examples of these types of buildings observed during the Mashiki damage survey had suffered only minor or negligible damage, despite being surrounded by other heavily damaged structures.

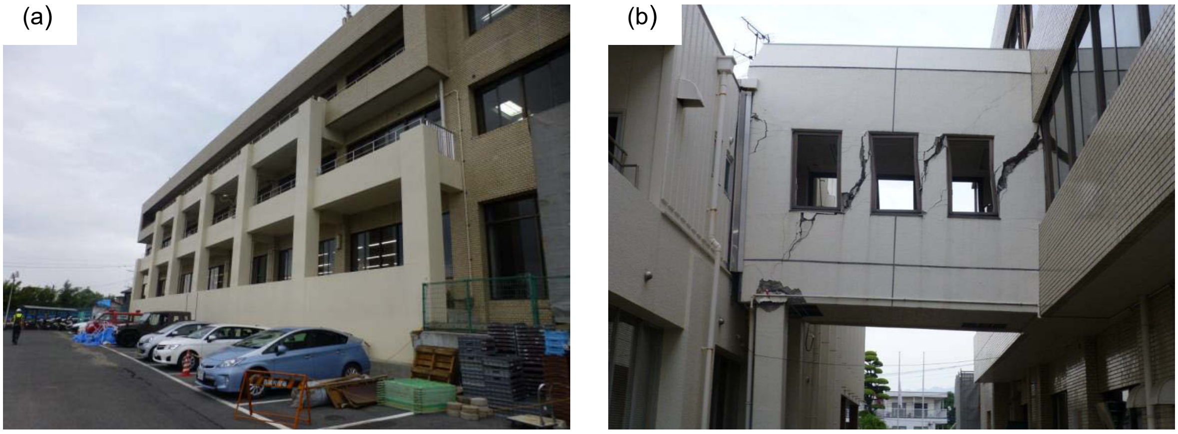


**Figure 4.9** Mashiki Town Office (strengthened RC frame): (a) strengthened south elevation and (b) damage to link bridge.


**Figure 4.10** Well-performing RC frame apartment building in Mashiki Town: (a) general view and (b) zoom showing no evidence of fine cracks.

## 4.5 Damage to steel frame buildings and hybrid construction

A number of steel building failures were observed along Road 28 in Mashiki Town. These were generally commercial properties with glazed ground level street side elevations. **Figure 4.11a** shows a typical failure observed to low-rise steel frame commercial buildings in Mashiki. The bottom storey suffered significant drift to the southwest. The drift caused infill blockwork to collapse exposing the interior of the building. The steel frame did not appear to have bracing. Similar failures were observed to other shops along the same high street which appeared to have suffered from a lack of bracing in the street side façade causing a weakness in an orientation parallel to the fault (see Section 3). Commercial buildings located along nearby perpendicular streets appeared to have fared better. Shops on Road 235 running north/south adjacent to the Mashiki Town Office were still trading, and did not exhibit visible damage. **Figure 4.11b** shows the partial collapse of a four-storey retail and residential building to the northern side of Road 28. The building appeared to be of hybrid steel and timber construction, and possibly had suffered from lack of continuity between the different structural sections. The collapse had occurred in the EW direction parallel to Road 28. This building was overhanging the pavement and looked likely to represent a hazard in case of aftershocks. Due to the density of buildings and narrowness of the road in this area, it was not possible for the building to be cordoned, and therefore the hazard to pedestrians and other road users was uncontrolled.

(a) (b)

**Figure 4.11** Steel building failures in Mashiki Town: (a) bottom-storey drift to the southern side of Road 28 and (b) four-storey collapse to the northern side of Road 28.

## 4.6 Damage to schools and hospitals

Nine days after the mainshock, the Asahi Shimbun newspaper (2016a) reported that approximately two thirds of school sites in Kumamoto City were closed due to building damage or because investigations were ongoing. Out of 1267 school buildings, 134 buildings were classified as red (11%), 354 as yellow (28%), and 779 as green (61%).

The EEFIT visited Mashiki Junior High School; the team was not able to inspect the building closely. Tajiri et al. (2016) carried out a damage survey at nearby Kiyama Junior High School immediately after the mainshock and observed damage to RC columns supporting the link bridge between two structures. The photographs of that survey are shown in **Figure 4.12**. The school building had a steel bracing retrofit to classrooms which was undamaged (**Figure 4.12a**), but lighter bracing to the gymnasium which had buckled (**Figure 4.12b**). Hazardous damage had occurred to the link bridges which were still standing, but exhibiting significant column drifts (**Figures 4.12c** and **4.12d**). This pattern of damage was similar to the Mashiki Town Office, showing low damage to strengthened blocks but concentrated damage to linking structures.

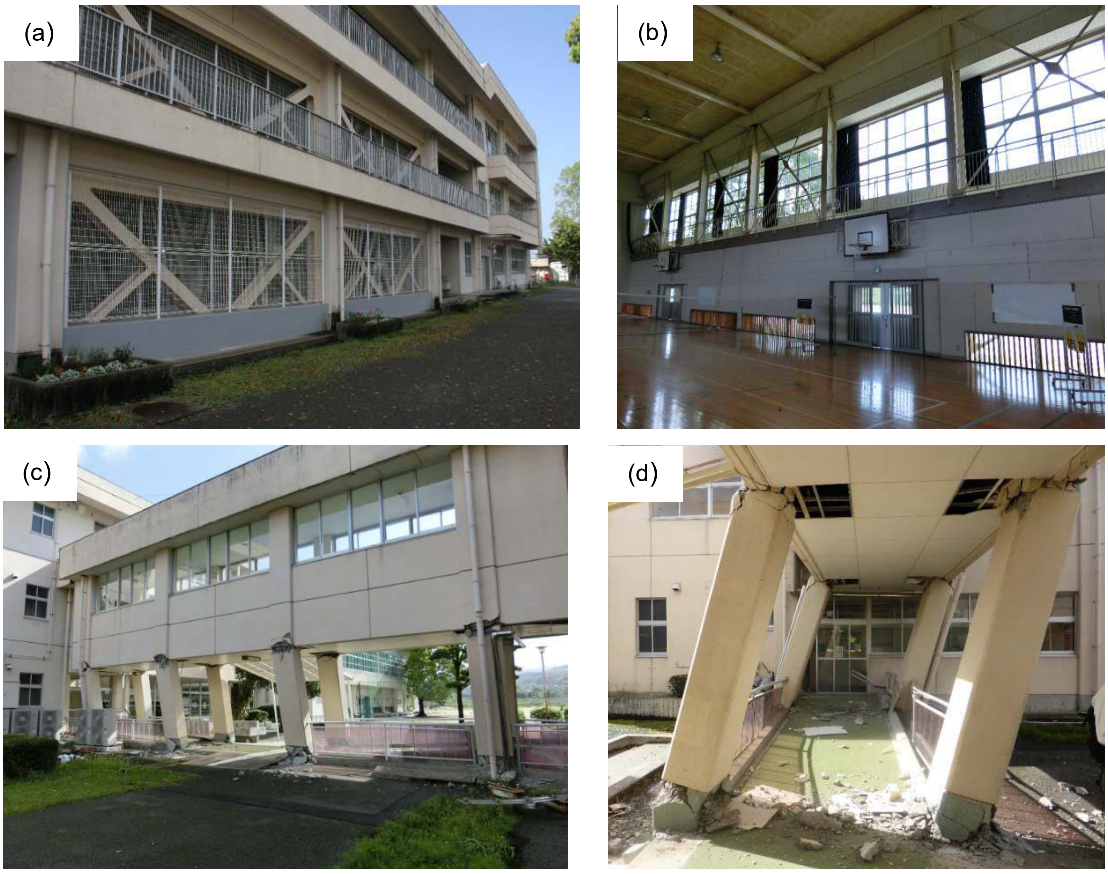

**Figure 4.12** Mashiki Junior High School: (a) RC frame retrofitted with steel bracing (undamaged), (b) buckled bracing to the gymnasium structure, (c) significant drift of link corridor, and (d) detailed picture of the same link corridor (Tajiri et al., 2016).

**Figure 4.13** shows a municipality-run nursery (previously an elementary school) in the Kawayo district of Minami Aso Village which comprised three RC frame blocks. The building frames were very regular and the RC structure was generally exposed. At the time of the visit, the buildings were in use as a disaster management centre instead of nursery. One of the buildings had been yellow-tagged but was still in use for storage of emergency supplies. The school playgrounds had been used for gathering debris from damaged buildings. The only visible external damage to the building was to a movement joint between two of the blocks (**Figure 4.13b**). Apart from this the exposed RC frames did not show earthquake damage, but appeared to be in a somewhat dilapidated state.

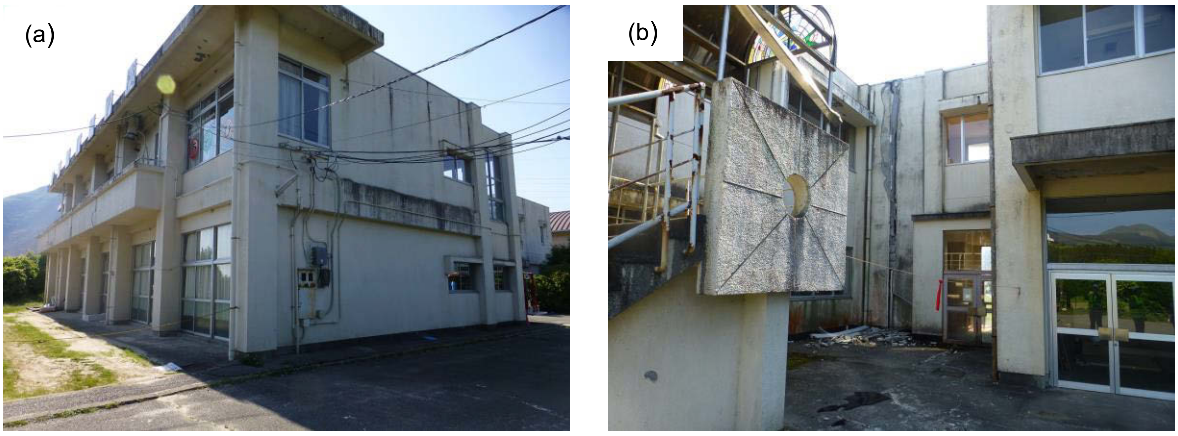

**Figure 4.13** Minami Aso Village Nursery: (a) regular RC frame construction and (b) damage to a movement joint between blocks (yellow-tagged).

The EEFIT also visited the Kumamoto City Hospital. News reports (Asahi Shimbun, 2016b) had stated that this hospital was forced to evacuate patients following the earthquakes due to damage to ceilings and walls (mainly non-structural components). At the time of the visit, the hospital staff were working in the building, but the building did not appear to be in full use. The team was not permitted to survey inside the building. From the outside, damage could be seen to the façades. The building appeared to be a RC frame with age of 20 to 40 years. There was no visible earthquake damage to the exposed RC structure, but the building appeared generally in a dilapidated state. The partial occupation of the building suggested that it was not in a hazardous state, but had lost its functionality.

### 4.7 Damage to buildings in the city centre of Kumamoto

The city centre of Kumamoto (**Figure 4.14**) experienced lower intensity of shaking than Mashiki Town, however accelerations were still considerable (**Figure 4.15**; note: the location of the KMM006 station is in the Higashi (Eastern) Ward, see **Figure 4.1** close to the Futagawa Fault). The shaking intensity in the city centre was registered as 6+ on the Japan Meteorological Agency's (JMA) intensity scale, which is roughly equivalent to IX to X on the Modified Mercalli Intensity Scale.

Typical building stock in the city centre is medium- to high-rise. The city does not have super tall buildings; very few buildings exceed 60 m high, which is a threshold in the Japanese building code above which analyses and approval requirements become more onerous.

Not many red-tagged buildings were seen during the damage survey in the city centre. The team observed some damage to cladding and spandrel walls (**Figures 4.16a** and **4.16c**), some minor damage at ground level (**Figure 4.16b**), and to contents and systems. For instance, a tall hotel car elevator did not have visible damage to structure or cladding, but the internal workings of the elevator and cars were heavily damaged (**Figure 4.16d**).

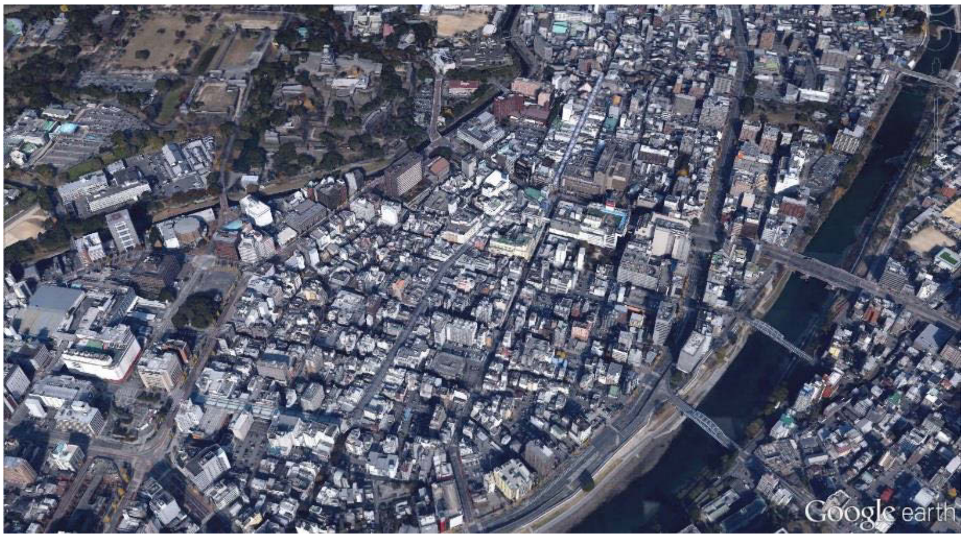


**Figure 4.14** Aerial view of Kumamoto downtown and Kumamoto Castle (image source: Google Earth).

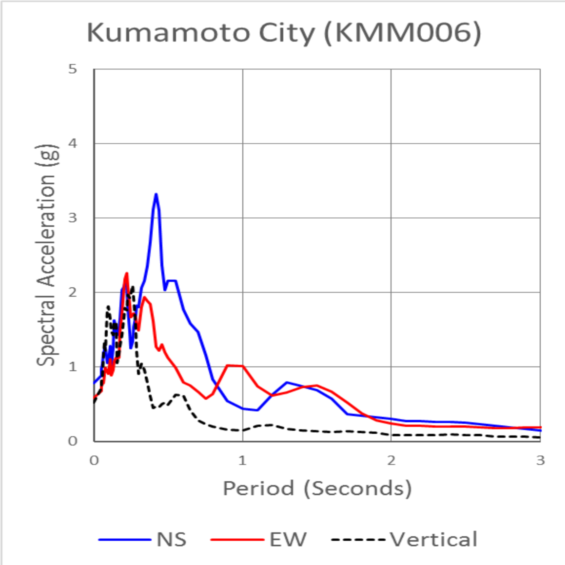


**Figure 4.15** Measured 5%-damped spectral accelerations in Kumamoto City (KMM006).


**Figure 4.16** Building damage in Kumamoto city centre: (a) damaged cladding being repaired, (b) buildings next to castle moat (ground damage), (c) shear cracking to façade, and (d) damage to contents and systems of a car elevator tower.

## 4.8 Damage to traditional buildings

### 4.8.1 *Kumamoto Castle*

Kumamoto Castle is a large complex of defensive earthworks and timber buildings (**Figure 4.17a**), originally dating from 1467 CE. The castle suffered damage to the steep, stone-faced earthworks, which collapsed at a number of locations. The main castle keep is a concrete reconstruction which was built in 1960 (**Figure 4.17b**). Minor damage could be seen to the timber ornamentation of the keep, but there was no visible lean or collapse. In some cases, the damage to the earthworks led to the collapse of timber structures on top of them. The team was able to observe the perimeter of the complex, including the north-eastern corner where a significant ground collapse had occurred, and the corner timber structure had collapsed to the bottom of the embankment and destroyed a shrine underneath (**Figure 4.17c**). The embankments are steep angled and faced in stone. In areas where collapse had occurred, it could be seen that the stone was generally unmortared. Material within the embankment generally looked granular with low cohesion (**Figure 4.17d**).

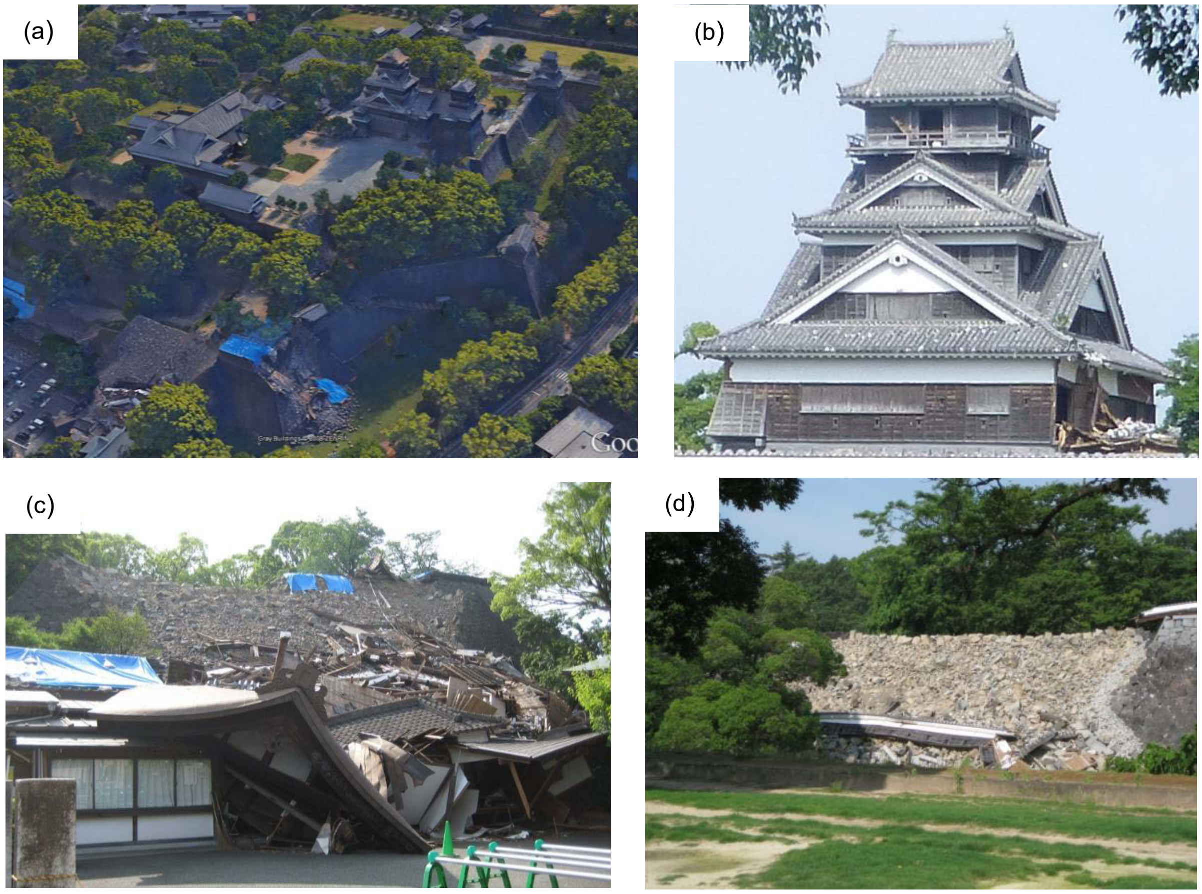


**Figure 4.17** Damage to Kumamoto Castle: (a) aerial view from northeast (image source: Google Earth), (b) main building, (c) north-western corner collapse, and (d) south embankment collapse.

### 4.8.2 *Aso Shrine*

Aso Shrine is located to the north of Mount Aso. The shrine is a complex of timber buildings. The central structures of the temple complex had all suffered storey collapse. The timber roofs were generally still intact, but the roofs were now at ground level because of partial or complete collapse of supporting walls and posts. The roofs were of thick construction, making them very heavy despite the relatively light density of supporting timber material. It was notable that despite significant collapse the roof structures had held their form (**Figure 4.18a**). Photographs of the shrine buildings before the collapse showed open-sided buildings supported with posts and with very few cross walls to provide lateral stability (**Figure 4.18b**).

(a) (b)

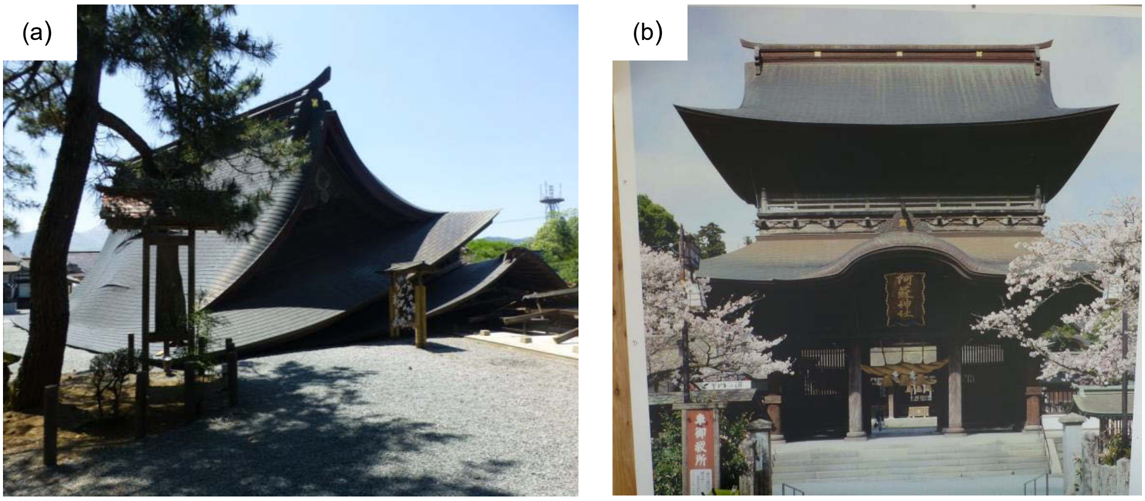

**Figure 4.18** Damage to Aso Shrine: (a) collapsed entrance structure and (b) photograph of the same structure prior to the earthquakes.

### 4.8.3 *Concrete temples*

In Mashiki Town, two examples of concrete temple structures were seen. These had both suffered heavy damage. The form of the concrete temples mimicked the timber pagoda, having circular RC corner columns, connected to RC beams. The heavy concrete roof structures, poor detailing, and insufficient strength of column heads appeared to have contributed to the partial collapse. The structures did not have clear ductile stability systems. **Figure 4.19** shows a temple close to the Mashiki Post Office. This building did not collapse during the foreshock but only suffered noticeable damage; it then had collapsed during the mainshock.

**Figure 4.19** Damage to a concrete temple in Mashiki Town: (a) a view from the eastern side and (b) failure of a column head at the north-western corner.

### 4.9 Systematic damage survey in Mashiki Town

The EEFIT carried out a systematic damage survey of 277 properties near the Mashiki Town Office (note: a JMA recording station was installed at the Town Office, which recorded the highest ground motions equivalent to JMA intensity of 7 during the foreshock and mainshock). The surveyed properties included timber, RC, and steel buildings. The surveyed areas were also close to the KMMH16 station (**Figure 4.2**). The purposes of the survey were to find spatial patterns in the damage and to gather data on the proportions of damage to different types of buildings.

The surveying was carried out by teams of two people as a walking survey based on external visual inspections of buildings. All properties on both sides of each surveyed street were logged. Information was logged in a simple data form (**Table 4.2**). One or two photographs of each building were taken, and the camera log numbers were used as the building references. GPS cameras were used, however the use of an independent GPS tracker in parallel was found to provide more accurate locating. These references were also marked onto a large scale map printed from Google Map, which included building outlines. Building damage severity was logged on a scale from 0 to 5, with 5 representing collapse. The earthquake damage grades are similar to the EMS-98 guidelines (Grünthal, 1998). **Figure 4.20** shows examples of building damage classifications from the survey. Prior to surveying, the teams carried out a sample of surveys all together as a large group in order to correlate interpretation of the different damage levels.

**Table 4.2** Damage survey data collection form.

| Camera ref | Building use | Structure/material type | No. of storeys | Damage grade | Comments |
|---|---|---|---|---|---|
| 797 | Shop | RC | 2 | 0 | Post Office; Minor ground movement |
| 798 | Shop | Steel | 1 | 0 | Supermarket |
| 803 | House | Timber | 2 | 2 | - |
| 800 | Hospital | Concrete | 2 | 1 | - |
| ⋮ | ⋮ | ⋮ | ⋮ | ⋮ | ⋮ |


**Figure 4.20** Examples of surveyed timber buildings in Mashiki Town: (a) damage grade 1 or 2, (b) damage grade 3, (c) damage grade 4, and (d) damage grade 5.

The results of the building damage survey in Mashiki Town are shown in **Figure 4.21**. Generally, newer timber houses as well as RC and steel buildings performed better than older timber houses. Houses in the south of the Mashiki Town Office were more severely damaged than those in the north, noting that the southern part of the surveyed areas was an older settlement. The geographic trend can be seen more clearly in **Figure 4.22**, which shows the same information filtered to timber buildings only, which was the dominant structural type. For the steel buildings (square markers in **Figure 4.21**), a trend of higher damage on Road 28 than Road 235 can be observed. The differences of the damage extent in the northern and southern areas may also be attributed to geological conditions of the two areas (approximately, Road 28 is a boundary between the volcanic sediments and the river terrace deposits; Seamless Digital Geological Map of Japan, 2016). Another important factor appeared to be the proximity to the Akitsu River, where severe geotechnical damage to bridges and embankments had occurred (Section 5). Therefore, at the local scale, micro-zonation of soil types and geomorphological features may have been useful for evaluating seismic risk potential in this region a priori.

**Figure 4.23** shows damage according to the structural/material type. It can be seen that RC buildings performed better than steel and timber buildings. Timber buildings were well distributed across the damage classifications, while steel frame buildings were more concentrated towards the two ends of the damage grade. It should be noted that all of the steel buildings were low-rise with a maximum of four storeys. **Figure 4.24** shows damage according to the number of storeys for steel and timber buildings. For the steel buildings, a significant trend can be seen of higher vulnerability of multi-storey buildings. For the timber buildings, however, the number of storeys did not appear to be a major differentiating factor in vulnerability.

It is important to clarify the limitations of the damage surveys conducted by the EEFIT. A systematic process is required to ensure that random samples of damaged and undamaged buildings are surveyed. There is a risk that damage surveyors can be drawn towards logging more damaged buildings. This bias can be resisted by using a systematic sampling process. For the Mashiki damage survey, a random sample was enforced by requiring that every building on a specific street was logged. The process could have been improved in a number of ways:

- While the logging of every property was enforced, the surveyors were free to choose which streets to survey within the survey area. This could be improved by preselecting the route to ensure that surveyors are not attracted towards the more damaged streets.
- Logging of every property is resource intensive, meaning that the area that can be covered is limited. A wider geographic spread could be obtained by surveying, for instance, every fifth property instead of every property.
- The rule of inspecting every building or every fifth building can be difficult to interpret in cases where there are double layers of buildings behind the street-side properties. Establishing a clear policy about non-street-side properties before the survey would help ensure a consistent approach.
- Another method of a random sampling would be to preselect the sample set from maps using a random method before the survey. This could have been done for the Mashiki area, which was found to be well represented in Google Map in terms of building outlines. The OpenStreetMap was also well represented due to a Missing Maps project prompted by the Kumamoto earthquakes (http://tasks.hotosm.org/project/1791). It is likely that future major earthquakes will also be supported by the Missing Maps project, which may be of benefit to future EEFIT missions, particularly in areas where commercial mapping websites contain limited data.

Some other limitations of the Mashiki damage survey were:

- Some buildings could not be recorded clearly, either because they were covered by weatherproofing or because buildings had been removed. However, there were relatively few empty plots in Mashiki Town; the impression was that very few buildings had been removed at the time of the survey.
- Differentiating between the different damage grades can be challenging, particularly at the low end of the damage scale (e.g. grade 1 or 2). This issue was partly mitigated by ensuring a clear photo log of all the buildings surveyed to enable retrospective review and moderation.

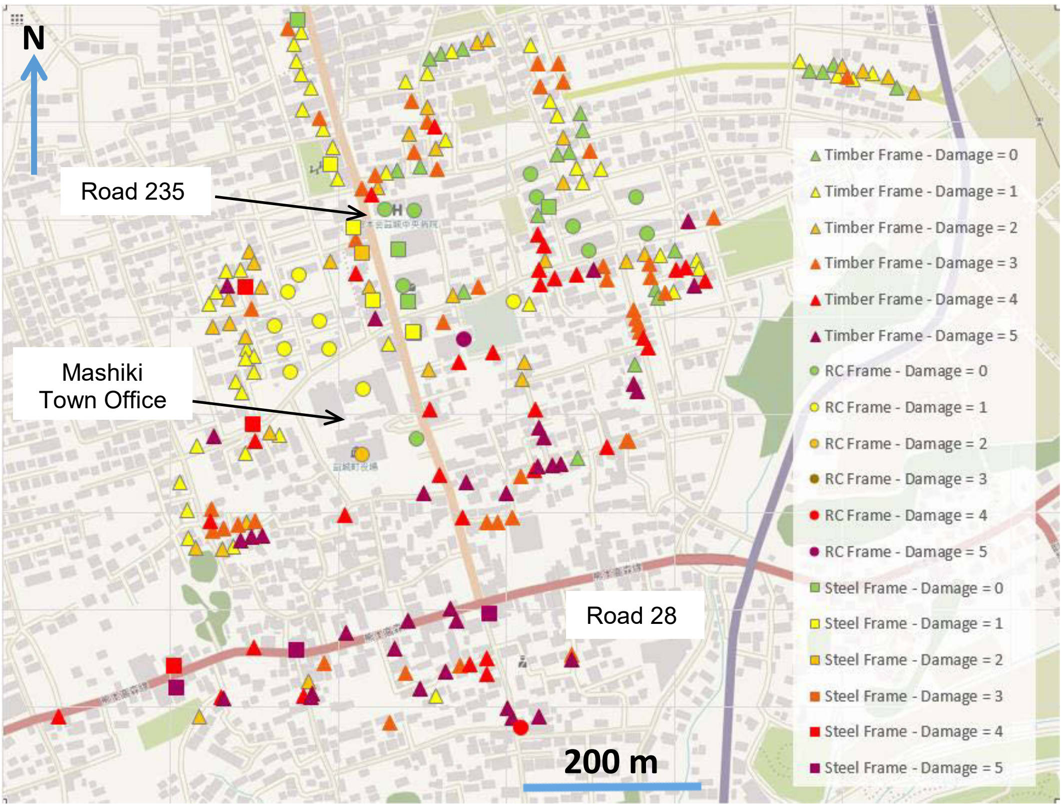


**Figure 4.21** Damage survey results in Mashiki Town. The base map was obtained from OpenStreetMap.

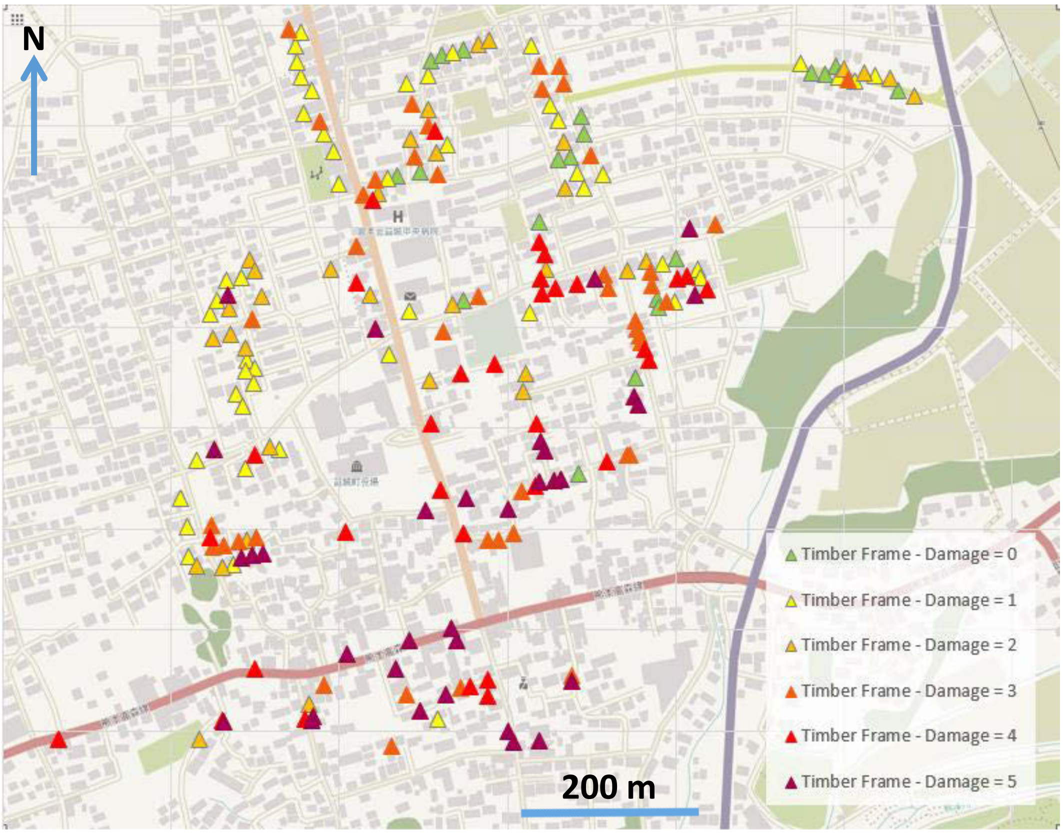


**Figure 4.22** Damage survey results for timber buildings only in Mashiki Town. The base map was obtained from OpenStreetMap.

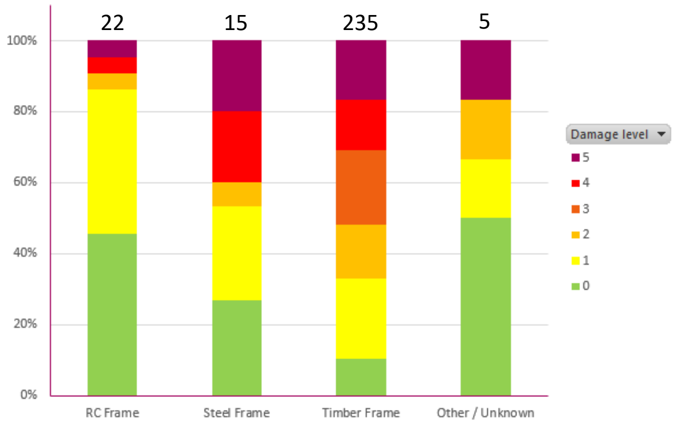


**Figure 4.23** Proportion of damaged buildings according to the structural material and their damage grade in the EEFIT survey in Mashiki Town.

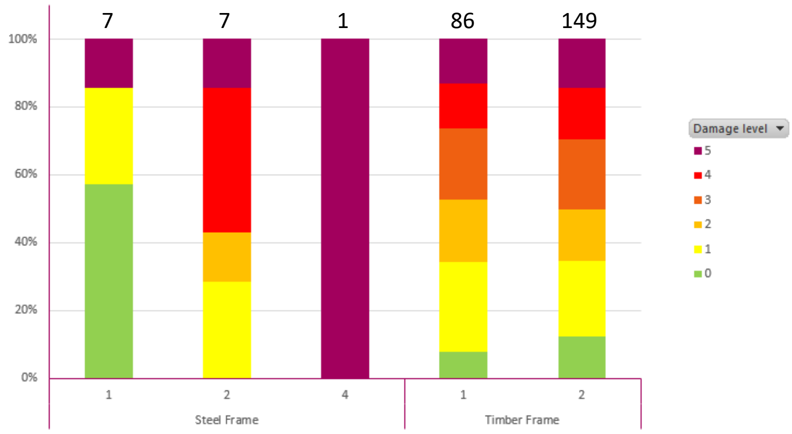


**Figure 4.24** Proportion of damaged steel and timber buildings according to the number of storeys and damage grade.

## 4.10 Conclusions on the building damage

The 2016 Kumamoto earthquakes highlighted certain vulnerabilities in Japanese building stock that had already been reported upon following the 1995 Kobe earthquake. These include poorly detailed pre-1981 RC frame buildings, soft-storey vulnerabilities, and poor performance of old timber houses. These issues have been resolved in new building codes, but are still critical to some older buildings. The seismic zone classification for Kumamoto was lower compared with other parts of Japan where historical seismicity has been more active. On the other hand, ground motions experienced in near-fault regions were quite intense and have exceeded the seismic design ground motion level in the region.

Since the Kobe earthquake there have been efforts to encourage retrofit or replacement of vulnerable structures, and the EEFIT observed evidence of strengthening programmes having been completed to school buildings and government buildings. Strengthening of privately owned existing structures is not currently mandatory, but recent changes to the law may indicate a shift towards future mandatory regulations. There were also some newer timber houses which performed poorly, which may be due to a combination of extreme loading beyond the code expectations and poor construction. There were a number of examples of hospitals losing operational capacity due to failures of non-structural components and systems. This is also likely to be an area of future attention and improvement.

### 4.11 References

Asahi Shimbun (2016a). Quakes leave 134 school buildings in Kumamoto at risk of collapse (26 April 2016). http://www.asahi.com/ajw/articles/AJ201604260060.html.

Asahi Shimbun (2016b). Healthcare takes a hit as quakes wreck hospitals in Kumamoto (19 May 2016). http://www.asahi.com/ajw/articles/AJ201605190057.html.

Earthquake Engineering Field Investigation Team (EEFIT) (1997). A field report on the Hyogo-Ken Nanbu (Kobe) Earthquake of 17 January 1995. Accessed on 15 December 2016 at https://www.istructe.org/downloads/resources-centre/technical-topic-area/eefit/eefit-reports/hyogo-ken-nanbu-kobe.pdf.

Earthquake Engineering Field Investigation Team (EEFIT) (2011). A field report on the $M_W$9.0 Tohoku earthquake and tsunami of 11th March 2011. Accessed on 15 December 2016 at https://www.istructe.org/getattachment/resources-centre/technical-topic-areas/eefit/eefit-reports/field-report-tohoku-japan-11-march-2011.pdf.aspx.

Earthquake Engineering Field Investigation Team (EEFIT) (2013). A return mission report on recovery two years after the 2011 Tohoku earthquake and tsunami. Accessed on 15 December 2016 at https://www.istructe.org/getattachment/resources-centre/technical-topic-areas/eefit/eefit-reports/EEFIT-Japan-Recovery-Return-Mission-2013-Report-(1).pdf.aspx.

Goda, K., Campbell, G., Hulme, L., Ismael, B., Ke, L., Marsh, R., Sammonds, P., So, E., Okumura, Y, Kishi, N., Koyama, M., Yotsui, S., Kiyono, J., Wu, S., and Wilkinson, S. (2016). The 2016 Kumamoto earthquakes: cascading geological hazards and compounding risks. *Frontiers in Built Environment*, **2**, 19, doi: 10.3389/fbuil.2016.00019.

Grünthal, G. (1998). European Macroseismic Scale 1998 (EMS-98). *Centre Européen de Géodynamique et de Séismologie*, Luxembourg, 99 p.

Ishiyama, Y. (1989). Japanese seismic design method and its history. In: *Proceedings of the Third U.S.-Japan Workshop on the Improvement of Building Design and Construction Practices*, Tokyo, Japan, 55–64.

Kuramoto, H. (2006). Seismic design codes for buildings in Japan. *Journal of Disaster Research*, **1**, 341–356.

Japan Building Disaster Prevention Association (JBDPA) (2001). Standard for seismic evaluation and guidelines for seismic retrofit of existing reinforced concrete buildings. Tokyo, Japan, 874 p.

Nakashima, M., and Chusilp, P. (2003). A partial view of Japanese post-Kobe seismic design and construction practices. *Earthquake Engineering and Engineering Seismology*, **4**, 3–13.

Okazaki, K. (2008). Institutional mechanism of building code implementation in Japan. Accessed on 15 December 2016 at http://www.uncrd.or.jp/hyogo/hesi/pdf/nepal08/training/okazaki2.pdf.

Seamless Digital Geological Map of Japan (2016). Access on 15 December 2016 at https://gbank.gsj.jp/seamless/index_en.html.

Tajiri, S., Kusuhara, F., Kabeyasawa, T., Trivedi, S., and Hun-Feng, H. (2016). Preliminary reconnaissance report on building damage of the 2016 Kumamoto Earthquake. Accessed on 15 December 2016 at http://peer.berkeley.edu/pdf/KumamotoEQ.pdf.

Takeda, K., Tanaka, K., Someya, T., Sakuda, A., and Ohno, Y. (2013). Seismic retrofit of reinforced concrete buildings in Japan using external prestressed concrete frames. *PCI Journal*, **58**, 41–61.

Tasdemir, E., and Paul, N. (2016). Overview of damage to reinforced concrete buildings in Kumamoto. EERI Clearing House. Accessed on 15 December 2016 at http://www.eqclearinghouse.org/2016-04-15-kumamoto/2016/05/06/overview-of-damage-to-reinforced-concrete-buildings-in-kumamoto/.

# 5 Infrastructure Damage and Geotechnical Failures

There was extensive damage to infrastructure throughout Kumamoto Prefecture as a result of ground shaking, fault rupture, ground settlement, liquefaction, and slope failure. Most damage was seen close to the Futagawa Fault where ground shaking was strongest and where there was also fault rupture at the surface (Sections 2 and 3). Damage to roads was most prevalent in areas of higher relief where lateral spread and slope failure occurred above and below the roads. Damage to bridges was also predominantly in areas of high relief, which coincides with being in close proximity to the Futagawa Fault. The EEFIT visited a number of locations to inspect damage to bridges and other infrastructure (**Figure 5.1**). Damage to over-ground utilities was seen in most areas where there was also damage to buildings and infrastructure in Kumamoto City, Mashiki Town, Minami Aso Village, and Nishihara Village (Section 4).

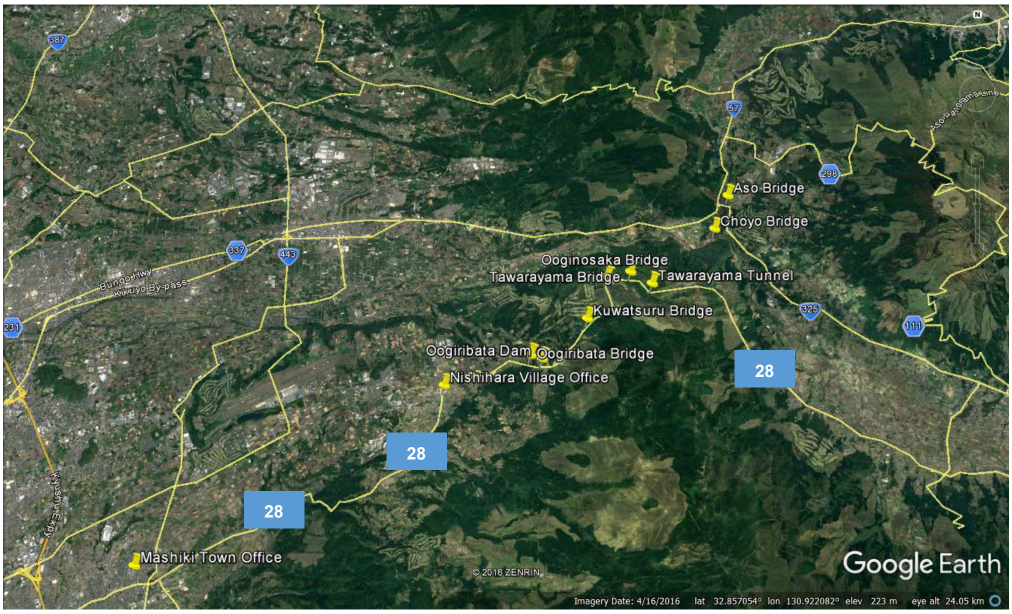


**Figure 5.1** Location map of damaged bridges or other infrastructure and of ground failures that were visited during the EEFIT mission (image source: Google Earth).

## 5.1 Bridges

There were multiple bridge failures across the Kumamoto region as a result of landslides, fault rupture and ground shaking. Numerous bridges along Road 28, which crossed above or were in close proximity to the Futagawa Fault, were damaged

### 5.1.1 *Oogiribata Bridge*

The Oogiribata Bridge (32.8425ºN, 130.9284ºE), constructed in 2000, is an approximately 250-m long 5-span steel girder bridge with two large concrete columns on piers. The body of the bridge remained structurally intact but the foundation connection failed, displacing the bridge from the road. The bridge appeared to have been moved by the earthquakes (**Figure 5.2**). Closer inspection of the bridge piers and deck-pier connections identified no cracking or leaning of the pier columns, indicating that a giant landslide immediately south of the bridge was not the cause of the failure. The rubber metal bearings at the foundation connection moved 1.2 m towards the north, suggesting that the seismic loading during the Kumamoto earthquake exceeded the design loading for these bearings (**Figure 5.3**). Images from Google Earth show that the slope failure and bridge displacement occurred during the mainshock on 16 April. The bridge appears to have replaced an old road that followed the topography across the slope which insinuates that slope stability was a concern prior to the seismic event.

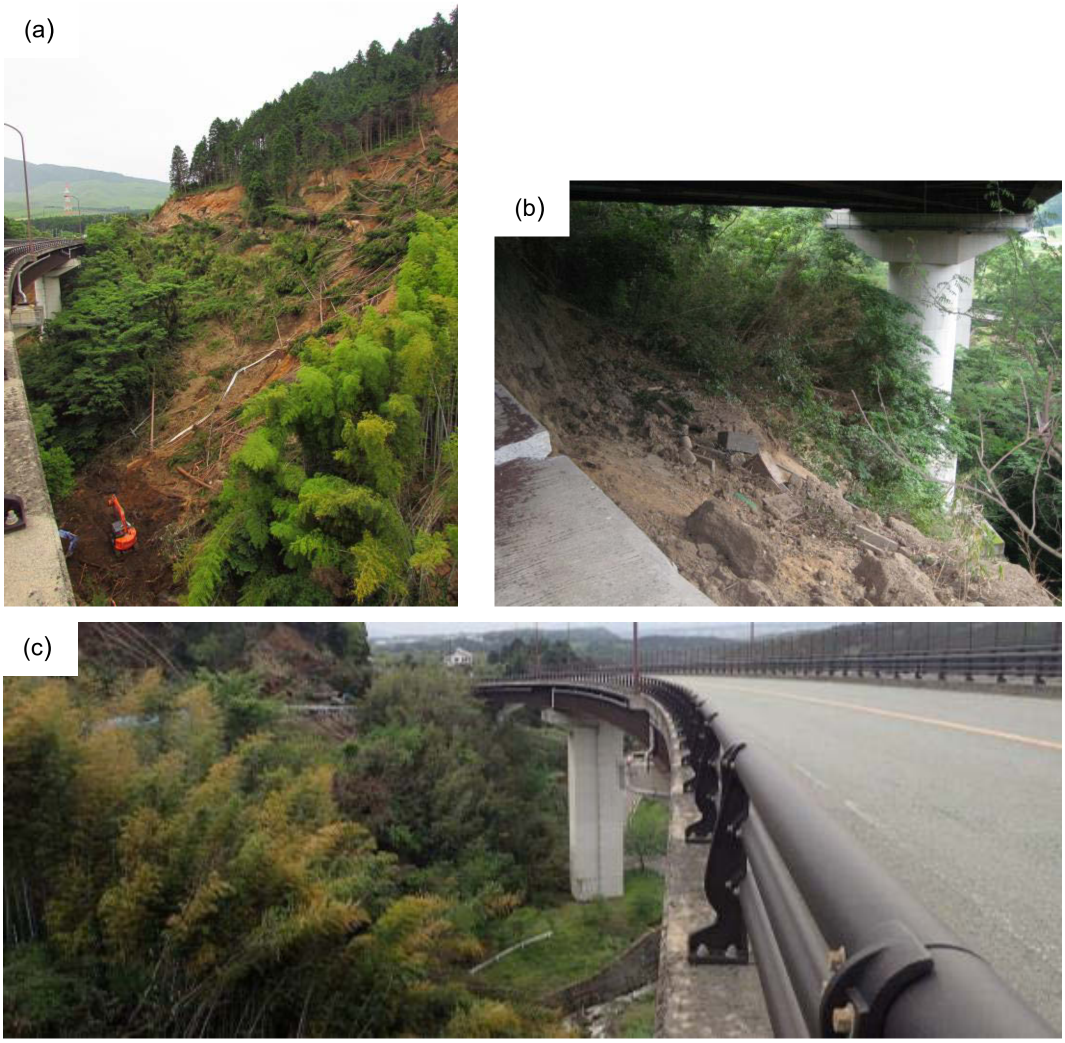


**Figure 5.2** Interaction between the landslide and bridge abutments of the Oogiribata Bridge: (a) view from the western end of the bridge looking east at the toe of the landslide, (b) looking west at the eastern pier from the underside of the bridge on the eastern end, and (c) looking west at the western pier (Ikeda et al., 2016).

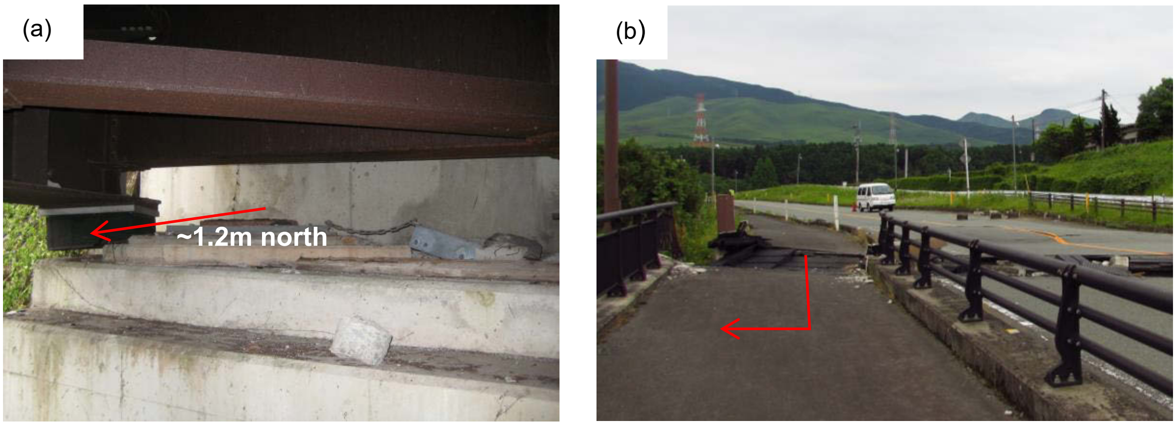


**Figure 5.3** Failure of the bearings beneath the Oogiribata Bridge: (a) view of the failed bearings from the underside of the bridge and (b) view from the top of the bridge.

### 5.1.2 *Kuwatsuru Bridge*

The Kuwatsuru Bridge (32.8516ºN, 130.9454ºE) is a 150-m (approximately) long cable-stayed bridge crossing a NW-SE low relief and heavily vegetated valley. The bridge is supported by one large concrete column. The damage observed was similar to that of Oogiribata Bridge; the road surface and barriers on the bridge remained relatively undamaged but there was failure at the foundation connection. Vertical displacement at the foundation connection was caused by settlement of the road and abutment rather than uplift of the bridge (**Figure 5.4**). Google Earth imagery identifies that the bridge withstood the foreshock on 14 April but failed during the mainshock on 16 April.

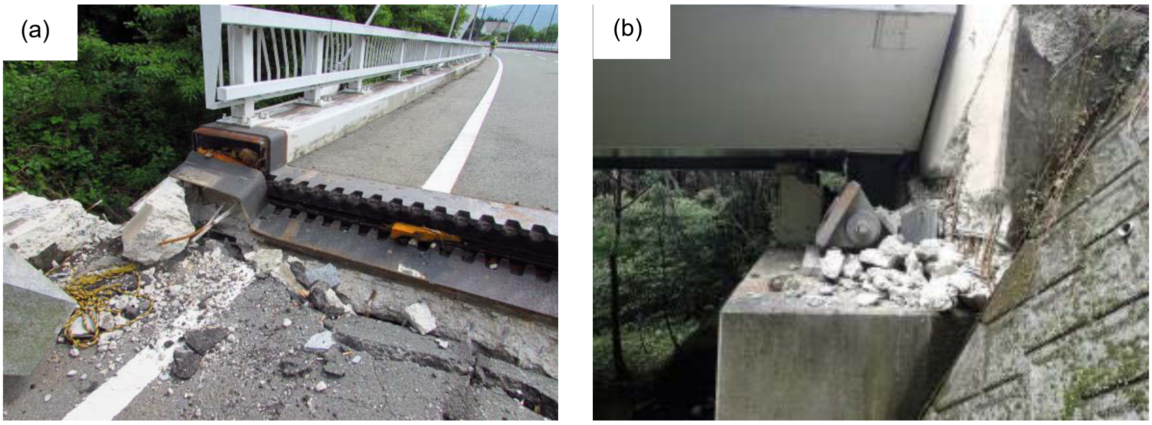


**Figure 5.4** Foundation connection damage of the Kuwatsuru Bridge: (a) failure of deck-abutment connection at the eastern end and (b) damage to the bearing at the eastern end (Ikeda et al., 2016).

### 5.1.3 *Ooginosaka Bridge*

The Ooginosaka Bridge (32.8622ºN, 130.9516ºE) is a 130-m long cantilever bridge on Road 28 that crosses an EW trending valley. The bridge road surface remained undamaged but the foundation connection experienced bilateral shearing (**Figure 5.5**). The abutments remained intact but the bearings were damaged as a result of this bilateral movement. Photos from Ikeda et al. (2016) show similar oblique shearing in the bearings at the top of the concrete columns.

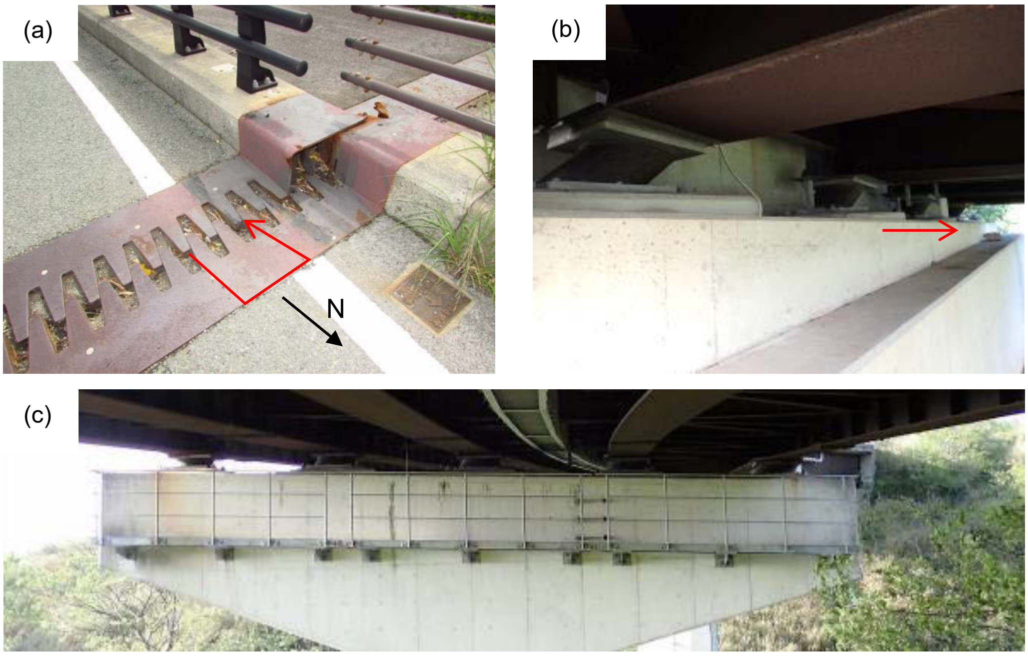


**Figure 5.5** Foundation connection damage of the Ooginosaka Bridge: (a) surface connection at the northern end; the relative movement occurred in N-S and E-W directions, (b) underside of the northern bridge abutment showing oblique shearing of the bearings (Ikeda et al., 2016), and (c) very little damage to the bearings at the top of the concrete columns (Ikeda et al., 2016).

5.1.4 *Tawarayama Bridge*

The Tawarayama Bridge (32.8634ºN, 130.9599ºE) is a 150-m long cantilever bridge with one large concrete column crossing a SSE-NNW trending, heavily vegetated valley. There were both horizontal and vertical displacements between the bridge and the road as a result of the bearings moving laterally and the embankment failing below the abutment foundations (**Figure 5.6**).


**Figure 5.6** Damaged foundation connections of the Tawarayama Bridge (Ikeda et al., 2016): (a) movement of the bearings at the eastern abutment and (b) damage to the foundations of the abutment of the west end.

5.1.5 *Bridges along the Kiyama River*

Settlements of the flood defence embankments occurred along the Kiyama River, south of Mashiki Town Office and as a result there were vertical displacements between the roads and the bridges. Vertical displacements between the road and bridge were measured by the EEFIT as (**Figure 5.7**):

Bridge 1: 0.48 m at the north-western end & 0.4 m at the south-eastern end
Bridge 2: 0.50 m at the north-western end & 0.6 m at the south-eastern end
Bridge 3: 0.35 m at the north-western end & 0.35 m at the south-eastern end

The embankment fill consisted of gravelly, slightly sandy silt with small amounts of clay. Poorly sorted sediments, if unconsolidated, could be prone to settlements during periods of intense shaking, which could explain the settlements of the embankments flanking the river. The abutments of the bridges 1 and 2 showed minimal signs of cracking and the piers remained intact. The reinforced concrete piers at the bridge 3 were damaged, with the reinforcement bulging and shearing in an approximately NE-SW direction (**Figure 5.7**).


**Figure 5.7** Settlements of flood defences and damage to bridges along the Kiyama River: (a,d) settled embankments relative to the bridge abutments, (b) embankment settlements causing collapse of concrete protection, (c,f) vertical displacement between the road on the embankments and the bridges, and (e) damage to bridge piers (image source: United States Geological Survey and Google Earth).

## 5.2 Tunnels

The Tawarayama Tunnel (32.8601ºN, 130.9646ºE) is a road tunnel (Road 28) 2057 m in length that passes through the caldera wall of Mount Aso (**Figure 5.8**). The tunnel portal in the west is located above the Futagawa Fault and as a result suffered high axial compression forces causing fracturing and collapse of the tunnel wall cladding. The fractures in the tunnel wall and the uplifted drain covers indicate a NEE-SWW compression. The shearing in the tunnel is dipping to the southwest and represents compression of the fault rather than lateral shearing of the Futagawa Fault at this location.

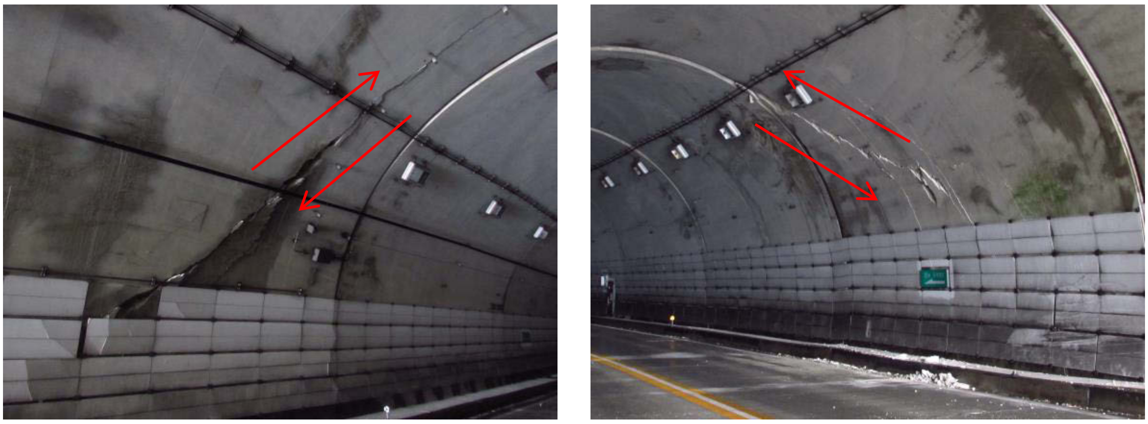

**Figure 5.8** Shearing on the side wall of the Tawarayama Tunnel showing a NEE-SWW compression.

## 5.3 Roads

The majority of road damage observed was either above or close to the Futagawa Fault or in the failed zone of landslides. Vertical displacements of roads were visible in the northern area of Aso Caldera where the fault ruptured at the surface, causing extension and therefore graben like structures on the road surfaces (**Figure 5.9**).


**Figure 5.9** Vertical road displacements in the northern area of Aso Caldera.

There was significant damage along Road 28 between Nishihara Village and Tawarayama Tunnel which is above and in close proximity to the Futagawa Fault (**Figure 5.10**). The straight sections on the road were less damaged compared to the road bends where slope failure above and below the road was common. Compression and shearing features in the road surface were representative of the tectonic stresses and fault rupture (**Figures 5.10a**, **5.10e**, and **5.10f**) as most compression was seen in a NEE-SWW direction and the shearing features trended approximately NE-SW. The connections between road and bridge were zones of weakness and commonly destroyed (**Figure 5.10d**). Slope failures above and below the road caused cracking and lateral movements and bulging of the road, respectively (**Figures 5.10b** and **5.10c**).

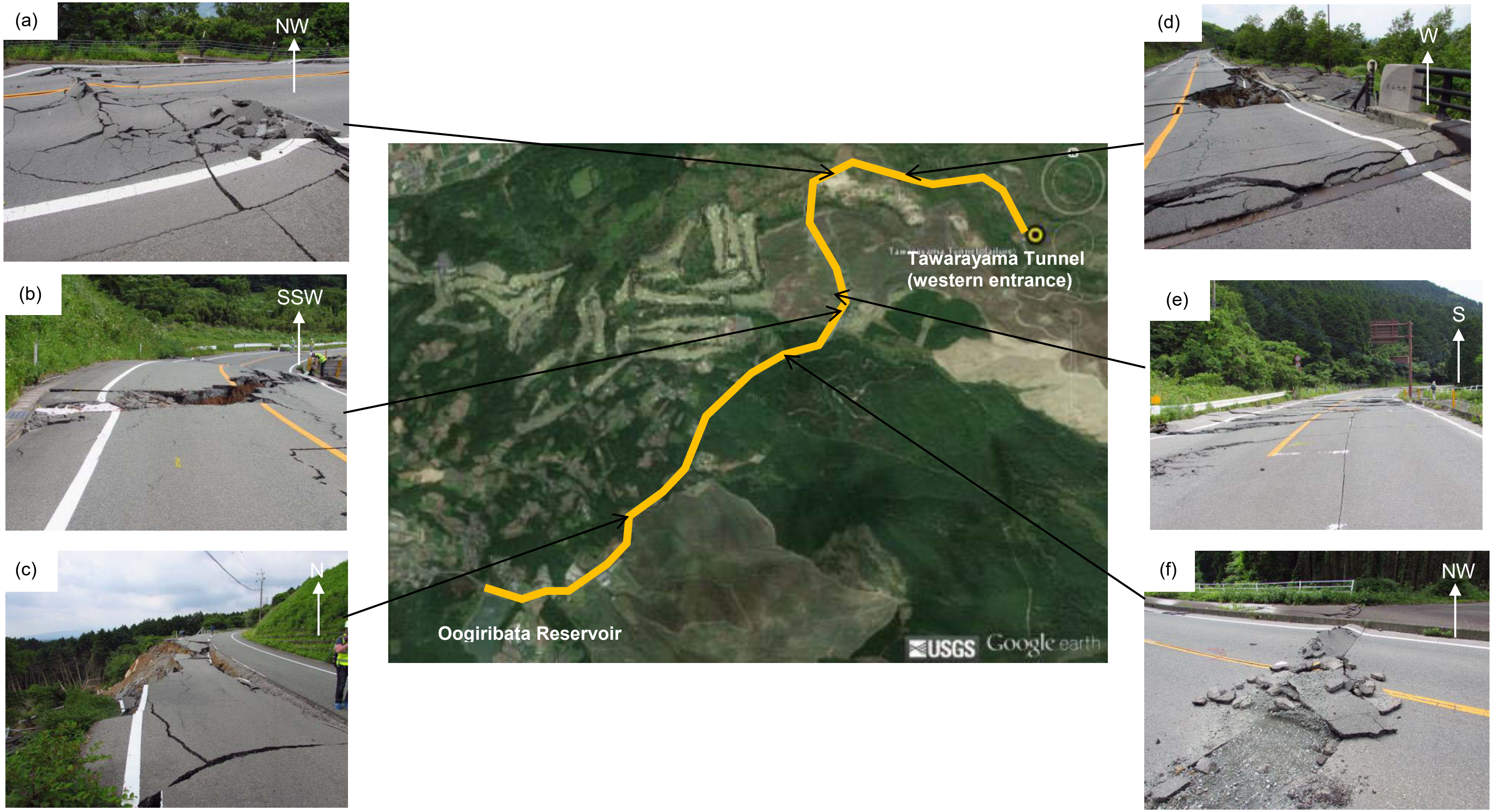


**Figure 5.10** Road damage along Road 28: (a) compression features on the road surface, (b) bulking at the road bend, either caused by compressional fault movement or bulging at the toe of a slope failure, (c) cracking and collapse of the road at the crest of a slope failure, (d) compression features at road-bridge connection and sinkhole, (e) shearing seen on the road surface trending roughly NE-SW, and (f) compression features on the road surface in E-W direction and signs of vertical ground shaking revealed as displaced tarmac cover (image source: United States Geological Survey and Google Earth).

## 5.4 Dams

The Oogiribata Dam (earth-fill; 32.8409ºN, 130.9318ºE) is located along Road 28 just outside of Nishihara Village (**Figures 5.1** and **5.11a**). The dam is located directly above the Futagawa Fault. The retaining walls of the spillway were damaged and tilted significantly; the control gates were not functional (**Figure 5.11b**). As a result, a large volume of water leaked out of the reservoir after the mainshock, however, there were no fatalities/casualties associated with this failure. The failure of the retaining walls appeared to be caused by movement of the soil behind the walls, causing lateral movement and tilting of the structures. Signs of the compression and shearing were evident in the northern and western sides of the dam (**Figures 5.11c** and **5.11d**). Much of the damage showed E-W to NE-SW compression and shearing which is expected when a segment of the Futagawa Fault is cutting NE-SW through the spillway. There was also a slope failure on the eastern side of the dam. This failure was probably caused by the water level change as the reservoir was drained.

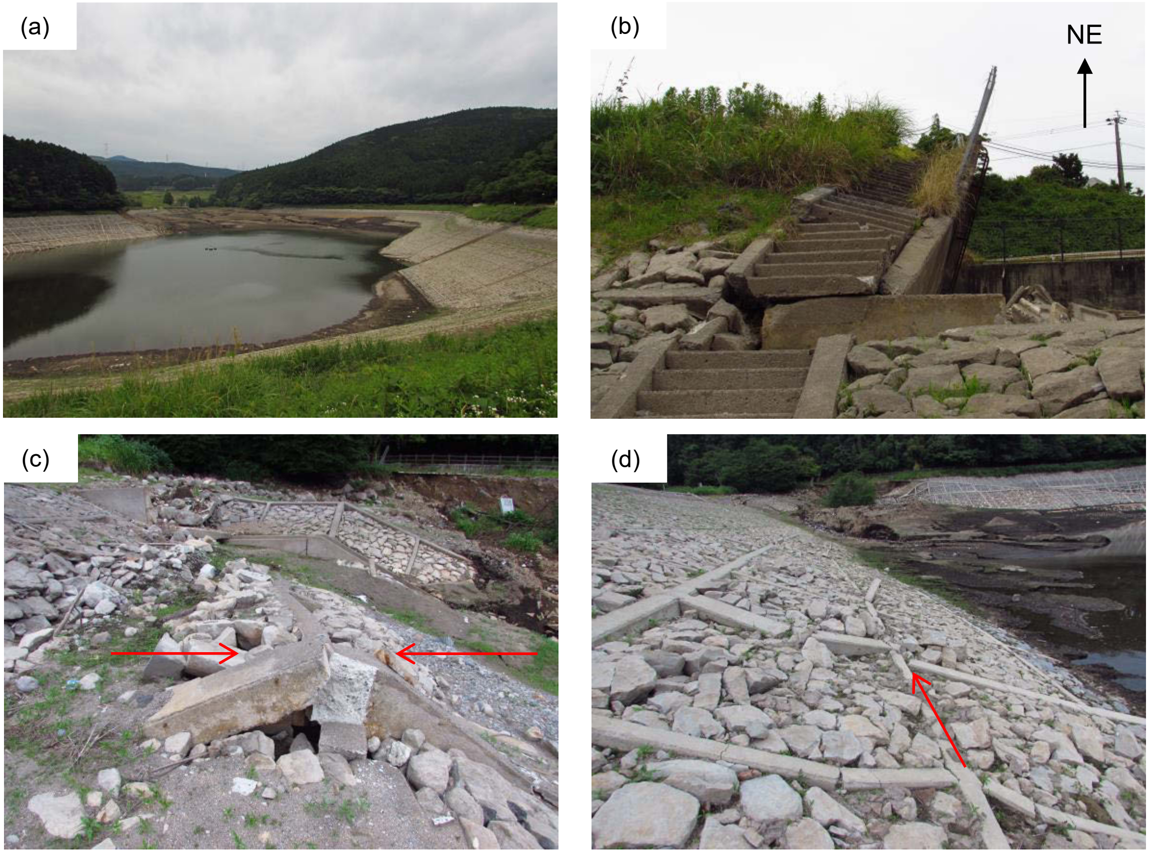


**Figure 5.11** Damage of the Oogiribata Dam: (a) reservoir, (b) failure of the retaining walls at the spillway, (c) compression features in the dam wall showing a NS compression, and (d) shearing features in the dam wall.

## 5.5 Landslides

Multiple landslides have been observed around Aso Caldera, including earth flows, debris flows, slides and slumps (**Figure 5.12**). 10 out of 49 deaths during the Kumamoto earthquakes were caused by landslides. The majority of the slope failures occurred around Aso Caldera and Mount Aso where the relief is high. The slopes are commonly gentle at the base (less than 10°) becoming steeper (>60°) towards the top of the Aso Caldera rim where volcanic vents are also observed (**Figure 5.13**). The upper slopes are generally formed of extrusive igneous rocks covered by a thin layer of residual soil and ash, whilst the gentle lower slopes are mainly mantled by thick layers of residual volcanic soils overlying pyroclastic deposits (**Figure 5.14**). Narrow steep valleys are common in this region and steep-side gorges can be up to 70 m in height, which are also prone to multiple cliff collapse during periods of high rain and seismic activity. The highest density of the landslides is concentrated in the areas where strong shaking was observed. This zone is in close proximity to the Futagawa Fault which intersects with the western Caldera wall.

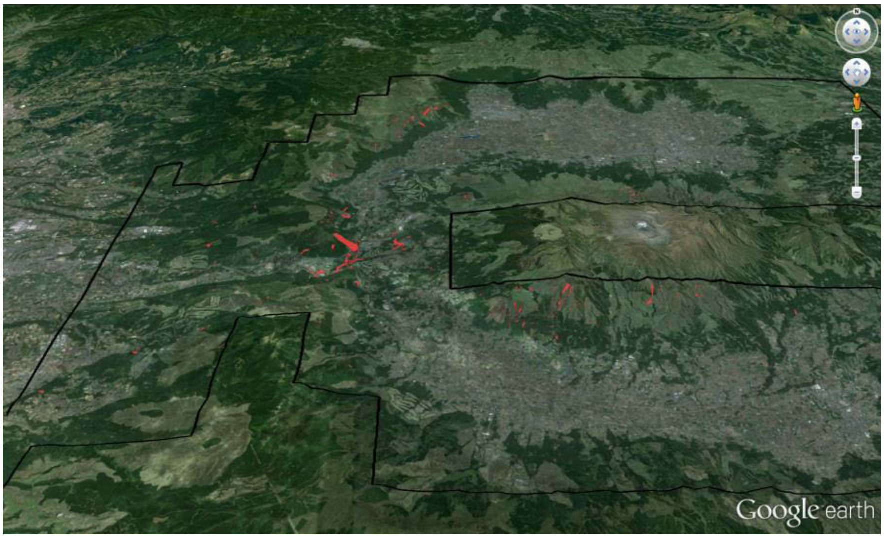


**Figure 5.12** Slope failures around Aso Caldera (highlighted in red) caused by the Kumamoto earthquakes (http://www.slope.dpri.kyoto-u.ac.jp/disaster_reports/2016KumamotoEq/map0418cont_s.jpg; image source: Goole Earth).

**Figure 5.13** Debris flows on the steep sides of Aso Caldera.

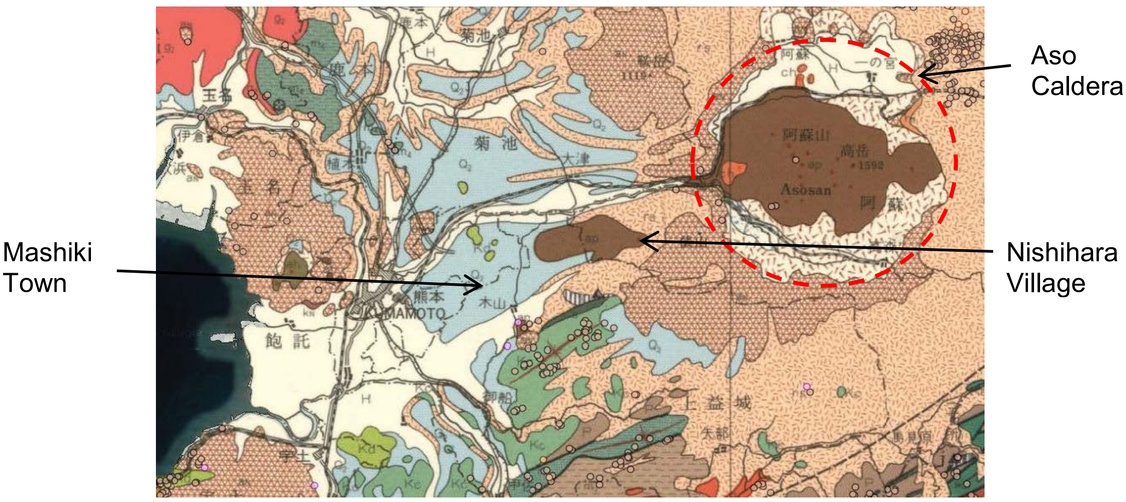


**Figure 5.14** Geology of Kumamoto Prefecture. The brown colours represent extrusive volcanic rocks, whereas the blue, green, and cream colours represent sedimentary deposits (image source: Geological Survey of Japan, https://gbank.gsj.jp/geonavi).

A giant landslide, 950-m long and 200-m wide, occurred near the Aso Bridge (32.8841ºN, 130.9889ºE) in Minami Aso Village (**Figure 5.15**). The failure was a large debris avalanche that originated at the slope crest, depositing hundreds of thousands of cubic metres of rock and soil into the gorge below. Multiple slope failures were also seen downstream. As is shown in **Figure 5.16**, the slide surface was smooth and neat, which implies that the failure was a flow rather than a slide or slump. Several highways nearby (Road 57 and Road 325) were overwhelmed and the Aso Bridge was destroyed. According to local media, one person who was driving near the bridge at the time of the event was killed. At the visit of the Aso Bridge, remotely controlled machinery was seen clearing away the debris and tidying the toe of the failure.

Approximately 1 km downstream of the Aso Bridge, a debris flow was observed near the Choyo Bridge (32.8750ºN, 130.9838ºE). Large rock/soil flowed down the 50º-60º valley side, as shown in **Figure 5.17**. Extensive cracking was observed at the upslope part of the landslide. The Choyo Bridge and ground transition zone showed significant settlement, thereby suffering great damage. This bridge and several highways nearby were blocked at the time of site visit.


**Figure 5.15** Large landslides near the Aso Bridge and Choyo Bridge (image source: Google Map).

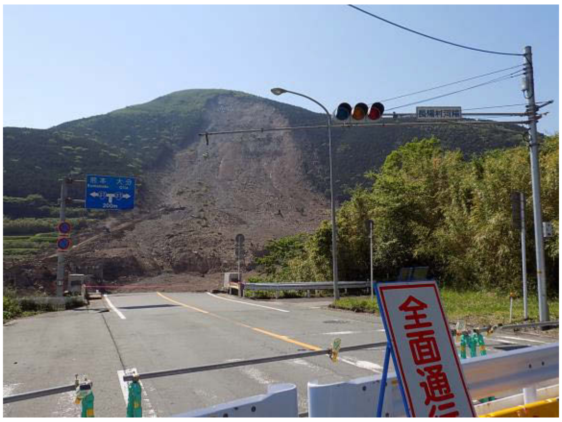


**Figure 5.16** Giant earthflow that destroyed the Aso Bridge.

**Figure 5.17** Debris flow near the Choyo Bridge.

A large landslide was observed at the Oogiribata Bridge (**Figure 5.18**). The landslide was approximately 200-m wide and 100-m long. It was a composite failure consisting of a mixture of toppling (trees tilting downslope), rotational failure (trees tilting upslope), rock falls, and transitional failure/earth flow. A road that was originally following the topography and hugged the valley side had been completely destroyed and carried downslope by the landslide. This suggests that the Oogiribata Bridge had been constructed because slope stability was already a concern. Shotcrete on the slope surface had been displaced down the slope with the soil that had moved beneath it. This is likely because there were no soil nails or rock bolts installed into the slope.

**Figure 5.18** Landslide at the Oogiribata Bridge looking south at the failure from the bridge deck.

A large number of landslides were observed along Road 28. The slopes in this region are mostly gentle, i.e. 10º-30º, which are mainly covered in ash rich volcanic soils, including pumice. Small to moderate avalanche/debris flows were observed along the road. Extensive cracking, ranging from a few centimetres to larger than 1 m at the crest of the landslides, was commonly seen on roads (**Figure 5.19**). As a result of slope failures, several facilities along the highway, such as pipelines, small power switching board stations, and guard rails, have been destroyed (**Figure 5.20**).

**Figure 5.19** Extensive cracking of roads.

**Figure 5.20** Damage to infrastructure facilities near the entrance of the Tawarayama Tunnel.

## 5.6 Slope stability measures and retaining structures

There were a number of slope failure mitigation measures seen across the Kumamoto region, some of which failed and some of which remained standing. At the most south-western closed section of Road 28, various slope stability structures had been put in place. The rock bolts and wire mesh that previously protected from rock falls and slope failures have completely collapsed probably caused by either too much material collapsing behind the wire mesh to exceed the mesh's capacity or due to the rock bolts failing. A concrete retaining wall with vertical and horizontal struts appears to have been distorted but has not failed completely (**Figure 5.21c**). The only slope failure mitigation structure that remained standing was a giant concrete retaining wall (**Figure 5.21b**).

Shotcrete was commonly seen across the region and on most occasions the slope had failed and sheared the shotcrete away from the slope (**Figure 5.22**). There were no rock-bolts or drainage installed with any of the shotcreted slopes observed. It appeared that without drainage and/or rock bolts this slope failure mitigation technique was unsuccessful.

**Figure 5.21** Slope stability measures along Road 28 at the westerly road blockage: (a) rock bolts and wire mesh supporting boulders and other fallen debris from the slope failed, (b) giant concrete retaining wall remained standing although large amounts of debris have fallen behind the structure, (c) deformed retaining wall with vertical and horizontal struts, and (d) cracking on the road at the crest of a slope failure downslope from the road.

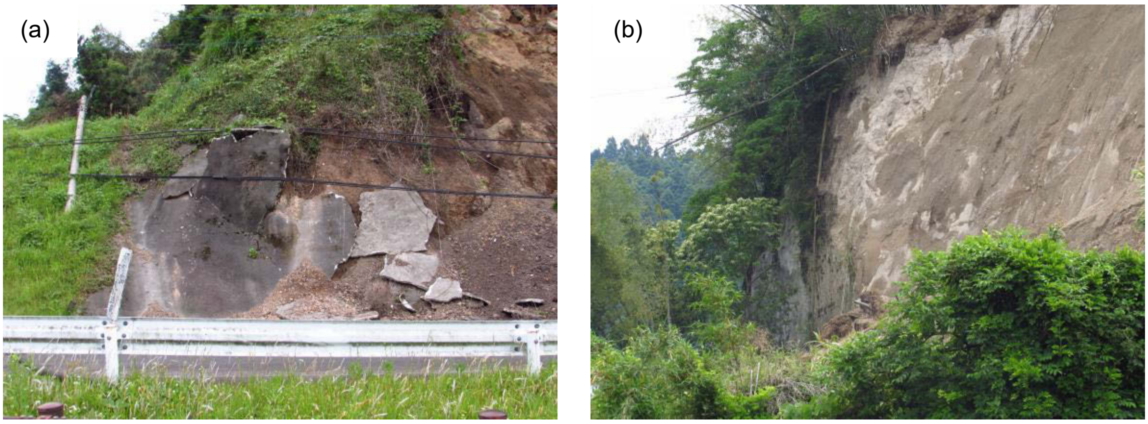

**Figure 5.22** Failure of sprayed shotcrete during slope failure: (a) eastern edge of the giant landslide at the Oogiribata Bridge and (b) near-vertical slope with shotcrete; the shotcrete has fallen but there has been minor failure of the soil.

A number of retaining walls failed in the Kawayo district of Minami Aso Village. Along the main road that passes through the Kawayo district, a concrete retaining wall was tilting towards the north and one of the blocks had completely toppled over (**Figure 5.23a**). The material behind the retaining wall was sandy silt with some clay. This failure likely occurred during ground shaking; soil movement behind the retaining wall causing it to tilt. In one of the side streets, a retaining wall had completely collapsed on the northern facing side while on the southern facing side remained standing. The material behind the retaining wall was sandy silt with small amounts of clay. The cause of the collapse was not apparent as remediation works had already started (**Figure 5.23b**). A large retaining wall in the form of large boulders also failed as a result of slumping of the soil behind the wall (**Figure 5.24**).

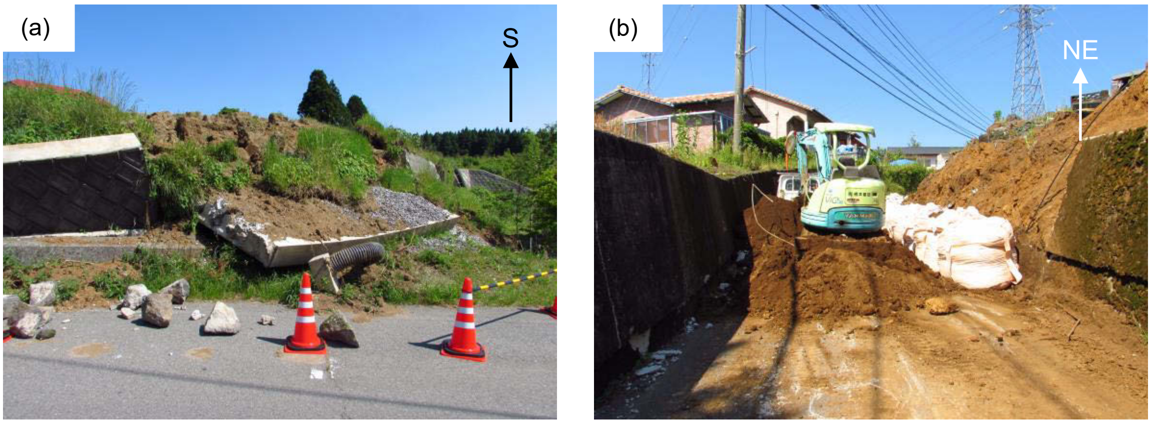


**Figure 5.23** Retaining wall failures in the Kawayo district of Minami Aso Village.

**Figure 5.24** Slumping of the soil behind a retaining wall in the Kawayo district causing it to collapse.

A concrete retaining wall opposite the Mashiki Town Office car park failed, whilst the adjacent retaining structure remained standing (**Figure 5.25**). The neighbouring, intact, retaining wall had in-build drainage, whereas the partly collapsed retaining wall did not. Seepage channels were visible in the soil behind the wall. A combination of these factors indicates that drainage was a major reason for the collapse.

**Figure 5.25** Retaining wall failure in Mashiki Town.

## 5.7 Liquefaction

Liquefaction is caused by the transformation of soil from a solid state to liquid. It occurs when the soil loses its strength during the application of cyclic loading or sudden loading. In saturated sand, excess pore water pressure is generated during the seismic loading, causing a decrease in the effective stress ($\sigma'$): $\sigma' = \sigma - u$, where $\sigma$ is the total overburden stress and $u$ is the pore pressure. In the extreme case, the effective stress becomes zero, and the soil grains lose contact with each other, so that they are floating in the pore water without any confining support from the surrounding soil. As a result, the soil loses its strength and behaves like viscous fluids rather than solid. As a consequence of the Kumamoto earthquakes, liquefaction was observed as sand boils, differential ground settlement, and localised lateral displacement. Liquefaction sites that were visited by the EEFIT during the field work were the Kumamoto Port, Akitsu River (Mashiki Town and Kumamoto City), and Kamiezu Lake.

### 5.7.1 *Kumamoto Port*

The Kumamoto Port (32.7639ºN, 130.5894ºE) is located west of Kumamoto City (**Figure 5.26**). This port is an artificial island built in Ariake Sea. Extensive liquefaction occurred, resulting in ejected sands at various locations (**Figure 5.27**). The possible explanation for sand boils is that, when the pore water pressure is increased during the seismic event, it applies pressure on the above strata causing many cracks and fissures. The pore water pressure is released through these gaps bringing the sands with it. At some locations, there was water on the ground, indicating that the water table was close to the surface. The soil profile for the Kumamoto Port shows that the ground is sand up to 3.5 m from the surface. The estimated peak ground acceleration at the Kumamoto Port was 0.5 *g* (Goda et al., 2016), which is sufficiently large to trigger liquefaction in sand soil layers (Idriss and Boulanger, 2008).

Large sinkholes were observed at different locations in the port which are likely results of poorly compacted fill at the path edges. Risen manhole covers were also observed, causing obstructions for pedestrians (**Figure 5.28**). When the soil beneath the manhole covers liquefies, the pipes lose the support from the surrounding soil. Consequently, under the effect of inherent buoyancy force due to rising pore water pressure, the pipes rise causing the manhole cover to pop up.

Liquefaction-induced settlements were observed at several locations in the port. The measured settlements ranged between 0.1 m to 0.15 m. **Figure 5.29** shows the induced settlement at the entrance of the main hall, inside the Kumamoto ferry terminal. Ground settlement occurs as water dissipates from soil, therefore, subsurface soil losses a large part of its total volume. This is sometimes accompanied by ejected sands which will also reduce the total volume of soil in the subsurface, resulting in settlement. **Figure 5.30** shows the damage at the ferry terminal where an overpass steel bridge was found to be out of service as a result of liquefaction-induced settlement.

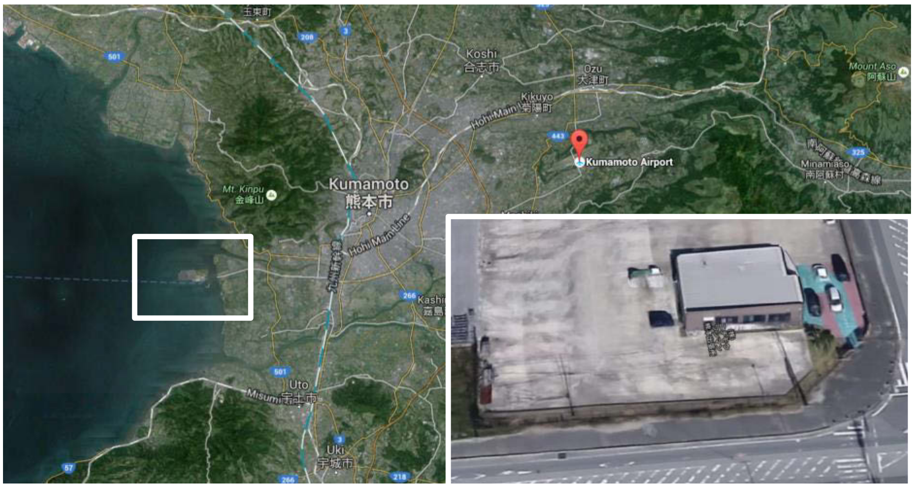


**Figure 5.26** Location of the Kumamoto Port (image source: Google Map).

**Figure 5.27** Sand boils at the Kumamoto Port.

**Figure 5.28** Liquefaction-induced failures at the Kumamoto Port.

**Figure 5.29** Liquefaction-induced failures near the ferry terminal.

**Figure 5.30** Damage to the steel overpass bridge at the ferry terminal due to liquefaction-induced settlement.

### 5.7.2 *Akitsu River*

The Akitsu River runs through Mashiki Town and Kumamoto City as shown in **Figure 5.31**. Liquefaction was observed along the river, where significant damage to the asphalt surface occurred. Within the residential area, polyester bags filled with soil and wrapped with polythene were laid along the embankments as a temporary flood defence (as seen in **Figure 5.7b** along the Kiyama River), indicating that there may have been overall settlement of the area.

Liquefaction was apparent at many locations along the river and signs of ejected sands were observed. As shown in **Figure 5.32a**, sand erupted from the edge of a foundation and footpath. Moreover, a tennis court was completely liquefied, and a large quantity of liquefied soil was apparent at the surface (**Figure 5.32b**). Another type of ground failure was apparent in the area as the ground concave down as shown in **Figure 5.33a**. **Figure 5.33b** shows pavement cracks, resulting in uplifting of manhole covers.

Relative lateral displacement of two bridge slabs was observed at a bridge over the Akitsu River. This failure may have been caused by lateral movement of the bridge abutment (liquefaction was observed close to the bridge), which may be the reason for no damage observed at the second pier (**Figure 5.34**).

Moreover, a high-rise reinforced concrete apartment building, located near the Akitsu River, suffered extensive diagonal shear cracks, especially at the first three floors (**Figure 5.35**), while several signs of liquefaction were observed around the building. A separation between the building's foundation and the main entrance was also observed due to the relative displacement between the building and the ground.


**Figure 5.31** Locations of the Akitsu River (white rectangle) and the Kamiezu Lake (orange rectangle) (image source: Google Map).

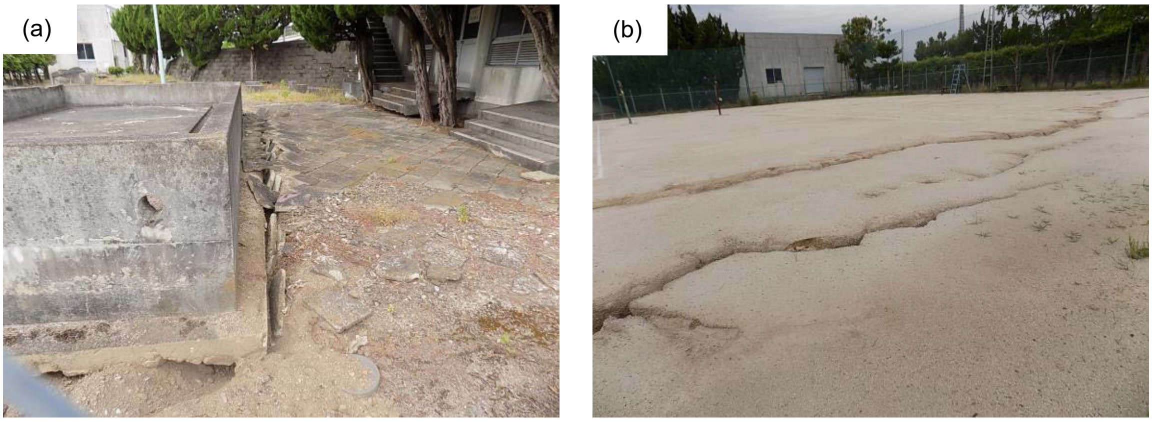


**Figure 5.32** Widespread of liquefaction at: (a) bottom of a foundation and (b) a tennis court.

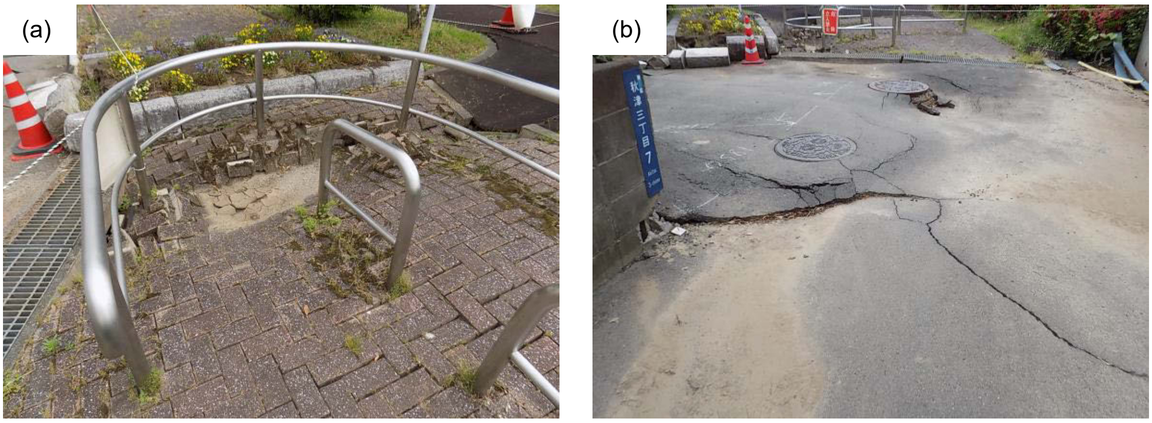


**Figure 5.33** Ground failures due to liquefaction: (a) ground settlement and (b) tension cracks.


**Figure 5.34** Lateral displacement of a bridge along the Akitsu River.


**Figure 5.35** Bearing failure of an apartment building near the Akitsu River.

### 5.7.3 *Kamiezu Lake*

Extensive ground settlements with localised lateral displacement and cracking occurred on the embankments of the Kamiezu Lake in Kumamoto City (**Figure 5.31**). Usually, man-made riverbanks have shallow slopes down towards the rivers. When the sub-layer liquefies and the generated excess pore water pressure is prevented from escaping to the surface (capped by a low permeable or impermeable layer at the surface), the lateral movement occurs for the whole liquefied layer. Tension cracks indicate that lateral spreading had occurred in this area (**Figure 5.36**).


**Figure 5.36** Liquefaction-induced lateral spreading at the Kamiezu Lake.

### 5.8 Conclusions on the infrastructure damage and geotechnical failures

Extensive investigations on infrastructure and geotechnical damage were conducted in Kumamoto City, Mashiki Town, Minami Aso Village, and Nishihara Village. The majority of the damage occurred close to the Futagawa Fault where ground shaking was strongest and there were fault surface ruptures. The types of observed ground failures included surface rupture, ground settlement, landslides, and liquefaction which resulted in damage to bridges, dams, tunnels, roads and over-ground facilities.

The main observations are as follows:

1 Multiple bridge failures across the Kumamoto region were observed as a result of landslides, fault rupture, and ground shaking. Extensive damage was observed along Road 28, which runs above and in proximity to the Futagawa Fault. All of the bridges between Nishihara Village and Tawarayama Tunnel were destroyed.

2 Significant cracking within the Tawarayama Tunnel was observed at the western portal which is located above the Futagawa Fault. The tunnel at this location suffered high axial compression forces, resulting in fracturing of the tunnel lining.

3 The Oogiribata Dam, which is located directly above the Futagawa Fault, showed damage in the retaining walls of the spillway. As a result, a large volume of water leaked out of the reservoir after the mainshock, however, there was no complete failure of the dam.

4 The roads that were above or close to the Futagawa Fault or were located at the toe of landslides were heavily damaged. Vertical displacements of the roads were visible in the northern area of Aso Caldera where the fault ruptured to the ground surface, causing extension and therefore graben like structures on the road surfaces. Intense ground shaking of the road fill also appears to have caused a significant amount of lateral spreading across the region with higher relief.

5 Multiple landslides have been observed around Aso Caldera in the form of earth flows, debris flows, slides, and slumps. The highest density of the landslides was concentrated in the areas where strong shaking was observed. This region was within close proximity to the Futagawa Fault which intersects the western caldera wall. The slopes were commonly gentle at the base (less than 10°) becoming steeper (>60°) towards the top of the caldera rim where volcanic vents were also observed.

6 Liquefaction, represented by sand boils, differential ground settlement and localised lateral displacement, was observed at the Kumamoto Port, along the Akitsu River (Mashiki Town and Kumamoto City), and near the Kamiezu Lake. In the Kumamoto Port, evidences of sand boiling were extensively observed, where building differential settlement occurred. Along the Akitsu River, the soil was mainly composed of sand and silt, which tend to develop liquefaction more easily under high excess pore water pressure. The bridges and buildings nearby showed differential settlements, tilting, and shear cracks. Extensive localised lateral displacement and ground cracking were observed on the embankments of the Kamiezu Lake. The surface of the man-made riverbanks was capped by a low permeable or impermeable layer which prevented the dissipation of excess pore water pressure, resulting in lateral spreading of liquefied soil.

### 5.9 References

Ikeda, T., Kiyota, T., and Konagai, K. (2016). The report on the damage along the prefecture road route 28. Accessed on 1 November 2016 at http://www.gdm.iis.u-tokyo.ac.jp/R28_v01b.pdf.

Goda, K., Campbell, G., Hulme, L., Ismael, B., Ke, L., Marsh, R., Sammonds, P., So, E., Okumura, Y, Kishi, N., Koyama, M., Yotsui, S., Kiyono, J., Wu, S., and Wilkinson, S. (2016). The 2016 Kumamoto earthquakes: cascading geological hazards and compounding risks. *Frontiers in Built Environment*, **2**, 19, doi: 10.3389/fbuil.2016.00019.

Idriss, I.M., and Boulanger, R.W. (2008). *Soil Liquefaction during Earthquakes.* Oakland, CA: Earthquake Engineering Research Institute, California, United States of America, 237 p.

# 6 Relief and Recovery

## 6.1 Emergency response

Whilst in Japan, the EEFIT was able to interview emergency response personnel from the Japan Voluntary Organisations Active in Disaster (JVOAD, http://jvoad.jp); representatives from the Kumamoto City Office and from the Kyoto Prefecture civil defence team; local volunteers and personnel from the Mashiki Town and Uki City Offices. The team members attended one of the nightly non-governmental organisation (NGO) coordination meetings at the Kumamoto City Office and also conducted interviews at evacuation centres, managed by both the city and regional offices, and talked to the managers as well as some evacuees. This section summarises the observations from these personal interviews and is supplemented by factual information on relief and recovery activities following the 14 and 16 April Kumamoto earthquakes from the Fire and Disaster Management Agency and other sources. Obviously, as of December 2016, the relief efforts and recovery planning are still ongoing, and some of these plans and information are subject to change in time.

### 6.1.1 *Organisation of city level and regional disaster management*

The population of Kumamoto Prefecture is 1,786,170 (2015 census). Over ten percent of the population were affected directly and at peak times, a day after the 16 April earthquake, there were 183,883 evacuees housed in 855 shelters. There are still 301 evacuees residing in 12 shelters at the time of writing this section (4 October 2016). The Cabinet Office disaster response mechanism is shown in **Figure 6.1**. Supported by the Kumamoto City Office, the other agencies involved in support of the disaster relief efforts after this earthquake included:

- Affected prefecture offices
- Japan Ground Self Defense Force (JGSDF)
- Non-profit organisations (NPOs), such as JVOAD; JVOAD is the main NPO in charge of coordinating the relief efforts
- Other prefecture volunteers

### 6.1.2 *Support from other prefectures*

Each prefecture civil protection team was assigned to support an affected area (**Figure 6.2**). The support teams from other prefectures have been working in rotation since mid-April and based at the Kumamoto City Office. The relief coordination has been divided into four regions:

- Centre: Kumamoto City
- North: Minami Aso Village, Nishihara Village, etc.
- West: Mashiki Town, etc.
- South: Mifune Town, Uto City, etc.

The coordinators of NPOs, national and local authorities meet every night at 19:00 PM at the Kumamoto Prefecture Office. There have been frustrations that despite these meetings, issues raised by the regional offices have not been addressed by the Kumamoto Prefecture Office. Kumamoto City operates separately from the rest of the affected region. In talking to officers from the Kyoto Prefecture Office and the World Food Programme during the visit, they also voiced their concerns at the slow pace of the relief efforts and lack of decisions made. An EEFIT member attended one of these meetings where each attendee (around 30 people) reported on progress, shared information and issues on their assigned area, but there was little in the form of exchanges of ideas and problem solving. Despite the intention of ensuring information flow between the local government authorities and all staff and volunteers working in the field, in reality, this process did not aid response efficiency (World Food Programme, personal communication). Moreover, there was frustration amongst municipality officers getting little or no responses to requests sent to the main Kumamoto Prefecture Office.

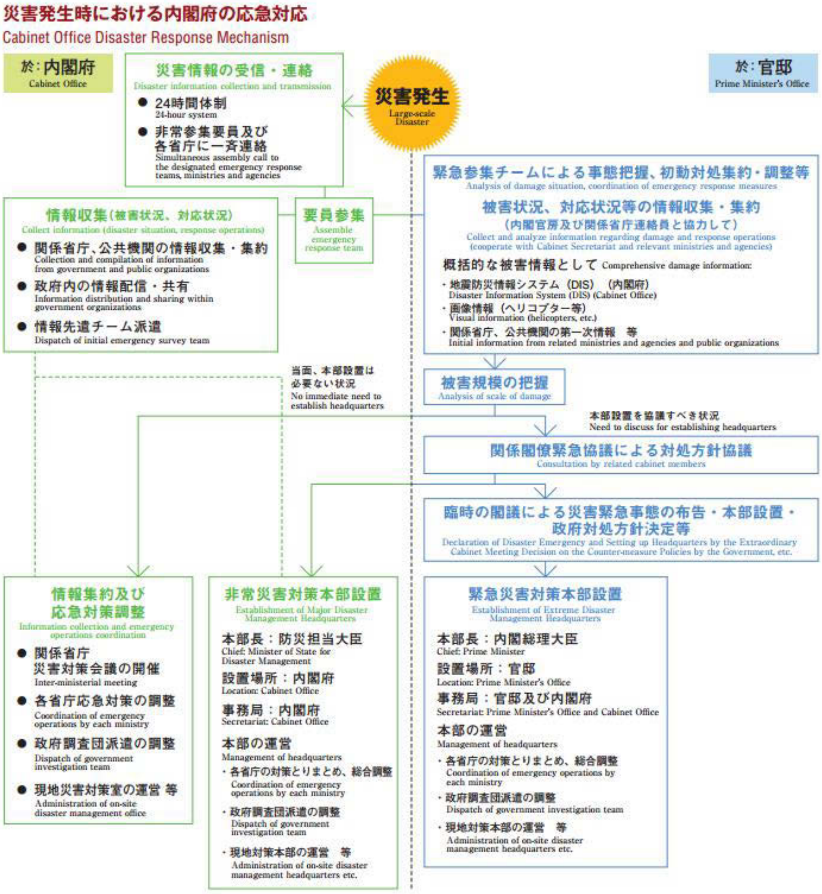


**Figure 6.1** Cabinet Office disaster response mechanism.

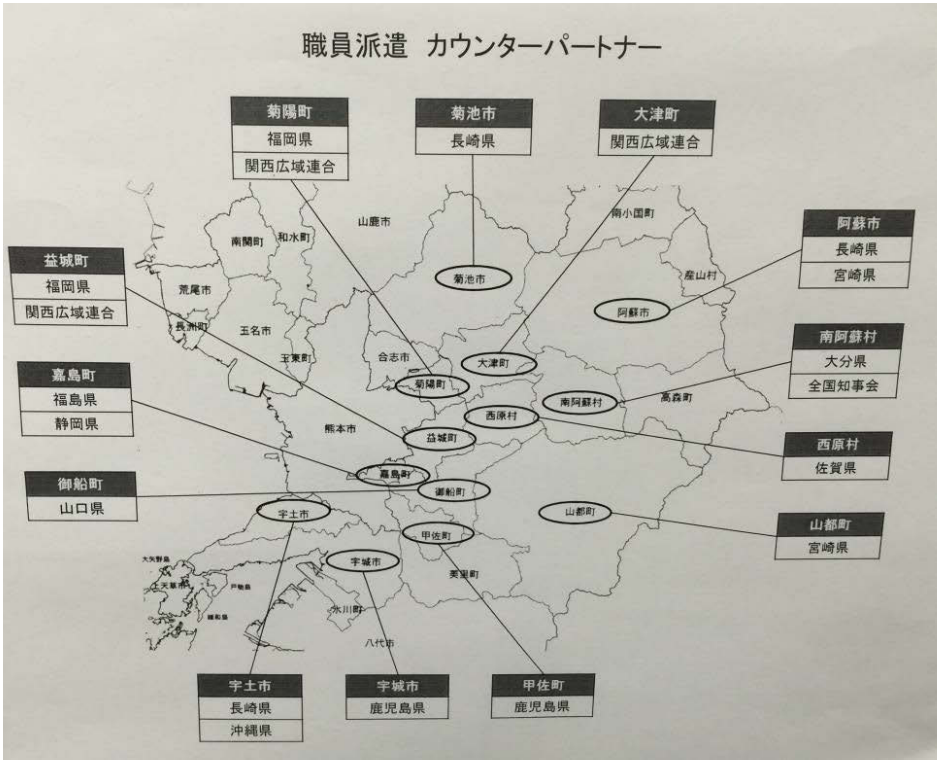


**Figure 6.2** Areas affected by the earthquake (in black) are supported by personnel from different prefectures. For example, Mashiki Town is supported by Fukuoka Prefecture and Union of Kansai Governments.

Some other issues were highlighted by relief responders as having an impact on the speed and effectiveness on the humanitarian response.

*Sequence of events*: Structural assessments and road repairs were underway after the 14 April event when the second, more damaging earthquake hit. Some residents who had been told that it was safe to return home after the first event were traumatised by the experience of the second event and refused to go home even though their homes were not significantly damaged. This increased the number of people needing temporary shelters in the weeks and months after the event.

*Damage to infrastructure*: There was extensive damage to infrastructure, railways, ports, and roads (Sections 4 and 5). This hampered initial response as personnel were unable to or there were significant delays in getting in and out of the affected areas.

*Damage to evacuation centres*: Some evacuation centres could not operate at their full capacity due to damage to parts of the designated buildings that were deemed unsafe. Evacuees were therefore either turned away, had to sleep in makeshift tents, in cars or in corridors. Though each household should have been assigned to an evacuation centre, there was confusion in post-event situations. One interviewee recounted how her family with a disabled daughter was turned away from three centres and ended up sleeping in their cars due to overcrowding.

*Secondary injuries and deaths*: In all, 115 people died as a result of the two earthquakes of 14 and 16 April 2016. Out of the 50 direct deaths, over two thirds (68%) were older people (age over 65 years) while 37 deaths were attributed to building collapses, with the remaining 13 deaths caused by landslides (**Table 6.1**). 7 of the 37 died on 14 April, and 30 died in the mainshock with Mashiki Town being the most affected area. At least 20 people died in collapsed houses built before 1981. After the 14 April 2016 event, some residents in fully or partially damaged homes had already moved to evacuation centres, and an interviewee in Minami Aso Village mentioned how he perhaps had 'escaped death' as his house completely collapsed after the 16 April event. There were also associated indirect deaths including cardiac arrests as shown in **Table 6.2**, which are attributed to the post-quake hardships, health and physical surroundings of the evacuees.

This event resulted in indirect deaths associated with 'economy class syndrome' because some evacuees slept in their cars for long periods of time. The association with deep vein thrombosis (DVT) was very worrying for the authorities and all around in the evacuation centres, there were notices giving advice to evacuees on how to avoid this condition as shown in **Figure 6.3**. Evacuees slept in their cars due to a variety of reasons. Some had to in the first few nights as the evacuation centres were over capacity due to damage to the evacuation buildings themselves. Others chose to stay in their cars as families were worried about security and privacy, some did not want their children to be sleeping in close proximity to strangers, and others because they had pets[1].

**Table 6.1** Direct and indirect deaths resulting from the two events by municipality (as of 4 October 2016).

| Municipality | Direct deaths | Indirect deaths |
|---|---|---|
| Kumamoto City | 4 | 45 |
| Uto City | 0 | 2 |
| Kikuchi City | 0 | 1 |
| Koshi City | 0 | 3 |
| Oozu Town | 0 | 3 |
| Aso City | 0 | 2 |
| Takamori Town | 0 | 1 |
| Minami Aso Village | 16 | 1 |
| Nishihara Village | 5 | 0 |
| Mifune Town | 1 | 1 |
| Kashima Town | 3 | 1 |
| Mashiki Town | 20 | 3 |
| Yatsushiro City | 1 | 1 |
| Hikawa Town | 0 | 1 |
| Kami Amakusa City | 0 | 0 |
| **Total** | **50** | **65** |

[1] A year on, the number of reported indirect deaths has risen to 170, with the total fatalities at 225 and with more than 47,000 people remaining on the list of displaced (Japan Times, 2017).

**Table 6.2** Trend of indirect deaths by municipality (as of 4 October 2016).

| Municipality | 3 May | 3 June | 4 July | 3 August | 5 September | 3 October |
|---|---|---|---|---|---|---|
| Kumamoto City | 10 | 10 | 10 | 23 | 30 | 45 |
| Uto City | 1 | 2 | 2 | 2 | 2 | 2 |
| Kikuchi City | 0 | 0 | 0 | 0 | 1 | 1 |
| Koshi City | 0 | 0 | 0 | 0 | 3 | 3 |
| Oozu Town | 0 | 0 | 0 | 0 | 3 | 3 |
| Aso City | 2 | 2 | 2 | 2 | 2 | 2 |
| Takamori Town | 0 | 1 | 1 | 1 | 1 | 1 |
| Minami Aso Village | 1 | 1 | 1 | 1 | 1 | 1 |
| Nishihara Village | 0 | 0 | 0 | 0 | 0 | 0 |
| Mifune Town | 1 | 1 | 1 | 1 | 1 | 1 |
| Kashima Town | 0 | 1 | 1 | 1 | 1 | 1 |
| Mashiki Town | 1 | 1 | 1 | 1 | 3 | 3 |
| Yatsushiro City | 0 | 0 | 0 | 0 | 0 | 1 |
| Hikawa Town | 1 | 1 | 1 | 1 | 1 | 1 |
| Kami Amakusa City | 0 | 0 | 0 | 0 | 0 | 0 |
| **Total** | **17** | **20** | **20** | **33** | **49** | **65** |


**Figure 6.3** Notice explaining preventative measures for 'Economy Class Syndrome' found in evacuation centres.

### 6.1.3 *Earthquake support programs*

The earthquake support programs were put in place for people affected by the 2016 Kumamoto earthquakes. The guidelines explained the different physical, financial, and social support available to evacuees as shown in **Figure 6.4**.

A victims' certificate was issued per household and was required for insurance claims. These were issued only after rapid structural assessments were carried out. It was noted during the team's visit that these assessments were carried out by different authorities and in many cases had to be repeated, resulting in delays in the issue of the disaster victims' certificates.

The evacuation centres housed three types of people: people with partially collapsed or completely collapsed houses; people living in residential blocks with disrupted services, and those who are too scared to return home. The affected municipal governments provided gymnasiums, schools and other public buildings for use as public shelters in Kumamoto, Oita, Nagasaki, and Fukuoka Prefectures. A day after the 16 April earthquake, there were 855 shelters and 183,883 evacuees recorded. Due to the restart of schools in the region, many shelters housed in school gymnasiums had to be closed on 8 May to allow school children to return to classes on 9 May 2016. All public shelters in prefectures other than Kumamoto were closed by 16 May 2016.

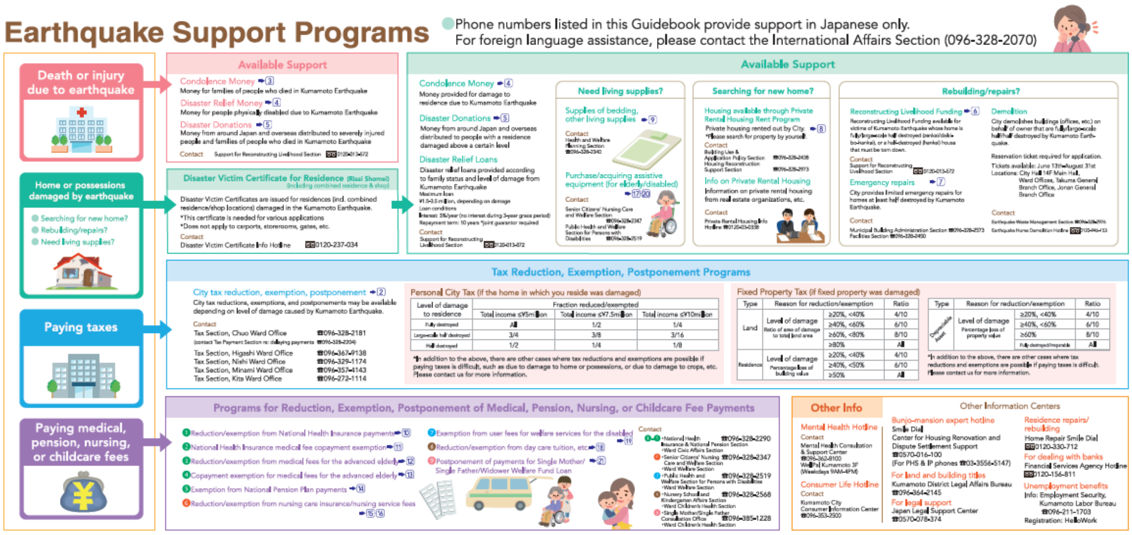


**Figure 6.4** A summary of the earthquake support programs for the people affected by the 2016 Kumamoto earthquakes. The full guidelines explain the physical, financial and social support available to evacuees.

The team visited evacuation centres in all four relief coordination regions in Kumamoto Prefecture. The organisation and management of these varied depending on location and size of the housed population. The largest centre was in Mashiki Town and was managed by three groups: the YMCA, the Mashiki Town Office, and a local NGO who coordinated the tented accommodation as shown in **Figure 6.5**. At this evacuation centre, an outdoor bathing facility was provided and managed by the JGSDF (**Figure 6.6**). Inside the Mashiki Town sports and community centre, which also includes a library, the affected population were sleeping where they could, in corridors as well as inside the main hall of the gymnasium. One of the problems mentioned by evacuees during interviews was lack of space for belongings and a fear of theft. This is in contrast to evacuation centres visited by the EEFIT after the Tohoku earthquake and tsunami, where the victims had very little in the form of possessions since most of these were washed away by the tsunami. There was a police presence at all the centres the team visited in Kumamoto but surprisingly at this evacuation centre, they did not have an updated register of the residents at the centre.

**Figure 6.5** Mashiki Town evacuation centre.


**Figure 6.6** Outdoor bathing facility operated by the Japan Ground Self Defense Force at the Mashiki Town evacuation centre.

During the team's visit, it was seen that trailers were used to house different amenities at the evacuation centre in Mashiki Town. For example, Japan Post provided a mobile post office from 25 April (**Figure 6.7**). **Figure 6.7** also shows part of a pet boarding facility, where about 60 cages in three buildings with an air conditioner and dog walking area were established from 16 May. This prevented people from bringing pets indoors and also helped in moving some families from their cars and tents into the main gymnasium. The Mashiki Town Office approved the use of the trailers as welfare shelters for victims at the end of May 2016. It is the first time that a local government has embarked on the use of these trailers in post-disaster situations in Japan.

The types of accommodation varied depending on where the displaced were housed. The team was given permission to take pictures inside the Uki City evacuation centre. **Figure 6.8** and **Figure 6.9** show the arrangements of the accommodation. Common to all of the centres visited, dedicated staff from the local municipality office and volunteers from other regions of Japan were managing the facilities. There were timetables of the daily activities, meal times and other services on notice boards, like the one shown in **Figure 6.10**. There were also notice boards with important announcements from the government related to the relief and recovery operations.


**Figure 6.7** Vehicle post office and the office of pet boarding facility at the Mashiki Town evacuation centre.

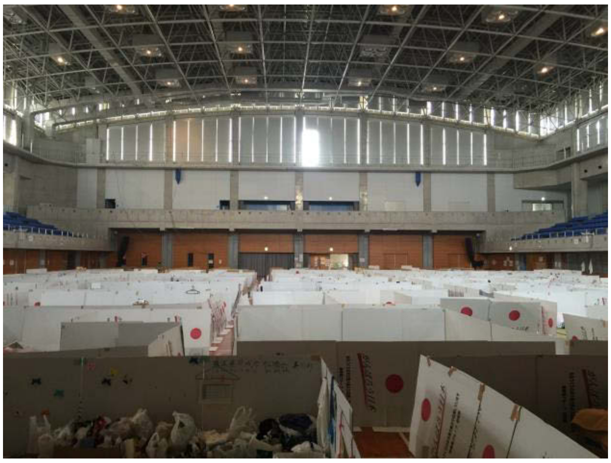

**Figure 6.8** Observed conditions inside a gymnasium at the Uki City evacuation centre. It accommodated around 30 people during the day and around 100 people at night at the team's visit on 27 May 2016.


**Figure 6.9** A family of three personalising their accommodation at the Uki City evacuation centre.


**Figure 6.10** An example of a notice board at the Uki City evacuation centre detailing the daily timetable for group activities, meal times, and health care services.

Though most of the interviewees EEFIT spoke to were happy to be taken care of by the local government and with the provisions and information received, some issues were identified by the evacuees and the managers of evacuation centres during the interviews conducted by the team.

From evacuees' points of view:

- There was a lack of privacy and excessive noise inside the centres, especially in the large gymnasiums.

- The Shigeru Ban cardboard column and curtain set-up (**Figure 6.11**) was criticised by families who were not able to see people approaching them and therefore felt insecure.
- Some families have been forced to stay in cars and tents as other residents complained about noise their children were making.
- Most have been moved a number of times since the earthquakes due to reopening of schools.
- Some of the elderly wanted the box beds (**Figure 6.12**) but these were not often available.

From evacuation centre managers' points of view:

- Some larger centres still (at the time of visit) did not have a register of the temporary residents.
- Some victims abused the system and the lack of formal registration by obtaining supplies and meals from the centres even though they were no longer living in the centres.
- Frustrations have been taken out on staff and most are not trained to deal with such issues.
- With the rainy season approaching (at the time of the visit), evacuees sleeping out in tents were asked but unwilling to move indoors due to a lack of privacy and space.
- Many of the prefecture staff have been affected themselves and are finding it hard to cope with managing the centres, their daily work at the municipality office and their own family lives.
- The elderly were in the centres all day and treating them as in day care centres but this is not part of the evacuation centre's remit.

As of 4 October, there are still 301 registered evacuees at 12 evacuation centres, significantly decreased in the six months since the beginning of the crisis.

**Figure 6.11** Shigeru Ban cardboard column and curtain temporary shelter design.

**Figure 6.12** Raised 'beds' made of paper boxes.

## 6.2 Plans for recovery

For Kumamoto City, the immediate plan at the time of the EEFIT mission was to move people from all temporary shelters to the base shelter in Kumamoto City. The Kumamoto Earthquake Recovery and Reconstruction Headquarters were formed and had their first meeting on 20 June 2016. The intention was to move people from temporary shelters to transitional houses by the end of July 2016.

For other regions in the prefecture, arrangements were different. For example, there was a lottery for assigning transitional housing on 10 June for Mashiki Town, while in Nishihara Village the local residents were consulted to collectively plan the relocation of their communities in June 2016.

As of 6 October 2016, the number of temporary housing constructed is shown in **Table 6.3**. As seen, six months after the event, over 90% of planned temporary housing have been constructed across the affected region.

**Table 6.3** The number of temporary housing planned and constructed (as of 6 October 2016).

| Municipality | Planned | | Constructed | |
|---|---|---|---|---|
| | Number of housing estates | Number of houses | Number of housing estates | Number of houses |
| Kumamoto City | 9 | 541 | 9 | 541 |
| Uto City | 6 | 143 | 4 | 117 |
| Uki City | 6 | 176 | 4 | 143 |
| Misato Town | 3 | 41 | 2 | 26 |
| Oozu Town | 6 | 91 | 6 | 91 |
| Kuyo Town | 1 | 20 | 1 | 20 |
| Aso City | 4 | 101 | 4 | 101 |
| Ubuyama Village | 2 | 9 | 2 | 9 |
| Minami Aso Village | 8 | 401 | 8 | 401 |
| Nishihara Village | 5 | 312 | 4 | 302 |
| Mifune Town | 21 | 425 | 17 | 328 |
| Kashima Town | 11 | 208 | 11 | 208 |
| Mashiki Town | 18 | 1,562 | 16 | 1,492 |
| Kosa City | 6 | 228 | 6 | 228 |
| Yamato Town | 1 | 6 | 1 | 6 |
| Hikawa Town | 3 | 39 | 3 | 39 |
| **Total** | **110** | **4,303** | **98** | **4,052** |

The Cabinet Office pledged 778 billion Japanese Yen (JPY) towards the restoration of the Kumamoto earthquakes. On 31 May 2016, 102.3 billion JPY was committed as a first financial injection for the reconstruction and recovery[2].

The proposed use of the funds is as follows:

- 18 billion JPY for small and medium-sized enterprises and agricultural assistance. The creation of a half price 'trip ticket' for trains and hotel charge to all seven prefectures in Kyushu Island to encourage commerce and tourism to the region (http://kyushu-fukkou.jp/). This is the first time that the Japanese Government has created a special grant for travel assistance.
- 400 billion JPY – for supporting medium-sized enterprises:
  - 75% of the funds to the recovery paid by the Government and Prefectures.
  - 25% of the funds to the recovery paid by affected companies.
- 53 billion JPY – for commerce, e.g. rebuilding of arcades along shopping streets affected by the earthquakes.

Since May 2016, the Kumamoto Prefecture Office has published a road map to provide housing and life support, recovery support of the affected residential land, medical care, prevention education, etc. (Kumamoto Prefecture Office, 2016). In all, there are four categories and 28 plans, and these goals are to be achieved within the next four years. The four categories are as follows:

[2] http://www.sankei.com/economy/news/160531/ecn1605310023-n1.html (in Japanese).

- Reconstruction of housing and social services: nine plans have been proposed, a timeline for some of the goals was translated and shown in **Figure 6.13**.
- Recovery of social infrastructure: seven plans.
- Reproduction of local industry: ten plans.
- Recovery of connection to the world (development of port facilities and sports): two plans.

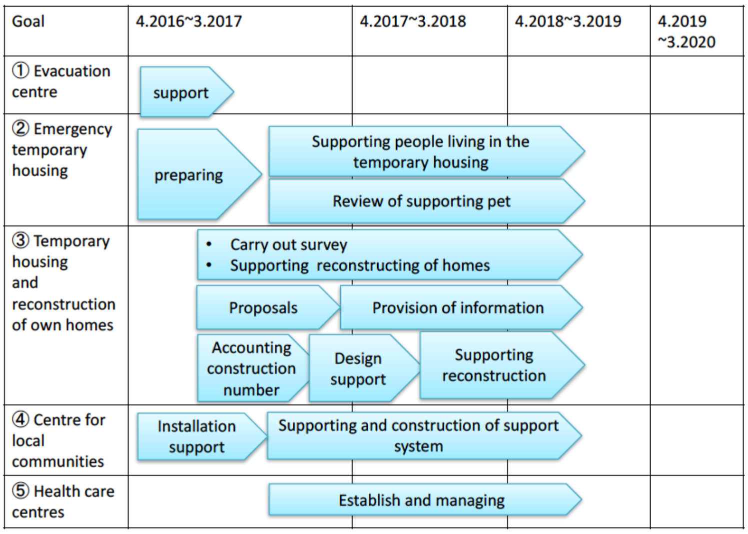


**Figure 6.13** Chart showing the timeline for different goals set out by the Kumamoto City Office for housing and social services.

The restoration-revival plan summary presents a future image for Kumamoto as one of:

Hope: The future is full of dreams and hopes.

Safety: Kumamoto can live in safety and security and be resilient against the disasters.

Pride: Treasures are inherited to the future with much pride.

Economy: Kumamoto has a stable and vibrant economy.

Municipalities in Kumamoto Prefecture have been developing their own recovery plans. For example, as of 7 October 2016, a second development committee was held in Mashiki Town to formulate a 10-year reconstruction plan. At this meeting, officials stated that they will request financial transactions, necessary business, and enactment of special legislation of the Government and Prefecture. For Mashiki Town, the key message for the future is to ensure that '*people want to continue to live in the city and want to inherit to the next generation*'. The reconstruction plan document is planned for publication in December 2016[3].

## 6.3 Conclusions on the relief and recovery

The organised but rigid pre-event disaster management structure and lack of power given to municipality officials and disaster management staff from other prefectures, may have worked against the relief efforts after the Kumamoto earthquakes. Even though many of the personnel deployed to Kumamoto from other prefectures have experience and important lessons learnt from previous national and international efforts, due to the traditional hierarchical structures, there were no means of implementing suggestions directly. This was seen by many interviewed as a waste of resources and time. One important observation from the EEFIT mission and the subsequent literature review is that relief and recovery strategies at the Kumamoto City level are deliberately separated from the surrounding regions. Though there is a need to differentiate due to the urban/rural mix and the number of population affected, the discrepancies have hampered coordination efforts and speed of the relief, and public consultation in the ensuing recovery. In Kumamoto City, decisions are

[3] http://www.town.mashiki.lg.jp/common/UploadFileDsp.aspx?c_id=137&id=859&sub_id=1&flid=3363 (in Japanese).

centralised, whereas in Nishihara Village for example, there is an emphasis on community consultation. The rate of recovery and the ability to 'build back better' may be dependent on the approach employed as seen in so many other examples of disaster recovery around the world (Platt and So, 2016).

Even though local governments should have designated nearby school gymnasiums and sports centres as public shelters, as part of the disaster management plans, there were reports of confusion in the first few days after the 16 April earthquake as to where the affected families should go. The team interviewed a family who was looking after a severely disabled girl during their visit and found the accounts of lack of provisions and consideration from the local authorities to accommodate people in the girl's situation troubling. The family had since decided to rent an apartment rather than wait for government support.

Every place the team visited, the members were overwhelmed by the level of volunteer support and generosity of the local and national population. The frustration and challenge, like in many post-disaster situations, were in better coordination and communication to utilise the goodwill and time of these volunteers more effectively.

'Ganbatte!' is a phrase that captures the Japanese spirit to *try one's best* and *never give up*. Six months on, the temporary housing construction plan is well under way and there are the beginnings of plans to address permanent housing, wellbeing, cultural heritage (including the restoration of the Kumamoto Castle and Aso Shrine amongst others; see Section 4), and the revitalisation of the region in the next four years. The new logo and motto from the Kumamoto Prefectural Government is 'Ganbaruken! Kumamoto-ken!' meaning, 'We won't give up! Kumamoto Prefecture!' (**Figure 6.14**).


**Figure 6.14** The new logo for the Kumamoto Prefecture's earthquake reconstruction efforts, featuring the prefectural mascot *Kumamon*. The text reads: 'Ganbaruken! Kumamoto-ken!' meaning 'We won't give up! Kumamoto Prefecture!' (image courtesy: Kumamoto Prefectural Government).

## 6.4 References

Kumamoto Prefecture Office (2016). Road map with new window of main approach for restoration and revival. Accessed on 3 October 2016 at http://www.pref.kumamoto.jp/common/UploadFileOutput.ashx?c_id=3&id=16643&sub_id=3&flid=81844.

Platt, S. and So, E. (2016). Speed or deliberation – a comparison of post disaster recovery in Japan, Turkey and Chile. *Disasters*, doi: 10.1111/disa.12219.

Japan Times (2017). Accessed on 20 June 2017 at http://www.japantimes.co.jp/news/2017/04/14/national/kumamoto-marks-one-year-anniversary-of-deadly-quakes-with-grief-and-resolve/#.WTw6CeRPpu0.

Earthquake Engineering Field Investigation Team

EEFIT is a UK based group of earthquake engineers, architects and scientists who seek to collaborate with colleagues in earthquake prone countries in the task of improving the seismic resistance of both traditional and engineered structures. It was formed in 1982 as a joint venture between universities and industry, it has the support of the Institution of Structural Engineers and of the Institution of Civil Engineers through its associated society SECED (the British national section of the International Association for Earthquake Engineering).

EEFIT exists to facilitate the formation of investigation teams which are able to undertake, at short notice, field studies following major damaging earthquakes. The main objectives are to collect data and make observations leading to improvements in design methods and techniques for strengthening and retrofit, and where appropriate to initiate longer term studies. EEFIT also provides an opportunity for field training for engineers who are involved with earthquake-resistant design in practice and research.

EEFIT is an unincorporated association with a constitution and an elected management committee that is responsible for running it activities. EEFIT is financed solely by membership subscriptions from its individual members and corporate members. Its secretariat is generously provided by the Institution of Structural Engineers and this long-standing relationship means that EEFIT is now considered part of the Institution.



This report can be downloaded from www.eefit.org.uk

EEFIT
c/o The Institution of Structural Engineers,
47 – 58 Bastwick St, London EC1V 3PS
Tel: +44 (0)20 7235 4535
Fax: +44 (0)20 7235 4294
Email: mail@eefit.org.uk
Website: http://www.eefit.org.uk